MODELLING AND CONTROL OF A MICROGRID INCLUDING PHOTOVOLTAIC AND WIND GENERATION

BY

MOHAMMED TOUSEEF HUSSAIN

A Thesis Presented to the

DEANSHIP OF GRADUATE STUDIES

KING FAHD UNIVERSITY OF PETROLEUM & MINERALS

DHAHRAN, SAUDI ARABIA

In Partial Fulfillment of the
Requirements for the Degree of

MASTER OF SCIENCE

In

ELECTRICAL ENGINEERING

April, 2012

KING FAHD UNIVERSITY OF PETROLEUM AND MINERALS

DHAHRAN 31261, SAUDI ARABIA

DEANSHIP OF GRADUATE STUDIES

This thesis is written by **MOHAMMED TOUSEEF HUSSAIN** under the direction of his thesis advisor and approved by his thesis committee members, has been presented to and accepted by the Dean of Graduate Studies, in partial fulfillment of the requirements of degree of **MASTER OF SCIENCE IN ELECTRICAL ENGINEERING**

Thesis Committee

A. H. Rahim

Dr. A.H.M. Abdur-Rahim (Advisor)
Professor, EE Dept.

Dr. Ali Ahmad Al-Shaikhi
Department Chairman

Dr. Ibrahim M. El-Amin (Member)
Professor, EE Dept.

Dr. Salam A. Zummo
Dean of Graduate Studies

8/4/12
Date

Dr. Zakariya M. Al-Hamouz (Member)
Professor, EE Dept.

Dedicated to

My Mother, Father
And
My Brothers and sister

Whose Prayers and Perseverance

led to this accomplishment

Acknowledgement

In the name of ALLAH, the Most Gracious and the Most Merciful

"Read! In the name of your Lord who created. He has created man from a clot. Read! And your lord is the most generous. Who has taught (the writing) by the pen. He has taught man that which he knew not."[Al Quran 96 Ayah 1-5].

All praise and glory be to Almighty Allah Subhanaho wa Taala; we praise Him; we worship Him alone without associating any partners and seek forgiveness from Him. Peace and blessings be upon his last messenger Muhammad sallallahu alaihi wa-sallam, his family, his companions, and all those who followed him until day of judgement.

Acknowledgement is due to King Fahd university of Petroleum & Minerals for providing support that has led my way through this point of undertaking my research work.

My deep appreciation and heartfelt gratitude goes to my thesis advisor Dr. A. H. Abdur-Rahim for his valuable time, suggestions and enormous effort that has spent for me. I am grateful for his guidance, encouragement and constant support that he provided throughout my master's program. I would like to express my deepest appreciation towards him.

I would like to express my grateful thanks to my committee member, Dr. Ibrahim-El-Amin, for his care, cooperation and support. I am very much thankful to him for his valuable recommendations in a leading company. Many thanks to my thesis committee member, Dr. Zakariya-Al-Hamouz, for his suggestions in the improvements in my thesis.

I also owe thanks and recognition to my seniors Abdurrahman, AbdulMalik, Mohammed Abdul Azeem Siddiqui, Akber Ali, Waheed and AbdulQadeer, Irfan Ali Khan and Rizwan Anwar, for their full support during my stay at KFUPM. I am also obliged to thank all my friends especially Jaaved Ali Khan, Khaleel Ahmed Mohammed and Mohammed Afzal Biyabani for their support, company and positive criticism throughout my master's which will be memorable for lifetime. I would also like to thank my other collegues Sameer Arastu, Aamer Ibn Ziyad, AbdulBaqi, AbdulHai Maaz, Asshad, Wajahat, Mohsin Ali and Fasi. I cannot forget some of my best childhood friends AbdulQuddus, Moin, Mohsin Khan, Afzal Khan, Moinulla Khan Ateeq and Mohammed AbdulWasay.

Finally, from the bottom of my heart, I thank my mother and father, my elder brothers {Mohammed Abid, Mohammed Adil, Mohammed Asif, Mohammed Altaf} and their families and my younger sister for their continuous love, encouragement, prayers, emotional and moral support throughout my life. Words fall short in conveying my gratitude towards them. A prayer is the simplest way I can repay them – May Allah give them good health and give me ample opportunities to be of service to them throughout my life.

Table of contents

List of Tables

List of Figures

THESIS ABSTRACT

Name: MOHAMMED TOUSEEF HUSSAIN

Title: MODELING AND CONTROL OF A MICROGRID INCLUDING PHOTOVOLTAIC AND WIND GENERATION

Degree: MASTER OF SCIENCE

Major Field: ELECTRICAL ENGINEERING

Date of Degree: April, 2012.

Extensive increase of distributed generation (DG) penetration and the existence of multiple DG units at distribution level have introduced the notion of micro-grid. This thesis develops a detailed non-linear and small-signal dynamic model of a microgrid that includes PV, wind and conventional small scale generation along with their power electronics interfaces and the filters. The models developed evaluate the amount of generation mix from various DGs for satisfactory steady state operation of the microgrid.

In order to understand the interaction of the DGs on microgrid system initially two simpler configurations were considered. The first one consists of microalternator, PV and their electronics, and the second system consists of microalternator and wind system each connected to the power system grid. Nonlinear and linear state space model of each microgrid are developed. Small signal analysis showed that the large participation of PV/wind can drive the microgrid to the brink of unstable region without adequate control. Non-linear simulations are carried out to verify the results obtained through small-signal analysis.

The role of the extent of generation mix of a composite microgrid consisting of wind, PV and conventional generation was investigated next. The findings of the smaller systems were verified through nonlinear and small signal modeling. A central supervisory capacitor energy storage controller interfaced through a STATCOM was proposed to monitor and enhance the microgrid operation.

The potential of various control inputs to provide additional damping to the system has been evaluated through decomposition techniques. The signals identified to have damping contents were employed to design the supervisory control system. The controller gains were tuned through an optimal pole placement technique. Simulation studies demonstrate that the STATCOM voltage phase angle and PV inverter phase angle were the best inputs for enhanced stability boundaries.

MASTER OF SCIENCE DEGREE

KING FAHD UNIVERSITY OF PETROLEUM and MINERALS

Dhahran, Saudi Arabia

2012

ملخص الأطروحة

الاسم: محمد توصيف حسين.

عنوان الأطروحة: أنمذجة والتحكم بالميكروجرد التي تشمل على خلايا شمسية وطواحين هوائية و مولدات موزعة.

الدرجة: ماجستير في العلوم الهندسية.

التخصص: الهندسة الكهربائية.

سنة التخرج: 2012

إن الزيادة المضطردة للمولدات المُوَزَّعِة ووجودها في مستوى التوزيعِ قدّما فكرةَ الشبكةِ الدقيقةِ. هذه الإطروحةِ تُطوّرُ نموذج متحرك لاخطّي واشارة صغيرة للميكروجرد الذي يَتضمّنُ خلايا شمسية،وطواحين رياح مع اجهزة توصيل الكترونيات القدرة والمرشحاتِ .

ولمعرفة تفاعل وأهمية المولدات الموزعة على الميكروجرد تم اعتبار نموذجان بسيطان. الأول يَشْملُ مولد مع خلايا شمسية وأجهزة الكترونيات القدرة الخاصة بهم، والنظام الثاني يَشْملُ مولد و طاحونة رياح كُلّ نموذج تم ربطه مع شبكة النظامِ الكهربائيةِ. وتم تطوير المعادلات التمثلية لكل من النظام الخطي والغير خطي لكل نموذج .

وباستخدام تحليل الاشارة الصغيرة تبين أن استخدام الخلايا الشمسية وطواحين الهواء يُمْكِنُ أَنْ يقُودَ الميكروجرد إلى حافةِ المنطقةِ الغير مستقرةِ بدون سيطرةِ كافيةِ. وتم أيضاً استخدام المحاكاة اللاخطّية لتَحقق من النَتائِجِ التي تم الحصول عليها خلال تحليل الاشارة الصغيرة .

وفي هذه الأطروحة تم دراسة نموذج يشمل على الخلايا الشمسية وطواحين الهواء والمولدات الموزعة. وتم اقتراح استخدام جهاز تخزين الطاقة مكثف مركزي مربوط مع جهاز الكترونيات القدرة المعروف باسم ستاتكم لمُرَاقَبَة وتَحسين عمل الميكروجرد.

وتم استخدام تقنيات التجزئة لتحسين عمل النظام. تم توظيف الاشارات المعرفة لتَصميم نظامِ السيطرةِ الإشرافيِ. وتمت معايرة جهازَ السيطرة من خلال تقنيةِ ازحة القطبِ المثاليةِ. تُبيّنُ دِراساتُ المحاكاةِ بأنَّ ستاتكم زاويةُ مرحلةِ فولطيةِ وعاكس خلايا الشمسية زاوية مرحلةِ كَانا أفضل المساهماتِ لحدودِ الإستقرارِ المُحَسَّنةِ.

ماجستير في العلوم الهندسية

جامعة الملك فهد للبترول والمعادن

الظهران, المملكة العربية السعودية

2012

CHAPTER 1

INTRODUCTION

1.1 Introduction to Microgrid

In traditional power systems a few large centralized power generation plants produce the bulk of the power. The generated power is then transferred to consumers over long transmission lines. Today, the world is more concern about the environmental issues and energy security; thus governments around the world are relying on renewable energy for reducing the environmental problems caused by the conventional energy sources. Due to rapid increase in global energy consumption and decline of fossil fuels, the demand for new generation capacities and their local connection at the distribution level has increased[1]. Utilizing renewable energy with distributed generation (DG) and distributed storage in large scale can potentially solve problems such as energy shortage and global climate change. Available and currently emerging technologies for DG units are selected depending upon the connection with the utility. The conventional DG units which can be directly connected to the grid are micro-alternators, low head hydro units, combustion engines, etc. The DG units which require voltage source inverter (VSI) for their connection to grid are fuel cells, wind systems, photovoltaic systems etc. [2].

Extensive increase of DG penetration and the presence of multiple DG units at distribution level have brought about the concept of the microgrid. A microgrid is a portion of power system which includes one or more DG units that can operate in islanded mode or in connection with the main grid[3]. A non-autonomous microgrid is connected to the utility usually through a 60Hz substation transformer. Unexpected

disturbances in the system such as sudden load change, three phase fault at PCC, may require microgrid to disconnect itself from the distribution system and remain operational as an autonomous entity[4]. A microgrid is designed to adapt necessary controls and operational strategies to meet at least a part of load in the islanded mode, if necessary. Modeling of microgrid is an important part for proper power management system. An accurate model helps to precisely regulate the active and reactive power flows in the network and ensure high power quality levels thus improving the reliability of the microgrid. Although the components of the microgrid are very well understood, the system performance as a whole is not. Thus modeling and simulating the microgrids become essential in order to maintain the good quality of the system performance.

Among renewable energy options photovoltaic and wind generations are favorite choices for many utilities[5]. But it is also observed that the power from these DG sources vary and is extremely unpredictable. Large participation of these power sources with rapid variations disturbs the power system stability and can cause critical problems. This difficulty can be overcome by employing energy storage devices in combination with static synchronous compensator (STATCOM) which can act as a central controller to the microgrid. Energy storage device with STATCOM act as a dispatchable DG source and can swiftly exchange power with utility grid[6]. Several fast response and bulk energy storage technologies can be employed into the DC bus of STATCOM namely batteries, Superconducting magnetic energy storage (SMES), energy capacitors, flywheels etc. However, energy capacitors have several benefits for energy storage that are useful in many applications. They are very robust and effective, need low maintenance, offer high power density and they can be operational through decades[7].

The microgrid central controller monitors the active and reactive power flows from various DGs in order to balance the total generation from DG units and the total load at the microgrid. It can enhance the safe operating region of microgrid by compensating the real and reactive power unbalance in the system.

1.2 Microgrid Development

Microgrids of variety of structures are an expected configuration of the future electricity supply system; they signify a drastic transition from a large centralized and normalized macrogrid. Benefits of small scale power generation and local control have been recorded from various perspectives. Before stating the advantages of microgrid, it is imperative to study the driving points towards the microgrid. Some of the concerns of centralized system[8] are,

- Restrictions on power system expansion.
- Limitations of centralized power system planning.
- Risks of volatile bulk power markets.
- Threats to an insecure system.
- Consequences of infrastructure interdependencies.
- Limits to the qualities of power delivered.
- Growth of gaseous emissions (mainly CO2).

A microgrid could potentially improve the technical performance of local distribution grid mainly in the following aspects:

- Energy loss reduction due to decreased line power flows.
- Mitigation of voltage variation via coordinated reactive power control and constrained active power dispatch

- Relief of peak loading of constrained network devices through selective scheduling of nearby DG outputs.
- Enhancement of supply reliability via partial or complete islanding during loss of main grid.
- Short construction times and lower capital costs of smaller plants.

1.3 Microgrid Operation Modes

A Microgrid can operate either in the grid connected mode or autonomous mode. In grid connected mode, the frequency and voltage magnitude is dictated by the main grid and DG units supply the total load or part of it. Thus it behaves as a controllable load or source by either absorbing or supplying power to the main grid depending upon the total generation and total load available at the microgrid.

In an autonomous mode, besides feeding total active and reactive power of the load, frequency and voltage magnitude should also be controlled by the DG units[9]. A microgrid sometimes intentionally isolates all DG units and operates in the standalone mode in the event of a fault in the grid. This strategy is adequate when the total generation of DG units is not sufficient and they can be removed without major impact on the system[10].

Microgrid is commonly designed for autonomous control. However, when multiple DG sources are incorporated, the control strategy for power balancing, within the microgrid, becomes difficult[11]. The microgrid reduces the frequency/voltage variations through its connection with the external power system which balances the power supply and load demand during normal and emergency condition[8].

1.4 Problem Statement

The increase of energy resources in the shape of distributed generation, distributed energy storage or a combination of both, challenges the control and stability of the microgrid. Major concerns of microgrid are the stability issues, power quality of the supply and penetration limitation of the electronically interfaced DG units. The presence of sensitive loads and continual imbalance in loads require the inverters to operate under unbalance conditions. This creates the switching harmonics, voltage and frequency variations in the microgrid, etc., and hence degrades the stability of the system. Steady state and transient stability studies in the utility-connected mode are required to ensure a safe operation with good performance.

In the grid-connected mode, the inverter-based DG faces the following problems:

- Large penetration of the DG sources in weak grid
- Attenuate the switching frequency ripple in the output voltage
- Avoid the resonance between the filter and coupling or grid inductance.
- Fast response of inverter can undesirably influence voltage/angle stability if suitable control actions are not taken.

1.5 Thesis Objective

This research aims at presenting an organized methodology and the mathematical description to derive a nonlinear and small-signal dynamic model of a microgrid that includes photovoltaic system and wind system in addition to the conventional generation. Effectively controlled design will guarantee stable and high quality power injection under disturbances and instabilities.

The main issues to be dealt with in this thesis are highlighted as:

- To identify the amount of generation mix from various DGs for satisfactory steady state and transient operation of the microgrid.
- To design a central controller and identify the control signals for stabilization and control of the tie-line power flow of microgrid under study.
- To optimize the controller parameters for providing satisfactory damping profile.
- To carry out the non-linear domain simulations to evaluate the effectiveness of the proposed controller in enhancing the stability boundaries.

1.6 Thesis Organization

This thesis is organized as follows

In chapter 2, a literature survey of the all components of microgrid configuration considered in this thesis and their issues is presented. The recent studies on hybrid microgrid models, stability issues and their solutions and various control techniques are included.

Chapter 3 presents the detailed nonlinear and linear models of photovoltaic and wind systems in addition to a microalternator. The converter interfaced microgrid components are connected to the common bus through LC filter and coupling inductances. A capacitor energy storage device interfaced through a STATCOM is modeled to act as a supervisory control of the complete microgrid is also modelled.

In chapter 4 two simple microgrid configurations are studied. The first one consists of microalternator and PV and the second consists of microalternator and wind system. A load is also considered to be connected at the common bus in individual microgrid system. The nonlinear and linear state space model of each microgrid connected to the grid is developed. Small signal analysis is performed to analyze the effect of large penetration of PV/ wind on the microgrid stability. Nonlinear simulations are also carried out to verify the results obtained through small signal analysis.

Chapter 5 presents a composite microgrid consisting of PV, wind, microalternator in addition to a central controller connected to the grid. A local load is also considered to be integrated. Both nonlinear and linear simulations are done to evaluate the suitable generation mix for the various distributed generation units for reliable and satisfactorily steady operation of microgrid.

Chapter 6 establishes the hierarchies of controls in terms of dynamic performance enhancement through minimum singular value decomposition, hankel singular value decomposition and residue principles. A pole placement technique is employed to optimize the controller parameters. Non-linear time domain simulations have been carried out to validate the findings of the small signal model and also to assess the controller performance in terms of enhancing system operation.

Chapter 7 includes conclusion and future work.

CHAPTER 2

LITERATURE REVIEW

The literature review on this subject is divided into the three sections. In the first section, the recent studies on photovoltaic system, wind system and the hybrid microgrid model are documented. In the second section, various stability issues involved in microgrid structure and their solution are discussed. In the last section, several control techniques and decomposition methods which help in improving the performance of microgrid have been discussed.

2.1 Components of Microgrid

A microgrid consists of rotating type DG and inverter type DG which requires power electronic converters for their connection to the main grid[12]. Rotating type DG includes internal combustion engines, gas turbine, microalternator etc. while inverter type DG includes photovoltaic, fuel cells, and wind generation technologies. All the DG components are usually small-scale power generation units typically in the range of 4kW to 10000kW.

2.1.1 Photovoltaic system

Photovoltaic is the method of generating electricity directly from the solar energy using the semiconductor by the photoelectric effect. PV power generation employs solar arrays composed of solar cells, usually connected in series-parallel arrangement. Electric power generated from the PV array depends upon the number of cells and their arrangement.

In literature, a lot of research has been conducted focused on a comprehensive PV model which is designed using power electronic components [13-16]. The detailed model

examines PV system and its control circuitry, but at the same time it is observed to be computationally complex, which limits its application for microgrid studies. PV systems were also represented as constant real power generations[17] or negative constant power loads[18]. These techniques for model simplifications are adopted for steady state analysis; however, they are not applicable for dynamic analysis and control implementation.

A PV dynamic model was modeled to comply with the practical data from a specified PV panel and a specified electronically controlled pulse modulated inverter by T. Yun in [19]. The mathematical equations were obtained irrespective of the actual system configuration, which hindered further control establishment. National Renewable Energy Laboratory(NREL) designed a simplified model of PV [20] and represented it as a current controlled source where only current magnitude and angle were taken into account. But no actual PV dynamics and closed loop controls were incorporated as the DC side was preset. Recently a simplified form of PV system modeled as voltage source was proposed[13]. This model is far more precise than current controlled source and it preserves many PV system signals and hence can be employed for control technique development. But its effect on dynamic stability of microgrid has yet to be studied.

A PV based stabilizer system has been developed to enhance the network dynamic stability in [21]. The system DC side was not considered and no control loops were applied in the model. Two dynamic models of PV generation systems, namely detailed dynamic and simplified models integrated into power network were studied in [22]. However the system is modeled as a non-dispatchable source hence it cannot be employed in microgrid to provide the controllable real power.

Large integration of PV systems can introduce unwanted conditions to power systems, such as current and voltage harmonics, voltage variations in distribution feeders, flicker and stress on distribution transformer. It has been observed that the voltage at the PCC in the large integrated system rises due to the reverse power flow from individual PV system on sunny days. In IEEE Std. 929 that is: "Recommend Practice for Utility Interface of Photovoltaic System" interconnection issues related to the PV system and their solutions are discussed.

2.1.2 Wind System

Since last 10 years, the wind turbine is the world's fastest expanding power generation technology. The worldwide market for the electrical power generated by the wind system generator has been rising progressively, which promptly impels the wind technology into a highly competitive environment.

(a) Fixed speed wind turbine

In the early 1990s, almost every wind turbine installed operated at fixed speed, irrespective of wind speed[23]. The rotor speed of the turbine is fixed to the speed defined by the normal frequency of the power grid to which the turbine is connected. The gear ratio and the design of generator permits the rotor to rotate at this fixed speed for variable wind speeds[24]. The standard electrical system for fixed speed wind turbine is the squirrel-cage induction generator (SCIG) directly connected to the grid. To compensate for the no-load current of the generator, a capacitor bank is installed which reduces the reactive power demand. Moreover, a thyristor based soft starter is employed to reduce the inrush current.

A conventional wind turbine rotating at fixed speed connected to the normal utility grid is modeled in[25]. Utilizing this model, the detailed short circuit analysis is done. A three-phase fault is applied in proximity to wind turbine generator, and detached immediately by disconnecting the faulted line. The base case is also used to analyze and discuss the effect of various mechanical, electrical and operating parameters for the certain critical fault-clearing time. The parameters examined are the wind speed, the power output, the short-circuit power at the connection bus, the distance to the fault ,the reactive power compensation, the hub-generator resonant frequency, the distance between generator and faulted point, the rotor inertia etc. The proposed methodology is very well organized to analyze the transient stability performance in fixed speed wind system.

Equivalent wind system models operating at fixed speed are proposed in[26] by accumulating the wind turbines into an approximate equivalent wind turbine which can operate on an equivalent wind system electric network. Two effective equivalent wind turbines have been designed. The first equivalent model for accumulated wind turbines operated efficiently for identical winds, the other equivalent model is extended to operate with different incoming winds.

Various dynamic models of fixed speed wind turbine, comprising of a comprehensive model and reduced third order equivalent model of wind systems with fixed speed wind turbine generators is presented in [27]. The power system stability studies were also presented with the stator flux transient incorporated. The fault ride through capability of the generator has been investigated for a symmetrical three phase fault on the grid bus.

(b) Variable speed wind turbine

A variable speed wind turbine runs at a certain speed relative to the current wind speed, defined by the optimal tip-speed ratio, in order to produce maximum power. The energy captured can be increased by using an active pitch, which adjusts the pitch angle instantaneously to the wind speed. Unfortunately, this advantage cannot be utilized only at low or medium wind speeds as the bandwidth of the pitch control results in overload due to large wind power fluctuations at high wind speed. The stall-controlled wind turbine can be designed to manage power overload but this increases the cost of the electrical system.

The dynamic model with pitch angle and stability control schemes of a variable speed wind turbine with permanent magnet synchronous generator (PMSG) is created in[30] The model comprises of a PMSG, the pitch angle controlled wind turbine and a drive train model. The drive train model employs single mass model to represent the generator mechanical characteristics. The control strategy development involves the pitch angle control for wind turbine and a speed control block for PMSG.

The comprehensive model and control strategy development of variable speed wind generator is also very well depicted in[31]. In order to find out the gain in energy obtained from one methodology over the other, many models of off-grid wind generator systems have been designed in matlab/Simulink. All methodologies under consideration have the same parameters and components. A new technique is proposed to track the maximum energy from a 20kW PMSG and a fair comparison is done with the results of previous control schemes.

A optimal tuning procedure for rotor side converter controllers for DFIG used for power system stability study are presented in [32]. It is particularly observed that both the stator and rotor dynamics should be incorporated for optimally tuning controller parameters. The paper is organized as modeling and stability study of microgrid and the impact of optimal control parameters on the system. Root loci technique and nonlinear time domain simulations show that the DFIG operation is viable over along range of operating conditions.

2.1.3 Microgrid Formation

The concept of microgrid evolved from operation of economically sustainable and reliable power system comprising of small scale generation units of distributed nature. Microgrid appears to the main grid as a single load or source depending on whether the load is higher than the generating sources in the area. Microgrid in parallel with the power grid has affected voltage, line current, power quality, line flow, protection and network reliability at the point of common coupling (PCC). The effect depends on the distribution circuit type, the location and the capacity of PCC, load characteristics of microgrid and so on[33]. Preliminary study on the technical requirements of grid connected microgrid such as power quality, voltage regulation, power control and so on are analyzed in [34].

To use solar and wind energy resources more efficiently and economically, a methodology for calculation of the optimal sizing of a PV array in hybrid PV/wind system for a given load is demonstrated in[35].An interesting study of an autonomous PV/Wind hybrid system has been reported in [36]. In this work, microgrid under study cannot always provide controllable power output with changing weather conditions due

to non dispatchable sources; hence an auxiliary generation apparatus that is used to store energy is employed. However, the maximum limit of storage unit is limited to 240W.

A comparatively larger standalone PV-diesel hybrid generation system for a small island has been proposed in [37]. This hybrid generation consists of 300kW of diesel power and 750kW of PV power that supplies the power to private houses in island and is relatively far away from main grid. Although it is a feasible work, the control strategies and MPPT has not been discussed.

F. Valenciaga[38] presented power control of a utility connected hybrid generation system which consists of PV and fuel cell. In this 500W hybrid system, an electrolyzed couple to the PV array is used for hydrogen production. A controller is also designed based on constant and continuous power generation using the hybrid combination. The details of controller are not depicted in the work.

Reference [39] reported a small scale hybrid PV/Wind system employing MPPT for both PV and wind with controllers. However the controller is designed without considering the environmental conditions such as irradiance and wind speed. The subjects relating to sizing and control of battery storage can be considered as shortcomings of the paper.

An organized technique is used to create a small-signal dynamic model of a several DG microgrid that incorporates synchronous generator including the exciter and the governor systems and electronically interfaced DG units is presented by F. Katiraei[40]. The system model incorporated the dynamic model of the transmission lines and hence is an acceptable depiction for the sub-synchronous frequency range. The designed model can be employed to develop controllers for the microgrid, optimize

controller parameters of EI-interfaced DG units, and recognize operating parameters of microgrid components and control blocks, investigation of torsional dynamics and low frequency power quality issues.

Various other configuration of microgrids have been discussed in the literature namely AC microgrids, DC microgrids and hybrid AC/DC microgrid. In AC microgrids, DC power from PV and fuel cells is converted into AC using DC/AC inverters. But the DC loads have to be converted in AC using AC/DC converters. In DC microgrids, AC power from wind and micro alternator has to be converted into DC and AC loads have to be converted into DC. To reduce energy loss due to reverse conversion, the concept of hybrid AC/DC microgrid is proposed[41].

2.2 Stability issues of microgrid

The microgrid stability has been affected by many factors in both on grid/ off grid mode. Presence of electronically interfaced DG units introduces new issues caused be network disturbances, overloading of DG units, switching harmonic generations etc. These disturbances extremely challenge the stability and control of weak microgrids. Moreover, in the traditional power system when the load changes, the frequency also changes due to the change in the kinetic energy of the rotating parts, but in microgrid the majority of the DG units do not contain rotating parts and are interfaced to the microgrid using power electronic devices. In other words, there is no frequency response when the load changes as in traditional power system. The interfacing inverter is controlled to imitate the operation of a synchronous generator. In this way, the power sharing mechanism is developed to share the powers between different DG units in the microgrid[42].

Poor power quality also results from the switching frequency and pre-existing grid voltage distortions. A well designed filter can accommodate the switching frequency components but has an impact on control bandwidth. “Control and filter design of three-phase inverters for high power quality grid connection” [43] describes a filter designed to incorporate an isolating transformer and the design of a complementary controller that rejects grid disturbance, maintains good waveform quality and achieves real and reactive power control.

“Harmonic Interaction between a large number of distributed power inverters and the distribution network”[44] investigates the power quality problems associated in extensive penetration of microgrid system at the PCC. This research is focused on observing the harmonic interference phenomena in multiple inverters and to compare the network interactions of various inverter configurations and control techniques. Laboratory experiments investigate the power quality issues of different inverter topologies and computer simulation validates the experimental results. It is observed that the parallel and series resonance phenomenon between the network and these inverters are responsible for higher than expected current and voltage distortion levels in DP networks.

A MATLAB/SIMULINK model of microgrid simulated is presented in “Stability analysis of microgrids with constant power loads” [45]. To extract the eigenvalues of the system, a small signal state space model is created. A sensitivity analysis is carried out to conclude on the possibility to shift right half plane poles to left half plane by regulating the current and voltage controller gain values.

A dynamic model of single shaft micro turbine generation(MTG) system is developed using SimPowerSystem toolbox in "Dynamic model of a microturbine used as a distributed generator" [46]. It is suitable for on grid/off grid operation. The bidirectional power flow between utility and MTG is allowed in the presented model.

A two-point estimate (TPE) based method for probabilistic analysis of small signal stability of a microgrid considering uncertainties is addressed in "Probabilistic analysis of small signal stability of microgrid using point estimate method" [47]. Stability indices and the judgment of unstable types for microgrids probabilistic small signal stability are also addressed. For a system with N random parameters, the TPE method employs 2N calculations to quantify the uncertainty while keeping enough precision in contrast with the Monte Carlo approach, where a long time simulation is performed for the same number of parameter evaluation.

2.3 Control of Microgrids

The power from the DG sources varies highly often and is extremely unpredictable. Large participation of electronically interfaced power sources with rapid variations disturbs the power system stability and can cause critical problems. This difficulty can be overcome by employing energy storage devices in combination with static synchronous compensator (STATCOM) which can act as a central controller to the microgrid. Reference[48] gives detail characteristics and performance of super capacitors, analyzing the structure and principles of the super capacitor energy storage system.

Utilization of battery super capacitor hybrid storage (BSHS) in microgrid is presented in [49]. BSHS composed of batteries (124V, 10 batteries), Supercapacitor module 20F, 324V), buck boost bi-directional converter, and a VSC. The control loop is

designed to compensate the fluctuating power from RES, and tries to extend the batteries lifetime by optimizing operation.

Supercapacitor centered dynamic support system for hybrid microgrids that assures the secure transition between operational modes (parallel / standalone) and the accurate power settlement in off-grid mode is introduced in "Design and development of a supercapacitor-based microgrid dynamic support system" [50]. The paper describes the design and development of the hardware and software components of a microgrid support system.

Oscillatory modes have been identified in microgrid simulation studies. There are some modes which are responsible for instabilities in the system at some operating conditions. These critical modes dictate the initiation of control action to improve the performance of the microgrid. In the design and evaluation of the controllers, the properties of linear models such as the controllability and observability are employed. It is always important to know the how difficult is to control the dominant mode from an input of the system. A theoretical explanation of the basics of singular value decomposition(SVD) used to measure the ability of inputs to control a mode is given in "An investigation of the significance of singular value decomposition in power system dynamics"[51].

In grid connected mode, the selected controller parameters, the filter inductance and the filter capacitance are very essential to attain the system stability. Trial and Error approach is mostly incorporated to select the controller parameters by understanding the system overall characteristics. But the trial and error method cannot reliably forecast all microgrid operational scenarios hence it may lead to weak power quality and

angle/voltage stability[52]. So the appropriate value of the controller and filter parameters should be obtained in order to maintain power quality within the coordinated range and assist the system against any load variation or any disturbances. Various approaches to choose the controller parameters and control strategies, wherein trial and error method is used, have been found in the literature[53].

Generally, it is observed that microgrid parameters change with generation and system loading making the system behavior quite different for different operating conditions. Whenever there is a drastic change in the power system operation parameters, the controller parameter which stabilize the system under normal operating condition, may no longer yield appropriate results due to the change of controller parameters in a complex manner. To maintain the required control performance and power quality during changing operating conditions, a fine tuning of controller parameters is required[54]. A method for shifting the complex open loop poles to any desired position while preserving the imaginary parts is presented in "Optimal pole shifting for power system stabilization" [55]. In every step of this technique, it is required to solve a first-order linear matrix lyapunov equation for shifting one real pole and a second order equation for shifting two complex poles. The solution obtained using this approach is optimal with respect to quadratic performance index.

Power electronic interfaces introduce new control issues and possibilities. The microgrid control techniques and their effectiveness are presented in "Control of microgrids" [56]. Strategies towards the well-organized and fault tolerant control with RES, smart loads and storage units are developed. These control strategies are completely based on local control and they do not need any communication between the DG units.

Control technique of DG plants using feedback of locally measurable variables are introduced in [57]. It has been shown that the islanding and paralleling procedures for portion of the distributed generations becomes cost effective with the proposed control logic for the inverter and offline communication to optimize real and reactive power sharing between the units.

The potential – function based method for secondary and tertiary is introduced in [58]. In this proposed method, various pieces of information from each DER unit e.g., voltage, current, real and reactive power etc. are communicated to the microgrid central controller at pre-specified time intervals. The central controller defines a potential function for each DER unit such that its minimum corresponds to the control goal. It is applied for the secondary voltage control of two microgrids with single and multiple feeders.

A control strategy to implement intentional islanding operation of microgrids is introduced in "Intelligent control for intentional islanding operation of microgrids" [59]. Sophisticated control, islanding recognition, load shedding and re-closure algorithms for the grid connected DG are well explained. Two interface controls are used, one for on-grid operation and other for pre-planned islanding operation. An islanding recognition algorithm is implemented to switch between the two controls. The synchronization of microgrids that operate with multiple DGs and loads cannot be controlled by a conventional synchronizer.

It is needed to control multiple generators and energy storage systems in a coordinated way for the connection of the autonomously operated microgrid to the main grid. Reference[60] proposes an active synchronizing control scheme that adopts the

network-based coordinated control of multiple DGs. The proposed controller assures the deterministic and reliable synchronization even under the power fluctuations from the renewable sources.

An Optimal design of microgrid in autonomous and grid connected modes [61] has been presented in KFUPM by Ali Hassan. Nonlinear time-domain-based as well as eigenvalue-based objective functions are proposed to minimize the error in the measured power and to enhance the damping characteristics, respectively. Also the nonlinear time-domain simulation has been done to evaluate the usefulness of the designed controllers under various loading and disturbances conditions. Dynamics of the DG unit itself has been ignored in this work and and the controllers are developed considering only one DG unit.

CHAPTER 3

MODELING OF A MICROGRID

The dynamic model of the various DG units along with the connecting electronics is developed in this section. The DGs considered are microalternator, photovoltaic system and a wind system. A capacitor energy storage is also modeled which acts as a supervisory control of the microgrid. The linearized model of each DG unit is also derived from their corresponding non-linear dynamics.

3.1 The Microgrid System

Figure 3.1 shows a single line diagram of the microgrid configuration. The system consists of three DG units connected to the grid with an integrated load. The system model also includes dynamic model of lines with filter for inclusion of sub-synchronous frequency range. DG1, the microalternator, is modeled so as to represent a gas-turbine or a diesel generator. The microalternator is equipped with an excitation control. The PV module (DG2) is interfaced to the grid through voltage source converter (VSC), filter and coupling inductance. The variable permanent magnet synchronous generator wind system (DG3) is interfaced through appropriate converters with an additional filter circuit at the grid side of the converter. A STATCOM along with energy storage capacitor supervises the overall flow conditions and takes corrective action, when needed.

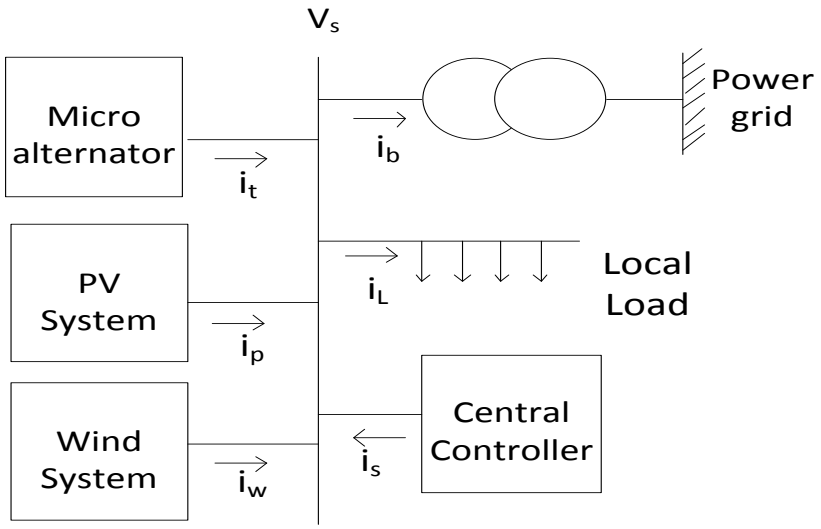

Figure 3.1 Microgrid Configuration

3.2 Micro-Alternator Model

The generator is represented by the 3rd order model consisting of the swing equation and the generator internal voltage equation [62]. The swing equation can be written as two first order differential equation as

$$\frac{d\delta}{dt} = \omega_o(\omega - 1) \quad (3.1)$$

$$\frac{d\omega}{dt} = \frac{1}{2H}[P_m - P_e] \quad (3.2)$$

In (3.1) and (3.2), δ and ω are the rotor angle and rotor speed, P_m and P_e are the mechanical power input and electrical power output of the generator.

The internal voltage ${e_q}'$ is given by

$$\frac{d{e_q}'}{dt} = \frac{1}{{T_{do}}'}\left[E_{fd} - {e_q}' - (x_d - {x'}_d)i_{td}\right] \quad (3.3)$$

where x_d, x'_d and T'_{do} are the d-axis synchronous reactance, transient reactance and open circuit field constants respectively, ${e_q}'$ is the voltage behind the transient reactance along q-axis.

The IEEE type ST is used for the voltage regulator excitation.

$$\frac{dE_{fd}}{dt} = \frac{1}{T_A}\left(K_A\{V_{tref} - V_t\} - (E_{fd} - E_{fd0})\right) \quad (3.4)$$

where E_{fd} is the field voltage along d-axis, K_A and T_A are the gain and time constant of the exciter respectively.

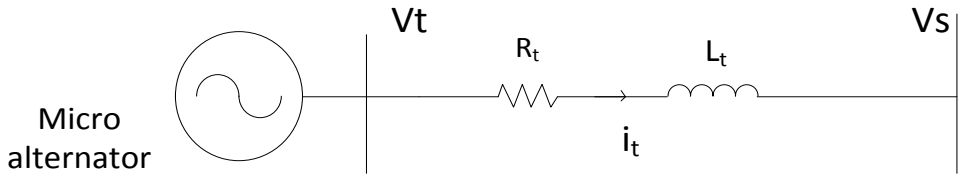

Figure 3.2 Microalternator connected to the grid.

The terminal voltage of the generator from the Figure 3.2 is given as

$$V_t = V_s + (r_t + jx_t)i_t$$

Writing in d-q terms

$$V_d + jV_q = V_{sd} + jV_{sq} + (r_t + jx_t)\left(i_{td} + ji_{tq}\right)$$

$$x_q i_{tq} + j\left(e_q{}' - x_d{}' i_{td}\right) = \left(V_{sd} + + r_t i_{td} - x_t i_{tq}\right) + j\left(V_{sq} + r_t i_{tq} + x_t i_{td}\right)$$

Real part:

$$x_q i_{tq} = V_{sd} + r_t i_{td} - x_t i_{tq}$$

$$(x_q + x_t)\, i_{tq} - r_t i_{td} = V_{sd} \quad (3.5)$$

Imaginary part:

$$e_q{}' - x_d{}' i_{td} = V_{sq} + r_t i_{tq} + x_t i_{td}$$

$$r_t i_{tq} + (x_d{}' + x_t) i_{td} = e_q{}' - V_{sq} \quad (3.6)$$

On solving (3.5), (3.6) and putting x_1=$(x_d{}' + x_t)$ and x_2=$(x_d{}' + x_t)$, we get

$$i_{td} = \frac{-r_t V_{sd} + (e_q{}' - V_{sq})\{x_q + x_t\}}{r_t{}^2 + \{x'_d + x_t\}\{x_q + x_t\}} \quad (3.7)$$

$$i_{tq} = \frac{V_{sd}[\{x'_d + x_t\}\{x_q + x_t\}] + r_t(e_q{}' - V_{sq})\{x_q + x_t\}}{\{x_q + x_t\}[r_t^2 + \{x'_d + x_t\}\{x_q + x_t\}]} \quad (3.8)$$

The terminal voltage of the generator is written as

$$V_t = \sqrt{V_d^2 + V_q^2}$$

$$V_t = \sqrt{(x_q i_{tq})^2 + (e_q{}' - x_d{}' i_{td})^2} \quad (3.9)$$

The power output is given as

$$P_e = V_d i_{td} + V_q i_{tq}$$

$$P_e = (x_q i_{tq}) i_{td} + (e_q{}' - x_d{}' i_{td}) i_{tq}$$

$$P_e = (e_q{}' i_{tq}) + (x_q - x_d{}') i_{td} i_{tq} \quad (3.10)$$

Substituting (3.7) and (3.8) in (3.9) and (3.10), the terminal voltage and power output of microalternator can be expressed in microgrid voltage components V_{sd} and V_{sq}.

3.3 Photovoltaic (PV) system

Solar cell is the basic building block of photovoltaic array made up of a semiconductor device which behaves as a current source driven by a flux of solar radiation from the sun. The characteristic of an ideal solar cell at no illumination is same as of an ideal diode. The operation of PV is greatly determined by the irradiation, array short circuit current, array open circuit voltage, cell temperature and load connected to the array[63]. The output current and power of the PV is approximately proportional to irradiance. Also at a given irradiance, the array voltage is determined by the load characteristics. PV system exhibits a nonlinear I-V and P-V characteristics which vary with the radiation intensity and cell temperature. The PV output current has very little effect on the temperature variation. By increasing the temperature, PV cell produces a slightly higher output current but this increase in the cell temperature forces the PV cell to conduct at a lower voltage thus greatly reducing the power output of PV[64].

A general mathematical description of I-V characteristics for a solar cell has been the subject of study for many years. The general equivalent model consists of a photo current, a diode, a shunt resistor representing a leakage current and a series resistance expressing an internal resistance to the current flow Figure 3.3 The net output current from the PV cell is the difference of photovoltaic current I_{ph} and the sum of normal diode current I_D and leakage current in the shunt resistanceR_{sh}.

$$i_{pv} = I_{ph} - I_D - \frac{(V_{pv}+i_{pv}R_s)}{R_{sh}} \quad (3.11)$$

The diode current I_D is given as

$$I_D = I_s\left(e^{\frac{(V_{pv}+R_s i_{pv})}{nv_T}} - 1\right) \quad (3.12)$$

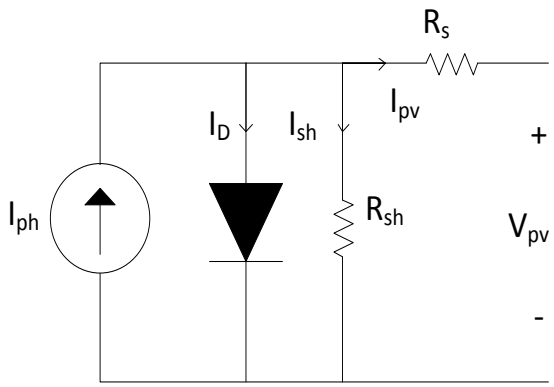

Figure 3.3 General equivalent model of solar cell

where, i_{pv} is the cell current, V_{pv} is the cell voltage, I_s is the reverse saturation current (strongly dependent on temperature), n is an ideality factor, Rs is a series resistor, R_{sh} is the shunt resistance $v_T \left(= \frac{kT}{q}\right)$ is the thermal voltage, K $(= 1.3807 * 10^{-19})$ is a Boltzmann constant, T is a cell's working temperature and q $(= 1.6022 * 10^{-19})$ is the charge of the electron.

The light generated current mainly depends on the cell's working temperature and solar irradiation. At a given cell temperature (T), the photocurrent is given as:

$$I_{ph} = \left[I_{sc} + a(T - T_{ref})\right]G \qquad (3.13)$$

In the above, I_{sc} is the cell's short current at a 25^0C and 1kW/m^2, 'a' is the temperature coefficient of Isc, T_{ref} is the cell's reference temperature and G is the irradiation in kW/m^2.

The reverse saturation current is also temperature dependent and at a given temperature (T) it is given as

$$I_s = I_{sref}\left(\frac{T}{T_{ref}}\right)^{\frac{3}{n}} e^{\frac{-qE_g}{nk}\left(\frac{1}{T}-\frac{1}{T_{ref}}\right)} \qquad (3.14)$$

where I_{sref} is the cell's saturation current at a reference temperature and solar irradiation, E_g is the energy band-gap of the semiconductor used in the solar cell.

The shunt resistance (R_{sh}) is inversely related to the shunt leakage current to ground. In general, the PV behavior is insensitive to $R_{sh,}$ and hence can be assumed to be infinity. On the other hand, a small variation in R_s will considerably affect the power output of PV. The approximate model of PV is shown in figure 3.3.

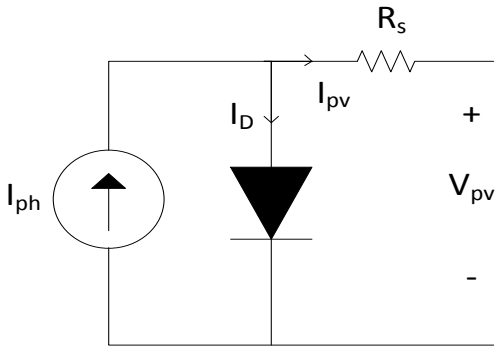

Figure 3.4 Approximate model of PV cell

The characteristic equation of the cell from approximate model is given as

$$i_{pv} = I_{sc} - I_s \left[e^{q\left(\frac{V_{pv}+i_{pv}R_s}{nv_T}\right)} - 1 \right] \quad (3.15)$$

The power generated by a solar cell is typically in the range of 2W at 0.5V. Since this power is very small, the solar cells are usually connected in series and parallel for generating power in the range of watts. The characteristic equation of the approximate photovoltaic array comprising of N_s series modules and N_p parallel modules can be obtained from the approximate PV cell equation and is given as

$$i_{pv} = N_p I_{ph} - N_p I_s \left[e^{\left(\frac{V_{pv}}{N_s}+\frac{i_{pv}R_s}{N_p}\right)/nv_T} - 1 \right] \quad (3.16)$$

It can be observed from (3.16) that for a PV cell, N_s=1 and N_p=1.

The current voltage relationship of a PV array in (3.16) is nonlinear. The Newton's method [65] is employed to solve this nonlinear equation.

Newton raphson algorithm

The iterative procedure for solving the nonlinear equation

$$f(x) = 0 \qquad (3.17)$$

starts from an initial solution x_n and updated as

$$x_{n+1} = x_n - \frac{f(x_n)}{f\prime(x_n)} \qquad (3.18)$$

The iterations can be continued until the error is less than or equal to pre-specified toleranceE_s, given as

$$\left|\frac{x_{n+1}-x_n}{x_n}\right| \leq E_s \qquad (3.19)$$

For the PV, the I-V characteristics are related as,

$$V_{pv}=N_s\left[ln\left(\frac{N_pI_{ph}-i_{pv}}{N_pI_s}+1\right)nv_T-\frac{i_{pv}R_s}{N_p}\right] \qquad (3.20)$$

Expressed as a function in (3.17), it can be related as

$$f(V) = V - N_s\left[nv_T * ln\left(\frac{N_pI_{ph}-i_{pv}-N_pI_s}{N_pI_s}\right)+\frac{i_{pv}R}{N_p}\right] = 0 \qquad (3.21)$$

Since $f'(V) = 1$, the recursive formula can be written as

$$V_{n+1} = N_s\left[nv_T * ln\left(\frac{N_pI_{ph}-i_{pv}-N_pI_s}{N_pI_s}\right)+\frac{i_{pv}R}{N_p}\right] \qquad (3.22)$$

3.3.1 The Power Conditioning Unit of PV system:

The power conditioning unit (PCU) contains the devices which required for connection of PV array to the microgrid. The main components of the PCU are DC/DC converter, DC link capacitor, DC/AC inverter and the output filter circuit as shown in figure 3.5. The DC power produced by the PV array is fed to the DC/DC converter. The converter transforms the PV output voltage from one level to another. The DC-link capacitor is a storage device used to maintain constant inverter voltage. The inverter is the core of grid-connected PV system which converts the DC to AC and injects it into the grid. For smoothing the output current, an LC filter is commonly employed between the PV system and utility network. The resistance R_{pdr} in series with the filter capacitor is used to avoid the resonance between the filter capacitor and the coupling inductance. The models for the different components of the PCU are presented in the following.

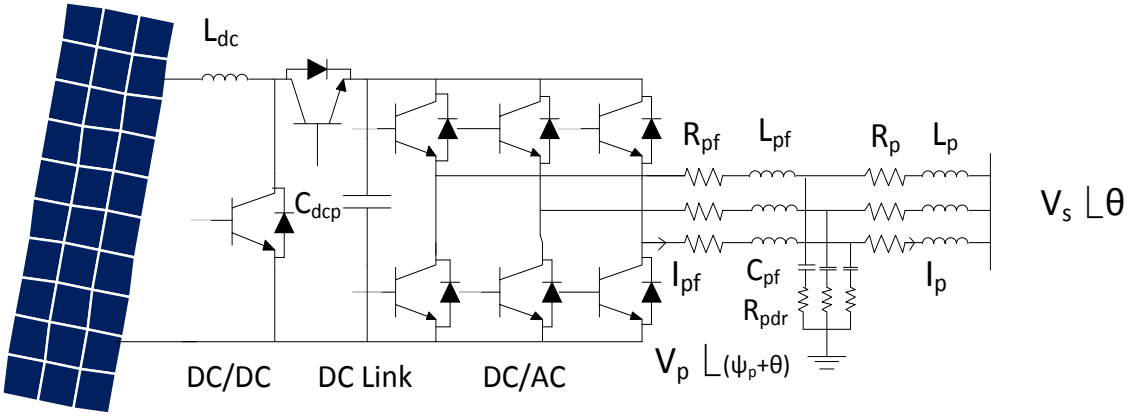

Figure 3.5 PV array connected to the microgrid

A. DC/DC converter model

As mentioned, the basic function of the DC/DC converter is to increase or decrease the DC output voltage. A DC/DC converter is composed of power electronic switches and storage elements connected in such a way that the dynamic power transfer from input to output can be controlled through switching. The configuration of the storage elements are such that they provide low output ripple voltage (less than 3%) which can be obtained by forming a low pass filter[67].

There are many different topologies of DC/DC converter, of which the two most fundamental ones are boost converter and buck converter. In this work, boost converter is employed because the PV output voltage always has to be stepped up. The duty cycle of the DC/DC converter, defined as the ratio of ON period to the switching time period (T), decides the level of DC output voltage.

A DC/DC converter can operate in continuous conduction mode (CCM) or discontinuous conduction mode (DCM). In CCM, current fluctuates but never goes down to zero. In DCM, the current fluctuates and goes down to zero before or at the end of switching period. In this work, continuous conductor mode of operation is employed as the photovoltaic array has to feed power into the grid without any interruption.

Boost converter:

The basic function of the boost converter is to step up the DC voltage level. It comprises of an inductor, a power electronic switch and a diode. It may have a capacitor to smooth the output.

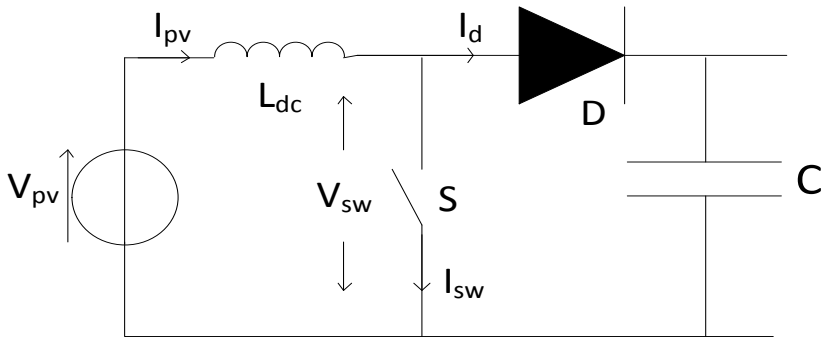

Figure 3.6 DC/DC converter Configuration

Dynamics of the DC/DC inverter can be easily obtained by applying as

$V_{pv} = \dot{L_{dc}} I_{pv} + (1 - dc) V_{dcp}$

which can be written as,

$$\dot{I_{pv}} = \frac{1}{L_{dc}} \left(V_{pv} - (1 - dc) V_{dcp} \right) \quad (3.23)$$

Here L_{dc} is the inductance of the DC/DC converter.

B. DC-link capacitor model

The purpose of the DC link capacitor of the pulse width modulated (PWM) inverter is to act as an energy storage and filter for the DC voltage. The DC/DC converter regulates the capacitor voltage irrespective of the inverter operation, while the inverter tries to provide the proper current to the grid at the expense of capacitor voltage variation. If the converter output current is made equal to the input current of the inverter, no current will flow through the DC-link capacitor which considerably reduces the size of the capacitor[68].

Dynamics of DC-link capacitor can be obtained by taking KCL at the DC-link node.

$$\frac{d\,V_{dcp}}{dt} = \frac{1}{C_{dc}}(I_{dc1} - I_{dc2}) \qquad (3.24)$$

where $i_{dc1} = (1 - d_c)i_{pv}$ and i_{dc2} is the input current to the inverter. The expression of the i_{dc2} can be obtained in terms of inverter output current,V_{dc} is the DC voltage across the capacitorC_{dc}.

C. Inverter Model

The inverter converts the PV array DC output and feeds the grid at the proper frequency. In this study, the voltage gain model of the voltage source inverter (VSI) operating in the PWM mode is adopted.

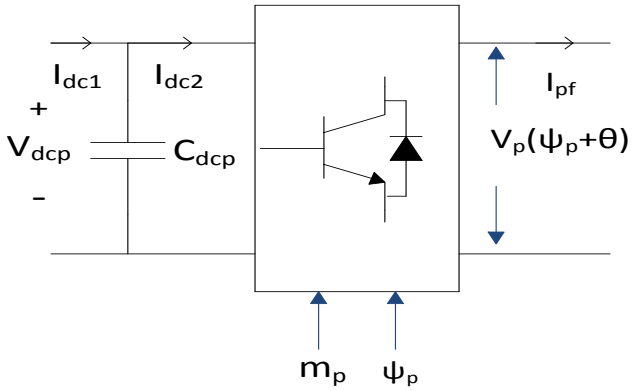

Figure 3.7 Inverter model

From Figure 3.7, the power on the Dc side of the inverter is expressed as

$$P_{dc} = V_{dcp} I_{dc2} \qquad (3.25)$$

The instantaneous active power on the AC side of the inverter is given as

$$P_{ac} = Re[V_p I_{pf}^*] \qquad (3.26)$$

where, V_p and I_{pf} are the inverter output voltage and inverter output current respectively.

In terms of d-q axes, V_p and I_{pf} are written as

$$V_p = V_{pd} + jV_{pq}$$

$$I_{pf} = I_{pfd} + jI_{pfq}$$

Substituting V_p and I_{pf} values in (3.26), we get

$$P_{ac} = V_{pd} i_{pfd} + V_{pq} i_{pfq} \qquad (3.27)$$

Equating the DC and AC side power gives,

$$P_{dc} = P_{ac}$$

$$V_{dcp}I_{dc2} = V_{pd}i_{pfd} + V_{pq}i_{pfq} \quad (3.28)$$

When the inverter operates in the PWM mode, the output voltage can be expressed in terms of the DC-link voltage, modulation index m_p and phase angle of the inverter ψ_p.

$$V_p = m_p * V_{dcp} \llcorner \psi_p \quad (3.29)$$

In terms of d-q axes, equation (3.29)

can be written as

$$V_{pd} = m_p * V_{dcp} * \cos(\psi_p + \theta) \quad (3.30)$$

$$V_{pq} = m_p * V_{dcp} * \sin(\psi_p + \theta) \quad (3.31)$$

Substituting the equations (3.30) and (3.31) into (3.28), we get the expression of I_{dc2}

$$I_{dc2} = \left(i_{pfd}m_p\cos(\psi_p + \theta) + i_{pfq}m_p\sin(\psi_p + \theta)\right) \quad (3.32)$$

D. LC Filter and the Coupling Inductance Model

A passive low pass filter is used to attenuate switching frequency ripple of the inverter output voltage. The filter contains a T section of an RL circuit shunted by a capacitor. The filter inductance and capacitance are the two reactive devices which respond to the change of frequency in opposite ways. The inductor blocks the high frequency harmonics and passes the low frequencies, while the capacitor allows high frequencies and blocks low frequencies. So these reactive devices can block most of the harmonics and reduce the ripples that go through the system[69]. To avoid the resonance that may arise with the coupling inductance and the filter capacitor, a passive damping circuit is added to the filter such as damping resistor.

Applying KVL around the PV inverter and filter capacitor gives a non-linear differential equation as

$$V_p = i_{pf}R_{pf} + L_{pf}\frac{di_{pf}}{dt} + V_{cp} + (i_{pf} - i_p)R_{pdr} \quad (3.33)$$

where, R_{pf} is the filter resistance, L_{pf} is the filter inductance, R_{pdr} is the damping resistance, V_{cp} is the capacitor voltage.

In d-q reference frame the above equation is written as

$$\frac{di_{pfd}}{dt} = \frac{-\omega_0 R_{pf}}{L_{pf}} i_{pfd} + \omega_0 \omega i_{pfq} + \frac{\omega_0 m_p V_{dcp}\cos(\psi_P+\theta)}{L_{pf}} - \frac{\omega_0 V_{cpd}}{L_{pf}} - \omega_0 R_{Pdr} i_{pcd} \quad (3.34)$$

$$\frac{di_{pfq}}{dt} = \frac{-\omega_0 R_{pf}}{L_{pf}} i_{pfq} - \omega_0 \omega i_{pfd} + \frac{\omega_0 m_p V_{dcp}\sin(\psi_P+\theta)}{L_{pf}} - \frac{\omega_0 V_{cpq}}{L_{pf}} - \omega_0 R_{Pdr} i_{pcq} \quad (3.35)$$

Similarly, a non-linear equation is obtained from the coupling transmission line between PV filter capacitor and microgrid as,

$$V_{cp} = i_p R_p + L_p\frac{di_p}{dt} + V_s - (i_{pf} - i_p)R_{pdr} \quad (3.36)$$

In d-q terms this gives,

$$\frac{di_{pd}}{dt} = \frac{-\omega_0 R_p}{L_p} i_{pd} + \omega_0 \omega i_{pq} + \frac{\omega_0}{L_p}\left(V_{cpd} - V_{sd}\right) + \omega_0 R_{Pdr} i_{pcd} \quad (3.37)$$

$$\frac{di_{pq}}{dt} = \frac{-\omega_0 R_p}{L_p} i_{pq} - \omega_0 \omega i_{pd} + \frac{\omega_0}{L_p}\left(V_{cpq} - V_{sq}\right) + \omega_0 R_{Pdr} i_{pcq} \quad (3.38)$$

where I_p is the coupling line current, R_p is the coupling resistance, L_p is the coupling inductance. The voltage across the filter capacitor is given as

$$C_{pf}\frac{dV_{cp}}{dt} = (i_{pf} - i_p) \quad (3.39)$$

where C_{pf} is the filter capacitor. Splitting the equation in d-q terms yields

$$\frac{dV_{cpd}}{dt} = \frac{1}{C_{pf}}\left(i_{pfd} - i_{pd}\right) + \omega_0 \omega V_{cpq} \quad (3.40)$$

$$\frac{dV_{cpq}}{dt} = \frac{1}{C_{pf}}\left(i_{pfq} - i_{pq}\right) + \omega_0 \omega V_{cpd} \quad (3.41)$$

3.4 Wind System Modeling

Permanent magnet synchronous generator (PMSG) type wind system is considered in the microgrid system. The model consists of a two mass drive-train, a synchronous generator, full-scale converter and filter circuit as shown in Figure 3.8. The wind turbine connects to the rotor of the synchronous generator through a gearless drive train. The permanent magnets are mounted on the generator rotor, providing a fixed excitation to the generator. The 3-phase stator windings of the generator feed power to the full frequency converter which converts variable frequency of the wind generator to the constant grid frequency.

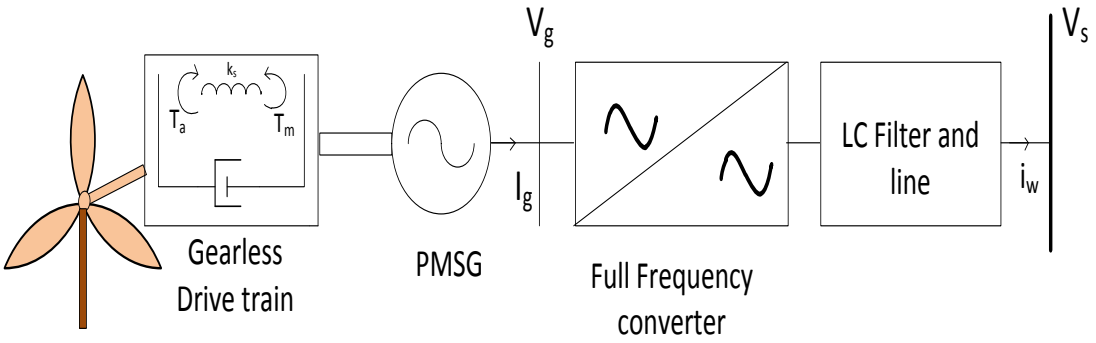

Figure 3.8 Wind energy conversion system model

3.4.1 Wind turbine model

The wind turbine extracts power from wind and converts it into mechanical power. The power output of the wind turbine depends on wind speed and rotor size. The mechanical power developed is proportional to the cubic power of wind speed hence a small increase in speed causes larger increase in the wind power. In addition, the power output of the turbine also increases with increase in blade area by allowing turbine to intercept more wind and energy capture. But the size of the blades in wind turbine has a limitation put by the economical and technical aspects. The amount of aerodynamic power produced by the wind turbine is given as follows

$$P_{mw} = \frac{1}{2} C_P(\beta, \lambda) S \rho V_V^3 \qquad (3.42)$$

where, ρ is the density of the air (kg/m^3), S is the area swept by the turbine (m^2), C_p is the power coefficient defining the aerodynamic efficiency of the wind turbine rotor, and is a function of the tip speed ratio λ and blade pitch angle β. The tip speed is defined as the ratio between the peripheral speed of the blades and the wind speed. The theoretical upper limit of C_p is 0.59 but in practical its value lies in range of 0.2-0.4. Power coefficient changes with the different values of β, but the wind turbine is most efficient for β=0.

A two mass model representation of the drive train is employed in this work. Higher inertia turbine rotor is connected to the lower inertia generator rotor through a flexible shaft having a stiffness of K_s. The high speed shaft is assumed to be stiff. No gear box is employed in this concept.

The electromechanical dynamics of the drive train in terms of the torsional angle θ_s and turbine speed ω_t are as follows

$$\frac{d\theta_s}{dt} = \omega_0(\omega_t - \omega_w) \quad (3.43)$$

$$\frac{d\omega_t}{dt} = \frac{1}{2H_t}(P_{mw} - K_s\theta_s) \quad (3.44)$$

where ω_w is the rotor speed and H_t is the inertia constant of the turbine.

3.4.2 PMSG Model

The equivalent circuit of a three phase permanent magnet synchronous generator considering sinusoidal flux distribution is as [70],

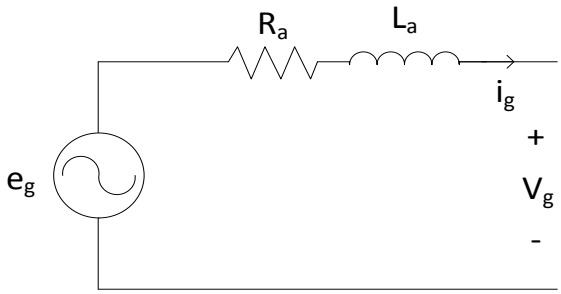

Figure 3.9 Equivalent circuit of PMSG

The voltage current relations of the stator circuit is,

$$e_g = L_a\frac{di_g}{dt} + R_a i_g + V_g \quad (3.45)$$

where, $R_a$and L_a armature resistance and inductance, V_g is the generator terminal voltage, e_g is the emf generated by the permanent magnet developed field. The above equation can be split in synchronously rotating d-q frame.

The emf generated by PMSG in d-q frame is written as

$e_g = e_{gd} + je_{gq}$

$e_{gd} = \omega_w x_{qw} i_{gq}$ (3.46)

$e_{gq} = -\omega_w x_{dw} i_{gd} + \omega E_{fdw}$ (3.47)

The equation (3.45) is represented as

$\frac{di_{gd}}{dt} = \frac{\omega_0}{x_{dw}}[-r_a i_{gd} + \omega_w x_{qw} i_{gq} - V_{gd}]$ (3.48)

$\frac{di_{gq}}{dt} = \frac{\omega_0}{x_{qw}}[-r_a i_{gq} - \omega_w x_{dw} i_{gd} + \omega E_{fdw} - V_{gq}]$ (3.49)

Here i_{gd} and i_{gq} are the d-q axes PMSG currents, $x_{dw}$and x_{qw} are the stator reactance in d-q axes, E_{fdw} is the field voltage along d-axis, ω_w is the generator rotor speed.

The above can be expressed in terms of the following 2 equivalent circuits in terms of d-q quantities.

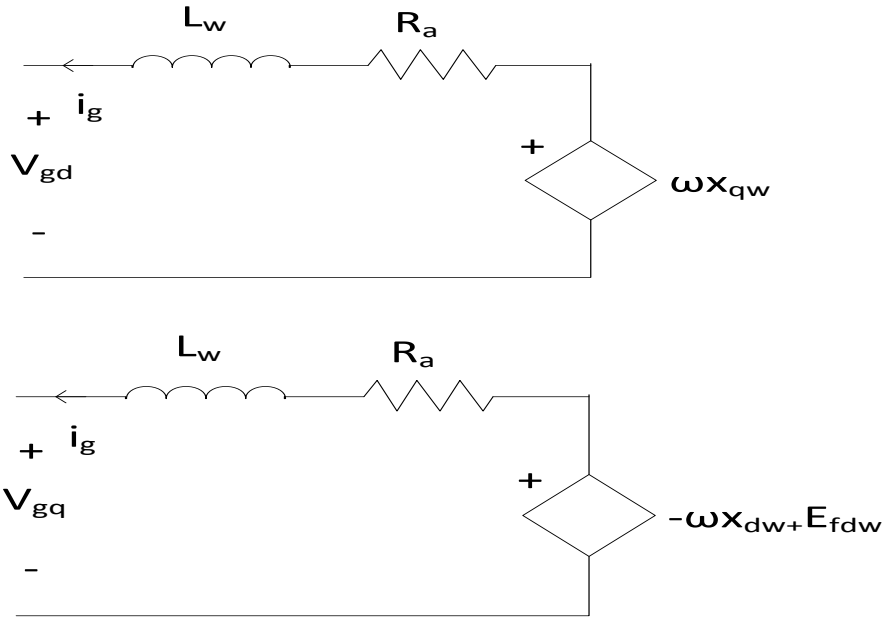

Figure 3.10 Equivalent circuit of PMSG in d-q axes.

The electromechanical torque generated by the machine is given as

$$T_{ew} = E_{fdw} * i_{gq} + \left(x_{qw} - x_{dw}\right) * i_{gd} * i_{gq} \quad (3.50)$$

The electrical power output of the generator is the product of torque and rotor speed, and is expressed as,

$$P_{ew} = \omega_w * T_{ew} \quad (3.51)$$

The electromechanical dynamics of the rotor can be expressed through the second order model,

$$\frac{d\delta_w}{dt} = \omega_0(\omega_w - 1) \quad (3.52)$$

$$\frac{d\omega_w}{dt} = \frac{1}{2H_g}(K_s\theta_s - P_{ew}) \quad (3.53)$$

where δ_w is the rotor angle of the PMSG and H_g is the generator inertia constant.

3.4.3 Full Converter Configuration

Full converter composed of a force commutated generator side converter and grid side converter connected with a common DC-link as shown in Figure 3.11. The advantage of such a system is that the DC-link capacitor decouples the two converters and hence a separate control on each converter can be employed. The generator side converter acts as rectifier which converts the generator's low frequency alternating current to direct current. The rectifier also acts on the pulse width modulated technique. The main advantage of using PWM is that it reduces the losses in the switching devices.

The DC link capacitor provides an intermediate energy storage, which isolates the generator side synchronous system and grid side synchronous system. The transfer of real power from the generator into the grid can be realized through this DC-link by keeping its voltage constant. The current in the DC-link is discontinuous as it is switched on or off

with respect to the switching frequency of the converter. This process induces voltage ripples in the DC-link capacitor which can be made small to the extent that the voltage appears virtually constant during switching period by selecting a large value of capacitor. On the other hand a small capacitor enables fast control of the DC-link voltage. Hence the selection of the size of the capacitor has to be a trade-off between the voltage ripples and fast changes in DC voltage.

The grid side converter acts as an inverter, which converts the DC power to fixed frequency AC power. The grid side converter also acts on the PWM technique. The magnitude of the inverter output voltage depends upon the modulation index m_W and DC link voltage.

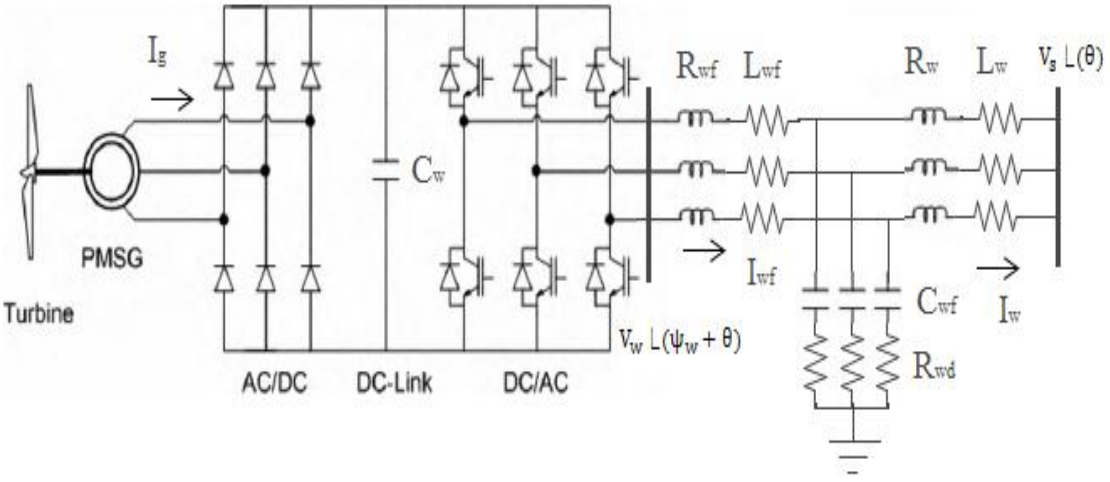

Figure 3.11 Full converter and filter configuration.

A. Generator side converter :

The terminal voltage of the synchronous generator can be expressed in terms of the modulation index of the rectifier, dc-link voltage and the rotor angle of the generator as.

$V_g = m_{wr} V_{dcw} \angle \delta_w$

In terms of d-q axes,

$V_{gd} = m_{wr} V_{dcw} \sin\delta_w$ (3.54)

$V_{gq} = m_{wr} V_{dcw} \cos\delta_w$ (3.55)

The power on the AC side of the converter is given as

$P_g = V_{gd} i_{gd} + V_{gq} i_{gq}$ (3.56)

B. Grid side converter:

The output voltage of the inverter in terms of the d-q axes is given as

$V_{wd} = m_{wi} V_{dcw} \cos(\psi_{wi} + \theta)$

$V_{wq} = m_{wi} V_{dcw} \sin(\psi_{wi} + \theta)$

Here, θ is the phase angle of the microgrid voltageV_s, V_{dcw} is the voltage across the dc-link, V_{wd} and V_{wq} are the d-q axes components of the inverter output voltage V_w.

The power on the AC side of the inverter is given as

$P_w = V_{wd} i_{wfd} + V_{wq} i_{wfq}$ (3.57)

i_{wfd} and i_{wfq} are the d- q axes component of the inverter output current i_{wf}.

C. DC-link capacitor:

Considering the DC link capacitor to be lossless, the dynamics of the DC-link voltage is given as,

$$C_w V_{dcw} \frac{dV_{dcw}}{dt} = P_g - P_w \quad (3.58)$$

Substituting the values of (3.56) and (3.57) into (3.58), the above gives

$$\frac{dV_{dcw}}{dt} = \frac{1}{C_w}[m_{wr} sin\delta_w i_{gd} + cos\delta_w i_{gq} - m_{wi}\cos(\psi_{wi} + \theta)\, i_{wd} - m_{wi}\sin(\psi_{wi} + \theta) i_{wq}] \quad (3.59)$$

D. LC Filter and the Coupling Inductance Model

For smoothing the output current, an LC filter is employed between the wind system and common bus. Referring to Figure 3.11, KVL and KCL on the left side of the filter section give the equations,

$$V_w = i_{wf} R_{wf} + L_{wf} \frac{di_{wf}}{dt} + V_{cw} + (i_{wf} - i_w) R_{wdr} \quad (3.60)$$

where, R_{wf} is the filter resistance, L_{wf} is the filter inductance, R_{wdr} is the damping resistance, V_{cw} is the filter capacitor voltage.

Breaking these in d-q axes and noting that the nonlinear model of the filter is obtained in a similar way as done for PV.

$$\frac{di_{wfd}}{dt} = \frac{-\omega_0 R_{wf}}{L_{pf}} i_{wfd} + \omega_0 \omega i_{wfq} + \frac{\omega_0 m_{wi} V_{dcw} \cos(\psi_{wi}+\theta)}{L_{wf}} - \frac{\omega_0 V_{0wd}}{L_{wf}} - \omega_0 R_{wdr} i_{wcd} \quad (3.61)$$

$$\frac{di_{wfq}}{dt} = \frac{-\omega_0 R_{wf}}{L_{wf}} i_{wq} - \omega_0 \omega i_{wfd} + \frac{\omega_0 m_{wi} V_{dcw} \sin(\psi_{wi}+\theta)}{L_{wf}} - \frac{\omega_0 V_{owq}}{L_{wf}} - \omega_0 R_{wdr} i_{wcd} \quad (3.62)$$

Similarly, equations from the right leg are,

$$V_{cw} = i_w R_w + L_w \frac{di_w}{dt} + V_s - (i_{wf} - i_w) R_{wdr} \quad (3.63)$$

In d-q terms the above is written as,

$$\frac{di_{wd}}{dt} = \frac{-\omega_0 R_w}{L_w} i_{wd} + \omega_0 \omega i_{wq} + \frac{\omega_0}{L_w} (V_{owd} - V_{sd}) + \omega_0 R_{wdr} i_{wcd} \quad (3.64)$$

$$\frac{di_{wq}}{dt} = \frac{-\omega_0 R_w}{L_w} i_{wq} - \omega_0 \omega i_{wd} + \frac{\omega_0}{L_w} \left(V_{owq} - V_{sq}\right) + \omega_0 R_{wdr} i_{wcd} \quad (3.65)$$

Where I_w is the coupling line current, R_w is the coupling resistance, L_w is the coupling inductance

The voltage across the filter capacitor is given as

$$C_{wf} \frac{dV_{cw}}{dt} = (i_{wf} - i_w) \quad (3.66)$$

Breaking in d-q axis gives,

$$\frac{dV_{cwd}}{dt} = \frac{1}{C_{wf}} \left(i_{wfd} - i_{wd}\right) + \omega_0 \omega V_{cwq} \quad (3.67)$$

$$\frac{dV_{cwq}}{dt} = \frac{1}{C_{wf}} \left(i_{wfq} - i_{wq}\right) + \omega_0 \omega V_{cwd} \quad (3.68)$$

where, C_{wf} is the wind filter capacitor

3.5 Controller Model

Since the microgrid system is composed of a number of distributed generators feeding various groups of loads, maintenance of system voltage requires coordinated generation of real and reactive power. A central control process is required for smooth steady operation as well for tackling emerging situations. This thesis considers a capacitor energy storage central controller which is interfaced through a STATCOM. The STATCOM can cater to reactive need of the system to a limited extent, while the capacitor energy storage can take care of transient power needs until a redistribution of DG power is implemented.

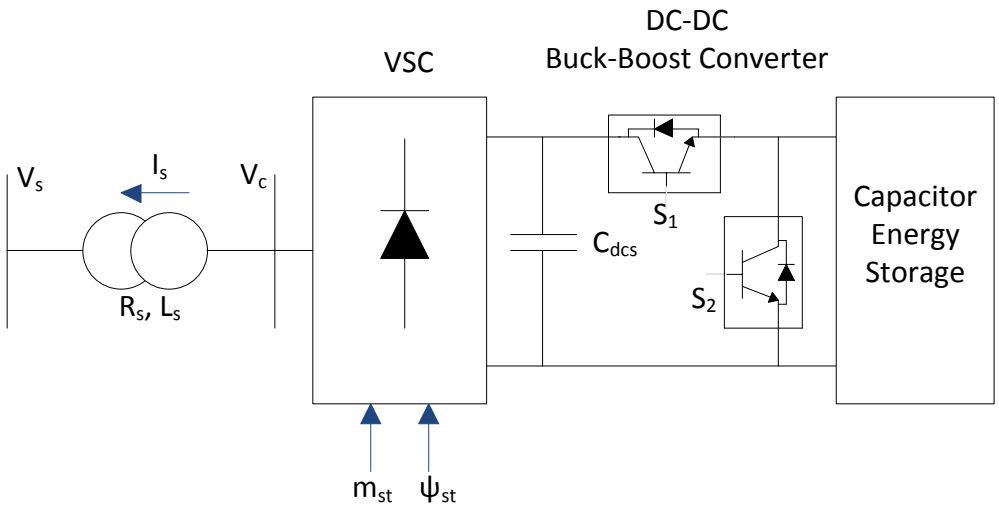

Figure 3.12 Controller Configuration

The central controller shown in Figure 3.12 consists of capacitor energy storage connected to the STATCOM through a bi-directional DC-DC buck boost converter. The operation of the buck-boost converter is controlled by varying the duty ratio through S_1 and S_2 to regulate the charge and discharge of the capacitor module. The STATCOM is modeled as a controllable voltage source which supplies the reactive power by varying

the modulation index (m_{st}) of the VSC. The storage capacitor caters for real power through the variation of the phase angle (ψ_{st})

Applying the KCL at the output node of the STATCOM one gets,

$$L_s \frac{di_s}{dt} + R_s i_s = V_c - V_s \quad (3.69)$$

Here, R_s and L_s are the resistance and inductance of the STATCOM, V_c and i_s are the STATCOM output voltage and output current.

The output voltage of the inverter in terms of the modulation index and phase angle of the converter is given as,

$$V_c = m_{st} V_{dcs} \angle(\psi_{st} + \theta) \quad (3.70)$$

Equation (3.70) can be rewritten in d-q axes as follows

$$V_{cd} = m_{st} V_{dcs} \cos(\psi_{st} + \theta) \quad (3.71)$$

$$V_{cq} = m_{st} V_{dcc} \sin(\psi_{st} + \theta) \quad (3.72)$$

Here, V_{cd} and V_{cq} are the d-q axes component of the inverter output voltage V_c

Writing (3.69) in d-q terms and substituting (3.71) and (3.72) gives,

$$\frac{di_{sd}}{dt} = \frac{-\omega_0 R_s}{L_s} i_{sd} + \omega_0 \omega i_{sq} + \frac{\omega_0 m_{st} V_{dcs} \cos(\psi_{st}+\theta)}{L_s} - \frac{\omega_0 V_{sd}}{L_s} \quad (3.73)$$

$$\frac{di_{sq}}{dt} = \frac{-\omega_0 R_s}{L_s} i_{sq} - \omega_0 \omega i_{sd} + \frac{\omega_0 m_{st} V_{dcs} \sin(\psi_{st}+\theta)}{L_s} - \frac{\omega_0 V_{sq}}{L_s} \quad (3.74)$$

Ignoring the detailed dynamics, storage capacitor current supplied is written approximately as

$$C_{dcs} \frac{dE_s}{dt} = i_{dcsc} \quad (3.75)$$

where i_{dcsc} is the current output from the storage capacitor, E_s is the storage capacitor voltage and C_{dcs} is the storage capacitor.

Applying KCL at the DC-link gives,

$$C_{dcs}\frac{dV_{dcs}}{dt} = -i_{dcs} + i_{dcsc} \quad (3.76)$$

where C_{dcs} is the STATCOM capacitor, V_{dcs} is the DC-link voltage of the STATCOM and i_{dcs} is the input current to the inverter and

For a lossless converter, in a steady state operation the instantaneous power on the DC side of the converter is equal to the instantaneous power on the AC side.

$$i_{dcs}V_{dcs} = V_{cd}i_{sd} + V_{cq}i_{sq} \quad (3.77)$$

Substituting (3.71) and (3.72) in (3.77) capacitor current i_{dcs} can be obtained as

$$i_{dcs} = i_{sd}m_{st}\cos(\psi_{st} + \theta) + i_{sq}m_{st}sin(\psi_{st} + \theta) \quad (3.78)$$

Substituting (3.78) in (3.76) we get the DC-link voltage as,

$$\frac{dV_{dcs}}{dt} = \frac{1}{C_{dcs}}\left[-\left(i_{sd}m_{st}cos\psi_{st} + i_{sq}m_{st}sin\psi_{st}\right) + i_{dcsc}\right] \quad (3.79)$$

3.6 Linearized model of the microgrid components

In this section the small signal model of the various components of the microgrid system is obtained by linearizing the non-linear equations developed in the previous section. Small signal analysis is used to determine the frequency response of the system for control design. The small signal model of the microgrid includes the linearized state space model of micro-alternator, photovoltaic system, wind system and that of the central controller. The linearized model is obtained by perturbing the set of equations around a normal operating point

3.6.1 Linearized model of microalternator

The linearized state equations of the microalternator is obtained from the non-linear model described in section 3.2 as follows

$$\Delta\dot{\delta} = \omega_0 \Delta\omega \qquad (3.80)$$

$$\Delta\dot{\omega} = \frac{1}{2H}[-\Delta P_e] \qquad (3.81)$$

$$\Delta\dot{e}'_q = \frac{1}{T'_{do}}\left[\Delta E_{fd} - \Delta e'_q - (x_d - x'_d)\Delta i_{td}\right] \qquad (3.82)$$

$$\Delta\dot{E}_{fd} = \frac{K_A}{T_A}\Delta V_t - \frac{1}{T_E}\Delta E_{fd} \qquad (3.83)$$

The generator output current is given as

$$\Delta i_t = \Delta i_{td} + j\Delta i_{tq} \qquad (3.84)$$

From (3.7) , the d-axis generator output current is given as,

$$i_{td} = \frac{-r_t V_{sd} + (e_q{}' - V_{sq})x_2}{r_t{}^2 + x_1 x_2}$$

Differentiating on both sides gives,

$$\Delta i_{td} = \frac{-r_t}{r_t{}^2 + x_1 x_2}\Delta V_{sd} + \frac{x_2}{r_t{}^2 + x_1 x_2}(\Delta e_q{}' - \Delta V_{sq}) \quad (3.85)$$

Similarly, from (3.8) , the q-axis output current is given as

$$i_{tq} = \frac{V_{sd}\left[\{x_d' + x_t\}\{x_q + x_t\}\right] + r_t(e_q{}' - V_{sq})\{x_q + x_t\}}{\{x_q + x_t\}\left[r_t^2 + \{x_d' + x_t\}\{x_q + x_t\}\right]}$$

Differentiating gives,

$$\Delta i_{tq} = \frac{\Delta V_{sd}}{x_1} + \frac{r_t}{x_d' + x_t}(\Delta e_q{}' - \Delta V_{sq}) \quad (3.86)$$

The terminal voltage is

$$V_t^2 = V_d^2 + V_q^2$$

$$\Delta V_t = \frac{V_{do}}{V_{to}}\Delta V_d + \frac{V_{qo}}{V_{to}}\Delta V_q$$

$$\Delta V_t = \frac{V_{do}}{V_{to}}\left(x_q \Delta i_{tq}\right) + \frac{V_{qo}}{V_{to}}\left(\Delta e_q' - x_d' \Delta i_{td}\right) \quad (3.87)$$

The power output of the generator from (3.10) is given as

$$P_e = \left(e_q{}' i_{tq}\right) + \left(x_q - x_d{}'\right) i_{td} i_{tq}$$

$$\Delta P_e = e_{qo}{}' \Delta i_{tq} + i_{tqo}\Delta e_q{}' + \left(x_q - x_d{}'\right)\left[i_{tdo}\Delta i_{tq} + i_{tqo}\Delta i_{td}\right]$$

$$\Delta P_e = e_{qo}{}' \Delta i_{tq} + i_{tqo}\Delta e_q{}' + \left(x_q - x_d{}'\right)\left[i_{tdo}\Delta i_{tq} + i_{tqo}\Delta i_{td}\right] \quad (3.88)$$

The values of Δi_{td}, ΔV_t and ΔP_e are substituted in the linearized model (3.80)-(3.83) to get obtain the model in terms of state variables and ΔV_{sd} and ΔV_{sq}.

3.6.2 Linearized Model of Photovoltaic System

Linearized model of the photovoltaic system consist of the small signal model of characteristic equation of the PV array and that of power conditioning unit.

From the equation (3.20) , the characteristic equation of the PV arrays as a function of PV output current is given as

$$V_{pv}=N_s\left[ln\left(\frac{N_pI_{ph}-i_{pv}}{N_pI_s}+1\right)nv_T-\frac{i_{pv}R_s}{N_p}\right]$$

Differentiating on both sides

$$\Delta V_{pv}=-N_s\left[\frac{nv_T}{N_pI_{ph}-i_{pvo}+N_pI_s}+\frac{R_s}{N_p}\right]\Delta i_{pv} \quad (3.89)$$

It can be written as

$$\Delta V_{pv}=K_{pv}\Delta i_{pv} \quad (3.90)$$

Where, $k_{pv}=-N_s\left[\frac{nv_T}{N_pI_{ph}-i_{pvo}+N_pI_s}+\frac{R_s}{N_p}\right]$

The small signal model of the power conditioning unit is obtained by linearizing its individual component which comprises of DC/DC converter, DC-link capacitor, LC output filter and coupling inductance. The corresponding non-linear state equation of the DC/DC converter is given in (3.15) along with the algebraic equation.

$$\Delta\dot{i}_{pv}=\frac{1}{L_{dc}}[\Delta V_{pv}-(1-d_c)\Delta V_{dcp}] \quad (3.91)$$

The non-linear equation for the DC link is the given in (3.24).

Differentiation (3.24) gives,

$$\Delta\dot{V}_{dcp}=\frac{-1}{C_{dcp}}[-i_{pfd0}m_p\sin(\psi_p+\theta)\Delta\psi_p+m_pcos(\psi_p+\theta)\Delta i_{pfd}+$$

$$i_{pfd0}\cos(\psi_p+\theta)\Delta m_p+i_{pfq0}m_p\cos(\psi_p+\theta)\Delta\psi_p+m_psin(\psi_p+\theta)\Delta i_{pfq}+$$

$$i_{pfq0}\sin(\psi_p+\theta)\Delta m_p-(1-d_c)\Delta i_{pv}] \quad (3.92)$$

The linearized state equations of the LC output filter and coupling inductance is obtained from the non-linear model given from (3.34) to (3.41) and are presented in APPENDIX A.

The linearized state variables are $\Delta\dot{\iota_{pfd}}$, $\Delta\dot{\iota_{pfq}}$, $\Delta\dot{\iota_{pd}}$,$\Delta\dot{\iota_{pq}}$, $\Delta\dot{V_{cpd}}$ and $\Delta\dot{V_{cpq}}$.

3.6.3 Linearized Model of Wind System

The small signal model of the wind system consist of linearized models of Wind turbine generator set, PMSG, DC link capacitor, LC output filter and coupling inductance.

Small Signal model of Wind turbine-generator set

The linearized model electromechanical dynamics of the drive train corresponding to the nonlinear model of (3.43)and (3.44), is given as follows

$$\Delta\dot{\theta}_s = \omega_o[\Delta\omega_t - \Delta\omega_w] \quad (3.93)$$

$$\Delta\dot{\omega}_t = \frac{1}{2H_t}[-K_s\Delta\theta_s] \quad (3.94)$$

Similarly the linearized model of PMSG swing equations corresponding to non-linear model given in (3.52) and (3.53) are shown below.

$$\Delta\dot{\delta}_w = \omega_o\Delta\omega_w \quad (3.95)$$

$$\Delta\dot{\omega}_w = \frac{1}{2H_g}[K_s\Delta\theta_s - \Delta P_{ew}] \quad (3.96)$$

Recall the output voltage of the PMSG given in (3.54)and (3.55)

$V_g = V_{gd} + jV_{gq}$

where $V_{gd} = m_c V_{dcw} sin\delta_w$ and $V_{gd} = m_c V_{dcw} sin\delta_w$

Differentiation of the above equations yield

$$\Delta V_{gd} = m_c V_{dcw} cos\delta_w \Delta\delta_w + m_c sin\delta_w \Delta V_{dcw} + V_{dcw} sin\delta_w \Delta m_c \quad (3.97)$$

$$\Delta V_{gq} = -m_c V_{dcw} sin\delta_w \Delta\delta_w + m_c cos\delta_w \Delta V_{dcw} + V_{dcw} cos\delta_w \Delta m_c \quad (3.98)$$

The electrical power generated by the PMSG is given as

$$P_{ew} = R_a\left(i_{gd}^2 + i_{gq}^2\right) + V_{gd} i_{gd} + V_{gq} i_{gq}$$

Differentiating on both sides

$$\Delta P_{ew} = 2R_a\left(i_{gdo}\Delta i_{gd} + i_{gqo}\Delta i_{gqo}\right) + V_{gdo}\Delta i_{gd} + i_{gdo}\Delta V_{gd} + V_{gqo}\Delta i_{gq} + i_{gqo}\Delta V_{gq}$$

Substituting the values of ΔV_{gd} and ΔV_{gq} in the above equation gives,

$$\Delta P_{ew} = 2R_a\left(i_{gdo}\Delta i_{gd} + i_{gqo}\Delta i_{gqo}\right) + V_{gdo}\Delta i_{gd} + i_{gdo}(m_c V_{dcw} cos\delta_w \Delta\delta_w$$

$$+ m_c sin\delta_w \Delta V_{dcw} + V_{dcw} sin\delta_w \Delta m_c) + V_{gqo}\Delta i_{gq} + i_{gqo}(-m_c V_{dcw} sin\delta_w \Delta\delta_w$$

$$+ m_c cos\delta_w \Delta V_{dcw} + V_{dcw} cos\delta_w \Delta m_c)$$

This can be rearranged as

$$\Delta P_{ew} = \left(V_{gdo} + 2R_a i_{gdo}\right)\Delta i_{gd} + \left(V_{gqo} + 2R_a i_{gqo}\right)\Delta i_{gq} + \Delta\delta_w(i_{gdo} m_c V_{dcw} cos\delta_w$$

$$- i_{gqo} m_c V_{dcw} sin\delta_w) + \Delta V_{dcw}(i_{gdo} m_c sin\delta_w + i_{gqo} m_c cos\delta_w) + \Delta m_c(i_{gdo} V_{dcw} sin\delta_w$$

$$+ i_{gqo} V_{dcw} cos\delta_w) \quad (3.99)$$

Hence the power output of the PMSG can be represented in terms of state variables as

$$\Delta P_{ew} = P_{ew1}\Delta i_{gd} + P_{ew2}\Delta i_{gq} + P_{ew3}\Delta\delta_w + P_{ew4}\Delta V_{dcw} + P_{ew5}\Delta m_c \quad (3.100)$$

Where $P_{ew1} = V_{gdo} + 2R_a i_{gdo}$ $\quad P_{ew2} = V_{gqo} + 2R_a i_{gqo}$

$$P_{ew3} = i_{gdo} m_c V_{dcw} cos\delta_w - i_{gqo} m_c V_{dcw} sin\delta_w$$

$$P_{ew4} = i_{gdo} m_c sin\delta_w + i_{gqo} m_c cos\delta_w \quad P_{ew5} = i_{gdo} V_{dcw} sin\delta_w + i_{gqo} V_{dcw} cos\delta_w$$

Small Signal model of PMSG armature currents:

The corresponding state equations are given in (3.48) and (3.49) along with the algebraic equations given in (3.54) and (3.55).

$$\Delta\dot{i}_{gd} = \frac{\omega_0}{x_{dw}}\left[-R_a\Delta i_{gd} + x_{qw}\Delta i_{gq} + x_{qw}i_{gq0}\Delta\omega - \Delta V_{gd}\right] \quad (3.101)$$

$$\Delta\dot{i}_{gq} = \frac{\omega_0}{x_{dw}}[-R_a\Delta i_{gq} - x_{dw}\Delta i_{gd} - x_{dw}i_{gd0}\Delta\omega + E_{fdo}\Delta\omega - \Delta V_{gq}] \quad (3.102)$$

From (3.54), $V_{gd} = m_c V_{dcw} sin\delta_w$

$$\Delta V_{gd} = m_c V_{dcwo} cos\delta_w \Delta\delta_w + m_c sin\delta_w \Delta V_{dcw} + V_{dcwo} sin\delta_w \Delta m_c \quad (3.103)$$

Similarly, from (3.55) $V_{gq} = m_c V_{dcw} cos\delta_w$

$$\Delta V_{gq} = -m_c V_{dcwo} sin\delta_w \Delta\delta_w + m_c cos\delta_w \Delta V_{dcw} + V_{dcwo} cos\delta_w \Delta m_c \quad (3.104)$$

Small Signal model of the power conditioning unit:

Recall the non-linear model of the DC-link voltage of the wind system from

(3.59),

$$\frac{dV_{dcw}}{dt} = \frac{1}{C_w}[m_{wr} sin\delta_w i_{gd} + cos\delta_w i_{gq} - m_{wi}\cos(\psi_{wi} + \theta)\, i_{wd} - m_{wi}\sin(\psi_{wi} + \theta) i_{wq}]$$

The linearized model of the above is given as,

$$\Delta\dot{V}_{dcw} = \frac{1}{C_w}[m_{wr} sin\delta_w \Delta i_{gd} + m_{wr} cos\delta_w \Delta i_{gq} + m_{wr}(i_{gdo} cos\delta_w - m_{wr} i_{gqo} sin\delta_w)\Delta\delta_w$$

$$+\left(sin\delta_w i_{gdo} + \cos\delta_w i_{gqo}\right)\Delta m_{wr} - m_{wi}\cos(\theta + \psi_{wi})\,\Delta i_{wd} - m_{wi}\sin(\theta + \psi_{wi})\,\Delta i_{wq}$$

$$-(i_{wdo}\cos(\theta + \psi_{wi}) + i_{wqo}\sin(\theta + \psi_{wi})\Delta m_{wi} + m_{wi}(i_{wdo}\sin(\theta + \psi_{wi})$$

$$-i_{wqo}\cos(\theta + \psi_{wi})\Delta\psi_{wi} \quad (3.105)$$

The linearized state equations of LC output filter and coupling inductance are obtained from the non-linear model given from (3.61) to (3.68) and are presented in APPENDIX A

The linearized state variables are $\Delta\dot{\imath_{wfd}}$, $\Delta\dot{\imath_{wfq}}$, $\Delta\dot{i_{wd}}$,$\Delta\dot{\imath_{wq}}$, $\Delta\dot{V_{cwd}}$ and $\Delta\dot{V_{cwq}}$.

3.6.4 Linearized model of the controller

The linearized state equations of the controller are obtained from the non-linear model given from (3.73) and (3.74).

$$\Delta\dot{i_{sd}} = \frac{-\omega_0 R_s}{L_s}\Delta i_{sd} + \omega_0\left(\Delta i_{sq} + i_{sq0}\Delta\omega\right) + \frac{\omega_0}{L_s}[m_{st}\cos(\psi_{st}+\theta)\Delta V_{dcso}$$

$$+V_{dcso}\cos(\psi_{st}+\theta)\,\Delta m_{st} - m_{st}V_{dcso}\sin(\psi_{st}+\theta)\,\Delta\psi_{st}] \quad - \frac{\omega_0\Delta V_{sd}}{L_s} \qquad (3.106)$$

$$\Delta\dot{i_{sd}} = \frac{-\omega_0 R_s}{L_s}\Delta i_{sq} - \omega_0(\Delta i_{sd} + i_{sd0}\Delta\omega) + \frac{\omega_0}{L_s}[m_{st}\sin(\psi_{st}+\theta)\,\Delta V_{dcso}$$

$$+V_{dcso}\sin(\psi_{st}+\theta)\,\Delta m_{st} + m_{st}V_{dcso}\cos(\psi_{st}+\theta)\,\Delta\psi_{st}] \quad - \frac{\omega_0\Delta V_{sq}}{L_s} \qquad (3.107)$$

The non-linear model of the DC-link voltage from (3.79) is given as,

$$\frac{dV_{dcs}}{dt} = \frac{1}{C_{dcs}}\left[-\left(i_{sd}m_{st}cos\psi_{st} + i_{sq}m_{st}sin\psi_{st}\right) + i_{dcsc}\right]$$

Differentiating the above gives,

$$\Delta\dot{V_{dcs}} = \frac{-1}{C_{dcs}}\left[-i_{sd0}m_s\sin(\psi_{st}+\theta)\Delta\psi_{st} + m_{st}cos(\psi_{st}+\theta)\Delta i_{sd} + i_{sd0}\cos(\psi_{st}+\right.$$

$$\left.\theta)\,\Delta m_{st} + i_{sq0}m_{st}\cos(\psi_{st}+\theta)\Delta\psi_{st} + m_{st}sin(\psi_{st}+\theta)\Delta i_{sq} + i_{sq0}\sin(\psi_{st}+\right.$$

$$\left.\theta)\,\Delta m_{st}\right] + \frac{1}{C_{dcs}}\Delta i_{dcsc}. \qquad (3.108)$$

CHAPTER 4

Microalternator-PV and Microalternator-Wind Non-autonomous Microgrids

In order to understand the interaction of the DG's on microgrid system two simpler configurations are considered in this chapter. The first one consists of microalternator and PV system and the second system consists of microalternator and wind system each connected to the power system grid. The load was considered to be integrated for both the systems. Both nonlinear and linearized integrated system models are developed. Non-linear simulations are carried out to verify the results obtained through small-signal analysis.

4.1 Microalternator and PV

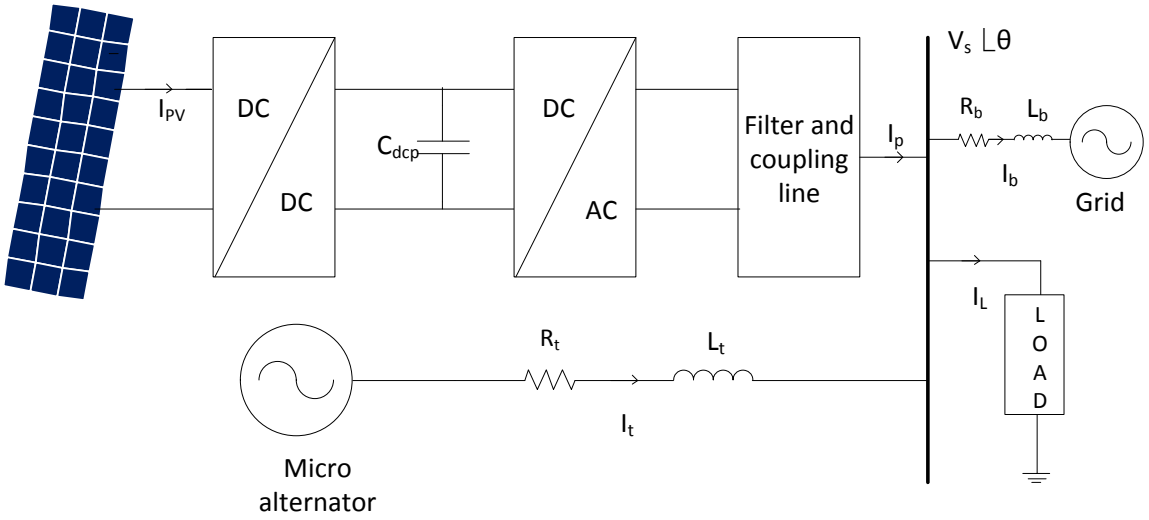

Figure 4.1 Microalternator and PV connected to grid.

Figure 4.1 shows a microgrid system containing a microalternator, a PV generator and an integrated load connected to the power grid, all connected to a common bus having voltageV_s. The dynamics of the microalternator and PV are given in sections 3.2 and 3.3, respectively. Note that the dynamic model of the component DG's contained the components of V_s along d-q axes (V_{sd}, V_{sq}). For getting a closed form representation of the composite state model, V_{sd} and V_{sq} have to be expressed in terms of chosen system states. This is done by applying KCL at the common bus V_s yielding

$$i_t + i_p = i_b + i_L$$

where i_t , i_p , i_b , i_L are the microalternator output current, PV output current, grid current and load current respectively.

Taking d-q components this gives the following equations,

$$i_{td} + i_{pd} = i_{bd} + i_{Ld} \quad (4.1)$$

$$i_{tq} + i_{pq} = i_{bq} + i_{Lq} \quad (4.2)$$

The next stage is to express the non-state current ($i_{td}, i_{tq}, i_{bd}, i_{bq}, i_{Ld,} i_{Lq}$) as a function of V_{sd} and V_{sq}.

Microalternator output current components i_{td} and i_{tq} have already expressed as a function of V_{sd} and V_{sq} and are given in (3.7) and(3.8) respectively.

Load Current:

The load at the microgrid is modeled as an admittance Y=g-jb

The load current is given as $I_L = V_s Y$

$$i_{ld} + j i_{lq} = (V_{sd} + j V_{sq})(g - jb)$$

Equating real and imaginary parts, we get

$$i_{ld} = gV_{sd} + bV_{sq} \quad (4.3)$$

$$i_{lq} = gV_{sq} - bV_{sd} \quad (4.4)$$

Grid Current:

From the Figure 4.1the main grid current i_b is given as

$$i_b = \frac{V_s - V_b}{r_b + jx_b}$$

$$i_{bd} + ji_{bq} = \frac{V_{sd} + jV_{sq} - (V_b sin\delta + jV_b cos\delta)}{r_b + jx_b}$$

Equating real and imaginary parts, we get

$$i_{bd} = \frac{(V_{sq} - V_b sin\delta)r_b + (V_{sq} - V_b cos\delta)x_b}{{r_b}^2 + {x_b}^2} \quad (4.5)$$

$$i_{bq} = \frac{(V_{sq} - V_b cos\delta)r_b + (V_{sq} - V_b sin\delta)x_b}{{r_b}^2 + {x_b}^2} \quad (4.6)$$

Finally substituting (i_{td}, i_{bd}, i_{Ld}) in (4.1) and solving for bus voltage components V_{sd} and V_{sq} as,

$$i_{pd} + i_{td} = i_{bd} + i_{Ld}$$

$$i_{pd} + \frac{-r_t V_{sd} + (e_q{}' - V_{sq})x_2}{z_1} = \frac{(V_{sq} - V_b sin\delta)r_b + (V_{sq} - V_b cos\delta)x_b}{z_b} + gV_{sd} + bV_{sq}$$

where $z_1 = {r_t}^2 + x_1 x_2$ and $z_2 = {r_b}^2 + {x_b}^2$

$$[gz_b z_1 + z_1 r_b + r_t z_b]V_{sd} + [bz_b z_1 + x_b z_1 + x_2 z_b]V_{sq} =$$

$$z_b z_1 i_{pd} + z_b e_q{}' x_2 + V_b cos\delta x_b z_1 + V_b sin\delta r_b z_1 \quad (4.7)$$

Substituting (3.8 **)** ,(4.4) and (4.6) in the above equation

$$i_{tq} + i_{pq} = i_{bq} + i_{Lq}$$

$$i_{pq} + \frac{V_{sd}z_1 - {r_t}^2 V_{sd} + r_t(e_q{}' - V_{sq})x_2}{x_2 z_1} = \frac{(V_{sq} - V_b cos\delta)r_b + (V_{sq} - V_b sin\delta)x_b}{z_b} \quad (4.8)$$

On simplifying the above we get,

$$-[x_b x_2 z_1 + b z_b x_2 z_1 + z_1 z_b - {r_t}^2 z_b]V_{sd} + x_2[\mathrm{g} z_b z_1 + z_1 r_b + r_t z_b]V_{sq}$$

$$= z_b z_1 x_2 i_{pq} + r_t z_b e_q{}' x_2 + V_b cos\delta r_b z_1 x_2 - sin\delta x_b x_2 z_1 \quad (4.9)$$

On solving equations (4.7) and (4.9) we get

$$V_{sq} = \mathrm{D}\, i_{pd} + E e_q{}' + \mathrm{F}\, i_{pq} + G V_b \quad (4.10)$$

$$V_{sd} = \frac{1}{A}[z_b z_1 i_{pd} + z_b x_2 e_q{}' + V_b z_1(r_b \sin\delta + x_b \cos\delta) - \mathrm{B} V_{sq}] \quad (4.11)$$

where A=$[\mathrm{g} z_b z_1 + z_1 r_b + r_t z_b]$ B= $[b z_b z_1 + x_b z_1 + x_2 z_b]$

C=$[x_b x_2 z_1 + b z_b x_2 z_1 + z_1 z_b - {r_t}^2 z_b]$ Den = $BC + A^2 x_2$

D= $\frac{1}{Den} C Z_b Z_1$ E= $\frac{1}{Den}(C Z_b x_2 + Z_b x_2 r_t A)$ F= $\frac{1}{Den}(A x_2 z_1 z_b)$

G=$\frac{1}{Den}[Z_1 C(r_b sin\delta + x_b cos\delta) + A x_2 z_1(r_b cos\delta - x_b sin\delta)]$ (4.12)

The values of V_{sd} and V_{sq} are substituted in the differential equations of the component models to get the closed form equation

$$\dot{X} = \mathrm{f}[\mathrm{X}, \mathrm{u}] \quad (4.13)$$

Where the state vector X is given as

$$X = [\delta, \omega, e'_q, E_{fd}, i_{pfd}, i_{pfq}, i_{pd}, i_{pq}, V_{cpd}, V_{cpq}, i_{pv,}\ V_{dcp}]$$

The control u is given as $U = [\, m_p, \psi_p]$

4.1.1 Linearized model of microalternator and PV:

Repeating the procedure for the linearized component system models, the small signal state model for the integrated microalternator, PV, load and the grid system is obtained by expressing the linearized microgrid voltage components along d-q axis ($\Delta V_{sd}, \Delta V_{sq}$) in terms of chosen states.

From (4.10) and (4.11), the microgrid voltage components are given as

$$V_{sq} = \mathrm{D}\, i_{pd} + E e_q{}' + \mathrm{F}\, i_{pq} + \left[\frac{1}{Den}[Z_1 C(r_b sin\delta + x_b cos\delta) + A x_2 z_1 (r_b cos\delta - x_b sin\delta)\right] V_b$$

$$V_{sd} = \frac{1}{A}[z_b z_1 i_{pd} + z_b x_2 e_q{}' + V_b z_1 (r_b \sin\delta + x_b \cos\delta) - \mathrm{B} V_{sq}]$$

On differentiating V_{sq} we get,

$$\Delta V_{sq} = \mathrm{D}\Delta\, i_{pd} + E\Delta e_q{}' + \mathrm{F}\Delta\, i_{pq} + V_b \left[\frac{1}{Den}[Z_1 C(r_b cos\delta_o - x_b sin\delta_o) - A x_2 z_1 (r_b sin\delta_o + x_b cos\delta_o)\right] \Delta\delta$$

$$\Delta V_{sq} = \mathrm{D}\Delta\, i_{pd} + E\Delta e_q{}' + \mathrm{F}\Delta\, i_{pq} + G_1 \Delta\delta \qquad (4.14)$$

where, $G_1 = V_b \left[\frac{1}{Den}[Z_1 C(r_b cos\delta_o - x_b sin\delta_o) - A x_2 z_1 (r_b sin\delta_o + x_b cos\delta_o)\right]$

Similarly on differentiating V_{sd} and substituting the value of ΔV_{sq} we get,

$$\Delta V_{sd} = \frac{1}{A}[z_b z_1 \Delta i_{pd} + z_b x_2 \Delta e_q{}' + V_b z_1 (r_b \cos\delta_0 - x_b \sin\delta_0)\Delta\delta - \mathrm{B}\left(\mathrm{D}\Delta\, i_{pd} + E\Delta e_q{}' + \mathrm{F}\Delta\, i_{pq} + G_1 \Delta\delta\right)]$$

$$\Delta V_{sd} = A_1 \Delta\, i_{pd} + B_1 \Delta\, i_{pq} + C_1 \Delta e_q{}' + D_1 \Delta\delta \qquad (4.15)$$

Where $A_1 = \left(\frac{Z_b Z_1}{A} - \frac{BD}{A}\right)$, $B_1 = \left(\frac{-BF}{A}\right)$, $C_1 = \left(\frac{Z_b x_2}{A} - \frac{BE}{A}\right)$

$$D_1 = \frac{z_1 V_b}{A}(r_b \cos\delta_0 - x_b \sin\delta_0) - \frac{B G_1}{A}$$

The values of ΔV_{sd} and ΔV_{sq} are substituted in the linearized differential equations of the component models to get the closed form equation

$$\left[\Delta \dot{X}_{GP}\right] = \left[A_{Gen-PV}\right]_{12x12}\left[\Delta X_{GP}\right] + \left[B_P\right]_{12x2}\left[\Delta U_P\right]$$

$$\text{where } \left[X_{GP}\right] = \left[\delta \quad \omega \quad e_q^{'} \quad E_{fd} \quad i_{pv} \quad V_{dcp} \quad i_{pfd} \quad i_{pfq} \quad i_{pd} \quad i_{pq} \quad V_{opd} \quad V_{opq}\right]^T \qquad (4.16)$$

$$A_{Gen-PV} = \begin{bmatrix} \left(A_{GG}\right)_{4x4} & \left(A_{GP}\right)_{4x8} \\ \left(A_{PG}\right)_{8x4} & \left(A_{PP}\right)_{8x8} \end{bmatrix}_{12x12} \qquad \left[\Delta U_P\right] = \left[\Delta m_p \quad \Delta \psi_p\right]$$

The sub matrix A_{GG} represents the system matrix of the microalternator and is given as,

$$A_{GG} = \begin{bmatrix} 0 & \omega_0 & 0 & 0 \\ -\frac{P_{e1}}{2H} & 0 & -\frac{P_{e3}}{2H} & 0 \\ \frac{-(\mathrm{x_d} - x_d^{'})i_{td1}}{T_{do}^{'}} & 0 & \frac{-(\mathrm{x_d} - x_d^{'})i_{td3}}{T_{do}^{'}} & \frac{1}{T_{do}^{'}} \\ \frac{K_A}{T_A}V_{t1} & 0 & \frac{K_A}{T_A}V_{t3} & \frac{-1}{T_A} \end{bmatrix}$$

The sub-matrix A_{PP} represents the system matrix of the PV system and is given as,

$$A_{PP} = \begin{bmatrix} \frac{K_{pv}}{L_{dc}} & \frac{(d_c - 1)}{L_{dc}} & 0 & 0 & 0 & 0 & 0 & 0 \\ \frac{(1-d_c)}{C_{dcp}} & 0 & m_p k_{pd1} & m_p k_{pd2} & 0 & 0 & 0 & 0 \\ k_{pf1} & 0 & -k_{pf} R_{eq} & \omega_o & k_{pf} R_d & 0 & -k_{pf} & 0 \\ 0 & 0 & -\omega_o & -k_{pf} R_{eq} & 0 & k_{pf} R_d & 0 & -k_{pf} \\ 0 & 0 & k_p R_d & 0 & -k_p (R_{eq1} + A_1) & -\omega_o - k_p B_1 & k_p & 0 \\ 0 & 0 & 0 & k_p R_d & -\omega_o - k_p D & -k_p (R_{eq1} + F) & 0 & k_p \\ 0 & 0 & \frac{\omega_0}{C_{pf}} & 0 & \frac{-\omega_0}{C_{pf}} & 0 & 0 & \omega_0 \\ 0 & 0 & 0 & \frac{\omega_0}{C_{pf}} & 0 & \frac{-\omega_0}{C_{pf}} & -\omega_0 & 0 \end{bmatrix}_{8x8}$$

The constants in the above matrices are given as

$$k_{pv} = -N_s\left[\frac{nv_T}{N_p I_{ph} - i_{pvo} + N_p I_s} + \frac{R_s}{N_p}\right] \qquad k_{pd1} = \frac{-1}{C_{dcp}}\cos(\psi_p)\, k_{pd2} = \frac{-1}{C_{dcp}}\sin(\psi_p)$$

$$k_{pf} = \frac{\omega_o}{L_{pf}} \qquad k_p = \frac{\omega_o}{L_p} \qquad R_{eq} = R_{pf} + R_{pdr} \qquad R_{eq1} = R_p + R_{pdr}$$

The other sub matrices are given as

$$A_{GP} = \begin{bmatrix} 0 & 0 & 0 & 0 & 0 & 0 & 0 & 0 \\ 0 & 0 & P_{e1} & P_{e2} & 0 & 0 & 0 & 0 \\ 0 & 0 & e_{q1} & e_{q2} & 0 & 0 & 0 & 0 \\ 0 & 0 & 0 & 0 & 0 & 0 & 0 & 0 \end{bmatrix}_{4x8} \qquad A_{PG} = \begin{bmatrix} 0 & \omega_o i_{pfq0} & 0 & 0 \\ 0 & \omega_o i_{pfd0} & 0 & 0 \\ -k_p D_1 & \omega_o i_{pq0} & -k_p C_1 & 0 \\ -k_p G & -\omega_o i_{pq0} & -k_p C_1 & 0 \\ 0 & \omega_o V_{cpq0} & 0 & 0 \\ 0 & -\omega_o V_{cpq0} & 0 & 0 \\ 0 & 0 & 0 & 0 \\ 0 & 0 & 0 & 0 \end{bmatrix}_{8x4}$$

4.1.2 Simulation results

The impact of the variation of microalternator and PV generation as well as the change of load pattern on the small signal stability of the test system given in Figure 4.1 was investigated through eigenvalue analysis. For nominal loading of microalternator=0.3pu, PV=0.7pu and load=1pu the eigenvalues of the subsystem are given in Table 4.1. The nominal bus voltage is considered to be 0.95pu.

Table 4.1 Eigenvalues of the microgrid containing microalternator and PV

DG unit	***Real***	***Imaginary***
PV	-298.776	±3097.842i
	-263.320	±2201.235i
	-183.262	±523.825i
	-98.860	
	-1.560	
Microalternator	-0.0489	±14.863i
	-0.4938	±1.714i

Figure 4.2 shows the variation of the real part of dominant eigenvalues of microalternator as the PV output changes in the range for 0.1-1.4pu for different values of the microalternator output. In all the cases the power absorbed by the load was kept constant at real power of 1p.u and reactive power of 0.15p.u. It can be observed that the stability of the system worsens as the participation of the microalternator is reduced. On the contrary, greater PV integration degrades the microgrid stability. For example if the PV output is 80% the system will enter into unstable mode if the microalternator generation is less than 10%.

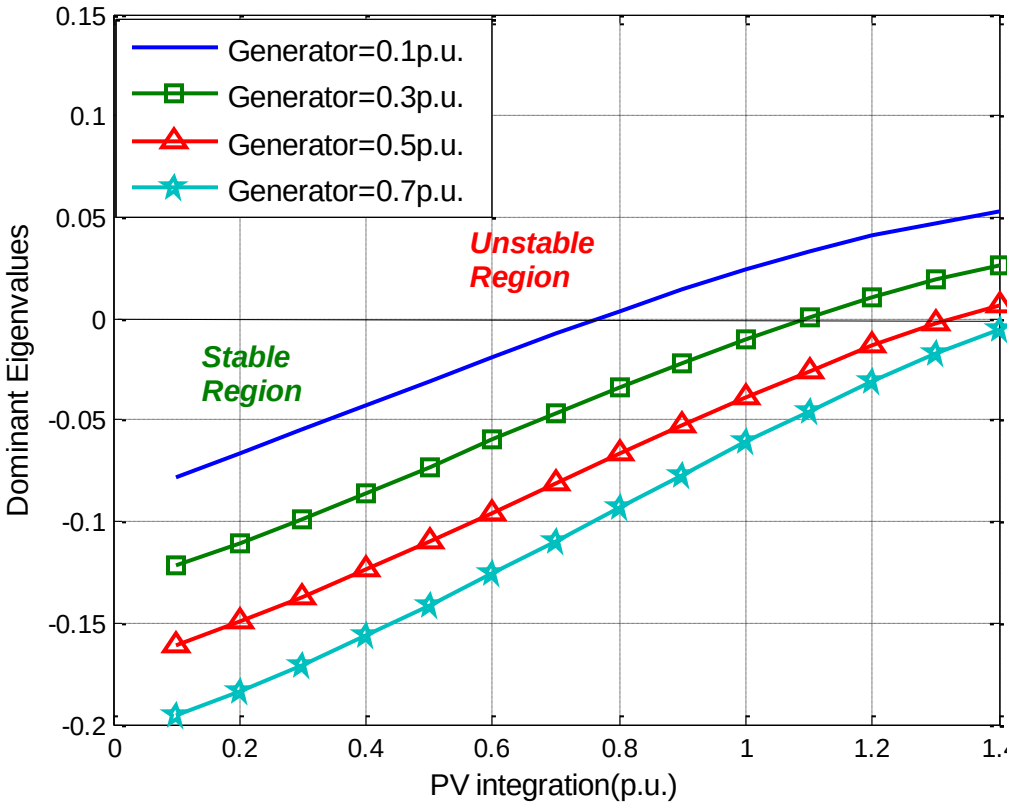

Figure 4.2 Dominant eigenvalues of microalternator for various PV and micro-alternator mixes, load is 1pu.

Figure 4.3 shows the effect of load changes at a constant microalternator and PV generation of 0.2p.u. It can be observed that the stability of the system worsens as the reactive power load at the microgrid increases. Increase in reactive power demand decreases the microgrid voltage and leads towards the voltage instability. It is also observed that increase in real power demand for fixed reactive load enhances the microgrid stability because it improves the load power factor and thus the voltage profile of the microgrid.

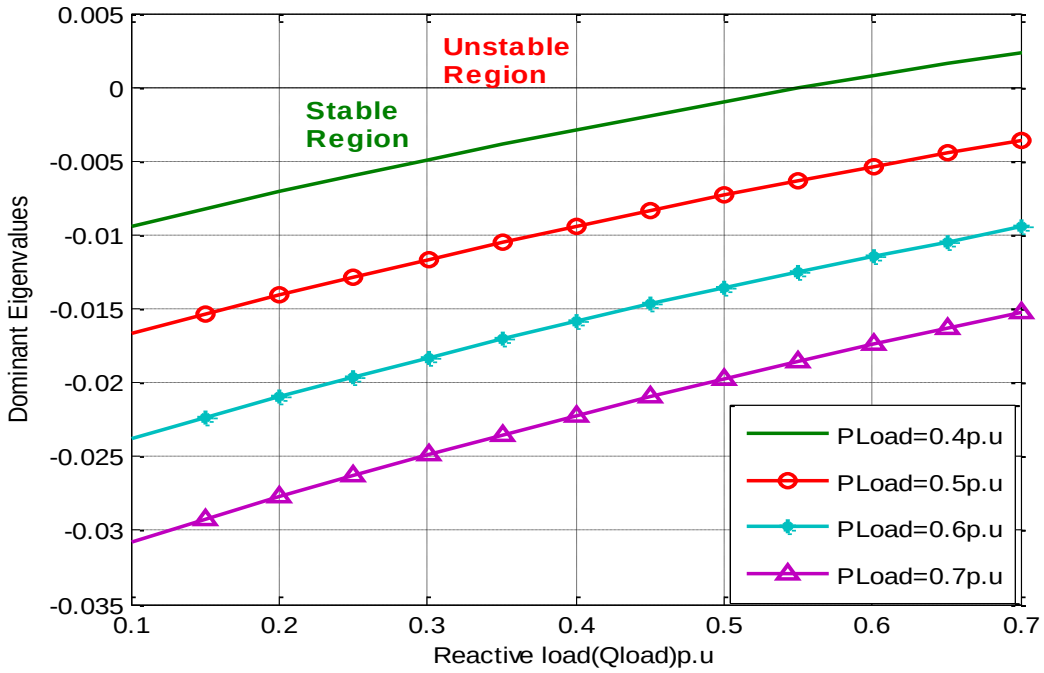

Figure 4.3 Dominant eigenvalues of microalternator for various real and reactive load variations, PV and microalternator generations are at 0.2pu.

Results obtained through a small signal analysis were verified by nonlinear system simulations. Figure 4.4 and Figure 4.5 show the variation of microalternator speed and converter DC-link voltage of PV respectively, following a 0.1pu input torque pulse for 0.3sec for two scenarios: (a) microalternator output 0.1pu, (b) microalternator output 0.5pu. The PV power and load are kept constant at 0.8pu and 1pu respectively. The results show that case ‘a’ renders the system unstable and it is stable for case ‘b’.

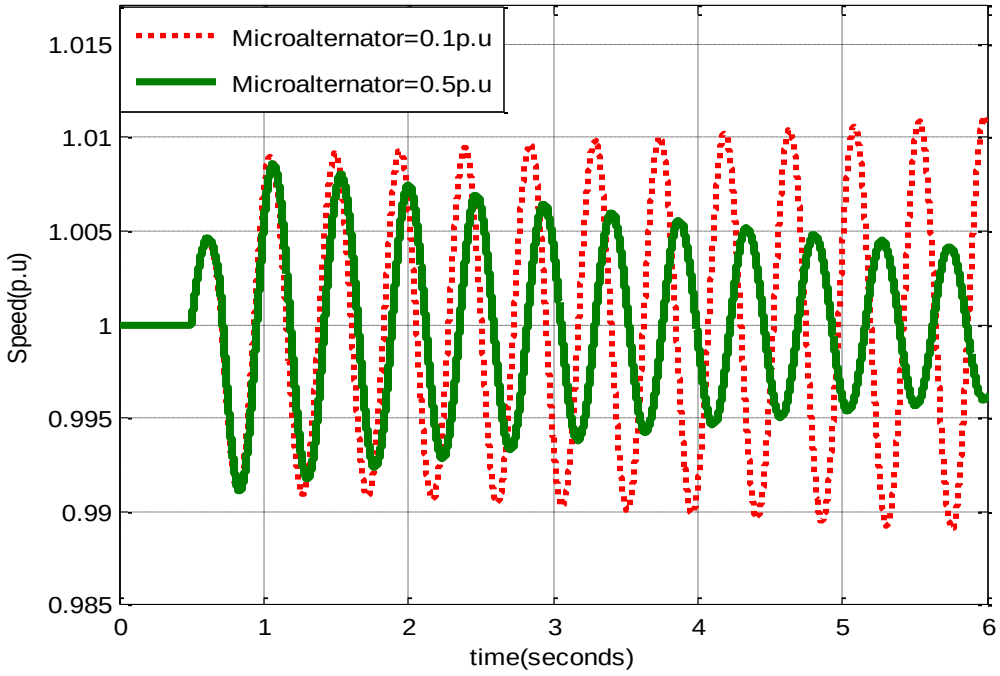

Figure 4.4 Speed variations of microalternator following a 10% input torque pulse for 0.3sec.

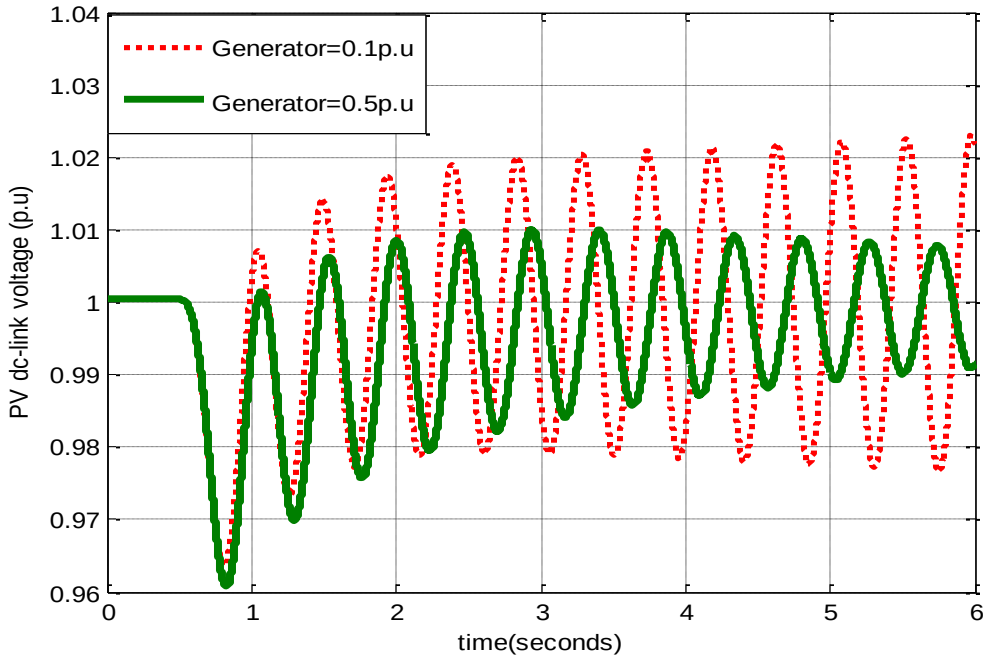

Figure 4.5 DC-link voltage variation following a 10% input torque pulse for 0.3sec

4.2 Microgrid with microalternator and wind generation

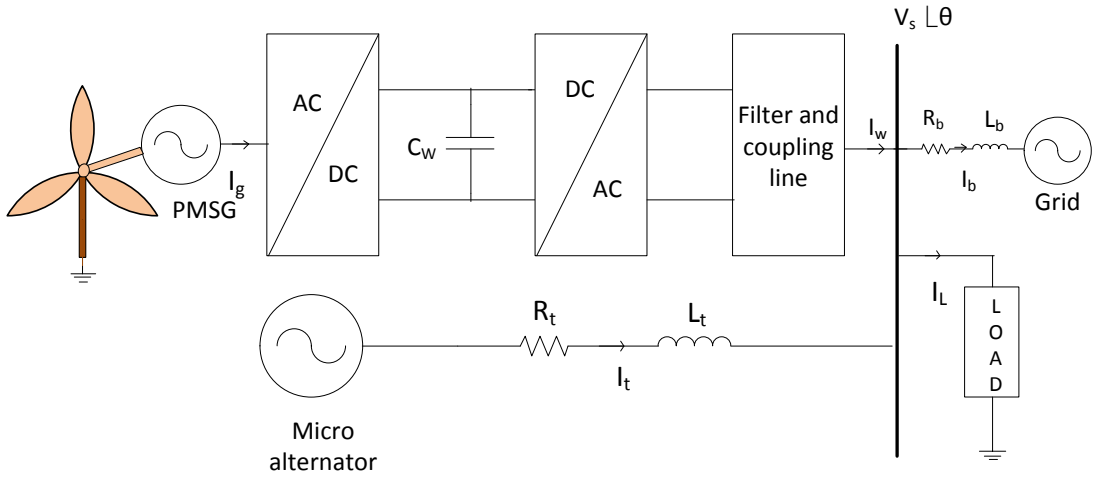

Figure 4.6 Microalternator and wind system connected to the grid.

Figure 4.6 shows the single line diagram of a non-autonomous microgrid consisting of microalternator and wind generation systems connected to the main grid with an integrated load at the common bus.

4.2.1 The dynamic model:

The composite model of the system given in Figure 4.6 is obtained by employing KCL at the common bus,

Microalternator output current + Wind output current = Load current +Grid current

$$i_t + i_w = i_b + i_L \qquad (4.17)$$

In d-q frame this will be

$$i_{td} + i_{wd} = i_{bd} + i_{Ld} \qquad (4.18)$$

$$i_{tq} + i_{wq} = i_{bq} + i_{Lq} \qquad (4.19)$$

The quantities i_{td}, i_{tq} and i_{wd}, i_{wq} are obtained from the individual models of microalternator and wind system respectively.

On simplification, we obtain the microgrid voltage components similar to (4.10) and (4.11) except that instead of PV current, we have the wind currents.

$$V_{sq} = \mathrm{D}\, i_{wd} + Ee_q{}' + \mathrm{F}\, i_{wq} + GV_b \quad (4.20)$$

$$V_{sd} = \frac{1}{A}[z_b z_1 i_{wd} + z_b x_2 e_q{}' + V_b z_1 (r_b \sin\delta + x_b \cos\delta) - \mathrm{B} V_{sq}] \quad (4.21)$$

The values of V_{sd} and V_{sq} are substituted in the differential equations of the component models to get the closed form equation

$$\dot{X} = \mathrm{f}[\mathrm{X}, \mathrm{u}] \quad (4.22)$$

Where the state vector X is given as

$$X = [\delta, \omega, e'_q, E_{fd}, i_{gd}, i_{gq}, \delta_w, \omega_w, \theta_s, \omega_t, V_{dcw}, i_{wfd}, i_{wfq}, i_{wd}, i_{wq}, V_{cwd}, V_{cwq}\ ]$$

The control u is given as $U = [\, m_w, \psi_w]$

4.2.2 Linearized model:

Proceeding in the same way as microalternator and PV, the linearized model for the system given in Figure 4.6 is,

$$\left[\Delta \dot{X}_{GW}\right] = \left[A_{Gen-Wind}\right]_{17x17}\left[\Delta X_{GW}\right] + \left[B_W\right]_{17x2}\left[\Delta U_w\right]$$

$$\text{where } \left[X_{Gw}\right] = \left[\delta \quad \omega \quad e'_q \quad E_{fd} \quad i_{gd} \quad i_{gq} \quad \theta_s \quad \omega_t \quad \delta_w \quad \omega_g \quad V_{dcw} \quad i_{wfd} \quad i_{wfq} \quad i_{wd} \quad i_{wq} \quad V_{owd} \quad V_{owq}\right]^T \quad (4.23)$$

$$A_{Gen-Wind} = \begin{bmatrix} (A_{GG})_{4x4} & (A_{Gw})_{4x13} \\ (A_{wG})_{13x4} & (A_{WW})_{13x13} \end{bmatrix}_{17x17} \quad (4.24)$$

$$\left[\Delta U_w\right] = \left[\Delta m_{wr} \quad \Delta m_{wi} \quad \Delta \psi_{wi}\right] \quad (4.25)$$

The sub-matrices are given as

$$A_{ww}=\begin{bmatrix}
-R_a k_{gd} & x_{qw}k_{gd} & k_{gd1} & k_{gd2} & 0 & 0 & k_{gd3} & 0 & 0 & 0 & 0 & 0 & 0\\
-x_{dw}k_{gq} & -R_a k_{gq} & k_{gq1} & k_{gq2} & 0 & 0 & k_{gq3} & 0 & 0 & 0 & 0 & 0 & 0\\
0 & 0 & 0 & \omega_0 & 0 & 0 & 0 & 0 & 0 & 0 & 0 & 0 & 0\\
P_{ew1} & P_{ew2} & P_{ew3} & 0 & \frac{K_s}{2H_g} & 0 & P_{ew4} & 0 & 0 & 0 & 0 & 0 & 0\\
0 & 0 & 0 & -\omega_0 & 0 & \omega_0 & 0 & 0 & 0 & 0 & 0 & 0 & 0\\
0 & 0 & 0 & 0 & \frac{K_s}{2H_t} & 0 & 0 & 0 & 0 & 0 & 0 & 0 & 0\\
k_{dcw1} & k_{dcw2} & k_{dcw3} & 0 & 0 & 0 & 0 & k_{dcw4} & k_{dcw5} & 0 & 0 & 0 & 0\\
0 & 0 & 0 & 0 & 0 & 0 & k_{wf1} & k_{wf}(R_{wf}+R_d) & \omega_0 & k_{wf}R_d & 0 & -k_{wf} & 0\\
0 & 0 & 0 & 0 & 0 & 0 & k_{wf2} & -\omega_0 & k_{wf}(R_{wf}+R_d) & 0 & k_{wf}R_d & 0 & -k_{wf}\\
0 & 0 & 0 & 0 & 0 & 0 & 0 & k_wR_d & 0 & k_w(R_w+R_d+A_1) & \omega_o-k_wB_1 & k_w & 0\\
0 & 0 & 0 & 0 & 0 & 0 & 0 & 0 & k_wR_d & -\omega_o-k_wD & k_w(R_w+R_d+F) & 0 & k_w\\
0 & 0 & 0 & 0 & 0 & 0 & 0 & \frac{\omega_o}{C_{wf}} & 0 & -\frac{\omega_o}{C_{wf}} & 0 & 0 & \omega_0\\
0 & 0 & 0 & 0 & 0 & 0 & 0 & 0 & \frac{\omega_o}{C_{wf}} & 0 & -\frac{\omega_o}{C_{wf}} & -\omega_0 & 0
\end{bmatrix}_{13x13}$$

$$A_{GW}=\begin{bmatrix}(0)_{4x9} & (a_{Gw})_{4x2} & (0)_{4x2}\end{bmatrix}_{4x13} \quad \text{where} \quad a_{Gw}=\begin{bmatrix}0 & P_{e1} & e_{q1} & V_{t1}\\ 0 & P_{e2} & e_{q2} & V_{t2}\end{bmatrix}^T_{4x2}$$

$$A_{WG}=\begin{bmatrix}
(0)_{7x1} & (0)_{7x1} & (0)_{7x1} & (0)_{7x1}\\
0 & \omega_0 i_{wfqo} & 0 & 0\\
0 & -\omega_0 i_{wfq0} & 0 & 0\\
-k_wD_1 & \omega_0 i_{wqo} & -k_wC_1 & 0\\
k_wG & \omega_0 i_{wdo} & -k_wE & 0\\
0 & \omega_0 V_{cwqo} & 0 & 0\\
0 & \omega_0 i_{wfqo} & 0 & 0
\end{bmatrix}_{13x4}$$

The constants used in the above matrices are presented in APPENDIX B.

4.2.3 Simulation results

The eigenvalues of the microalternator and wind microgrid shown in Figure 4.6 for 0.3pu microalternator and 0.7pu wind participation is shown in Table 4.2. The load was considered to be 1p.u.

Table 4.2 Eigenvalues of the microgrid containing microalternator and PV

DG unit	***Real***	***Imaginary***
Wind	-298.775	±3097.848i
	-263.318	±2201.246i
	-183.234	±523.901i
	-4.673	±377.746i
	-98.860	
	-0.00452	±4.102i
	-0.00454	14.864i
	-0.348	±34.132i
Microalternator	-0.066	±14.865i
	-1.489	±0.3372i

Figure 4.7 shows the real part of the dominant eigenvalues of microalternator for various amount of wind participation at a fixed load of real power 1pu and reactive power 0.15pu consumption. It can be observed that as the power from microalternator increases, the microgrid gets more stable. The system stability worsens as the PMSG power output increases reaching the stability margin at around 1.1pu.

Figure 4.8 shows the effect of variation of real and reactive power load on microgrid for constant microalternator and wind generation of 0.2p.u. The real power is varied from 0.4 to 0.7p.u and the reactive power is varied from 0.1 to 0.7p.u. It can be observed that the stability of the system worsens as the reactive power load at the microgrid increases. It is also observed that increase in real power demand at constant reactive power load enhances the microgrid stability.

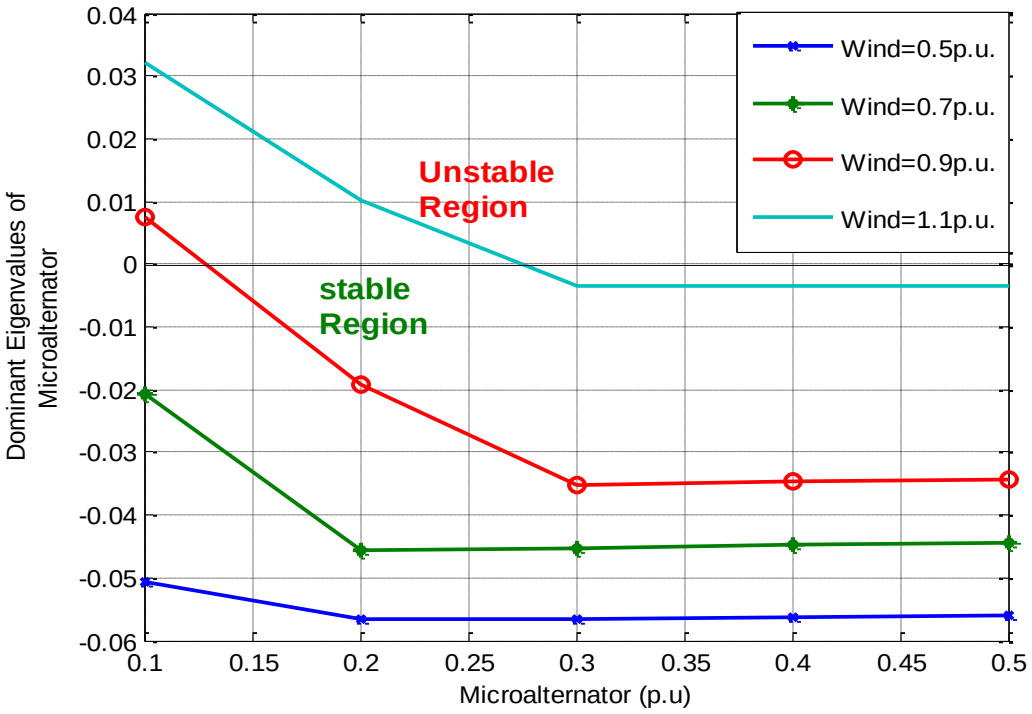

Figure 4.7 Dominant eigenvalues of microalternator for various wind participation, load is 1pu

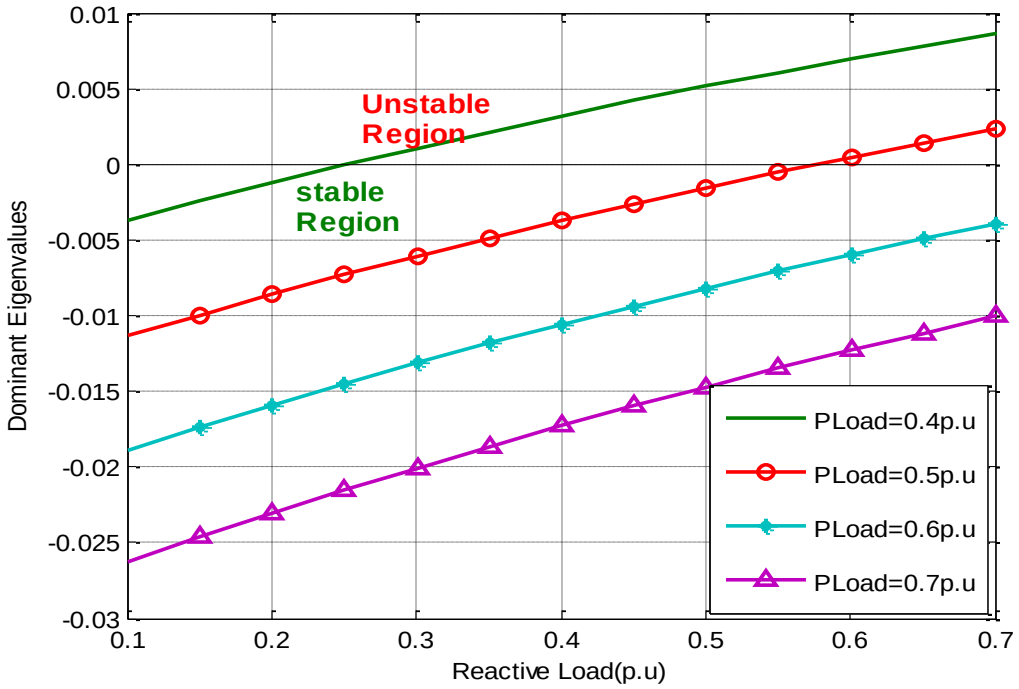

Figure 4.8 Dominant eigenvalues of microalternator for varying real and reactive power demand, microalternator and wind power are at 0.2p.u.

Figure 4.9 and Figure 4.10 show the variation of wind speed and converter DC-link voltage respectively following a 0.1pu input torque pulse for 0.3sec for two scenarios (a) wind system delivers 1.1p.u; (b) wind system delivers 0.9p.u. The microalternator power and load were maintained constant at 0.2pu and1pu for both cases. Fig-8 shows that case ‘a’ is unstable and case ‘a’ gives rise to damped oscillations as was also shown through linear analysis. Nonlinear simulations carried out for these cases verify the validity of the results obtained in Figure 4.7 through small signal analysis.

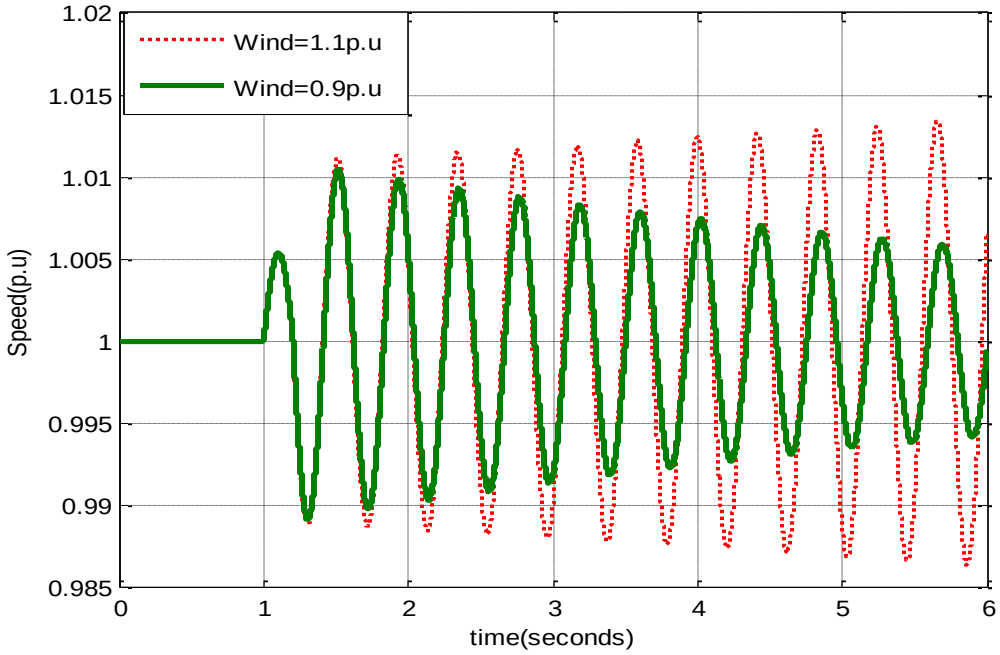

Figure 4.9 Speed variations of microalternator following a 10% input torque pulse for 0.3sec

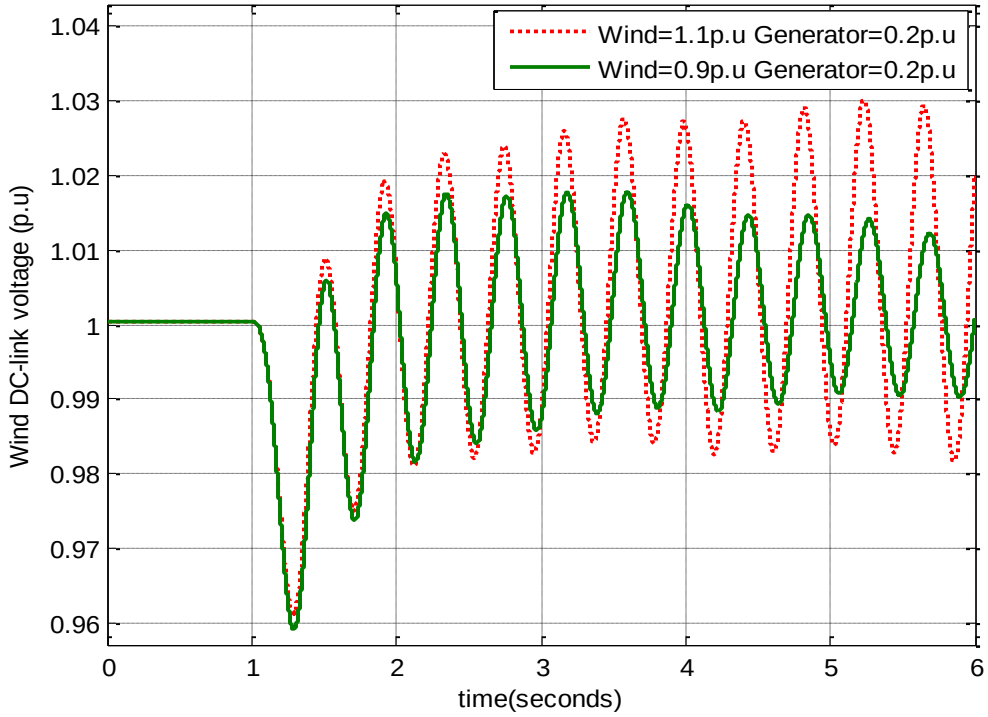

Figure 4.10 DC-link voltage variations following a 10% input torque pulse for 0.3sec

CHAPTER 5

A Microgrid with PV, Wind and Conventional Microalternator Generations

In this chapter a microgrid model including PV, wind in addition to microalternator generation is considered. Small signal analysis is carried out to find a suitable generation mix from the various distributed generation unit for reliable and satisfactorily steady operation of microgrid. Non-linear time domain simulations are made to verify the results obtained from the linear analysis.

5.1 System model

Figure 5.1 shows the single line diagram of the microgrid system considered. The PV and wind system are connected through voltage source converters and LC output filter. An integrated load connected at the common bus. None of the DG units acts as a spinning reserve for back-up generation. This is in contrast to interconnected power systems. Hence a central controller is included which can meet real and reactive power needs for transient period. A capacitor energy storage system interfaced through a STATCOM is considered in this study.

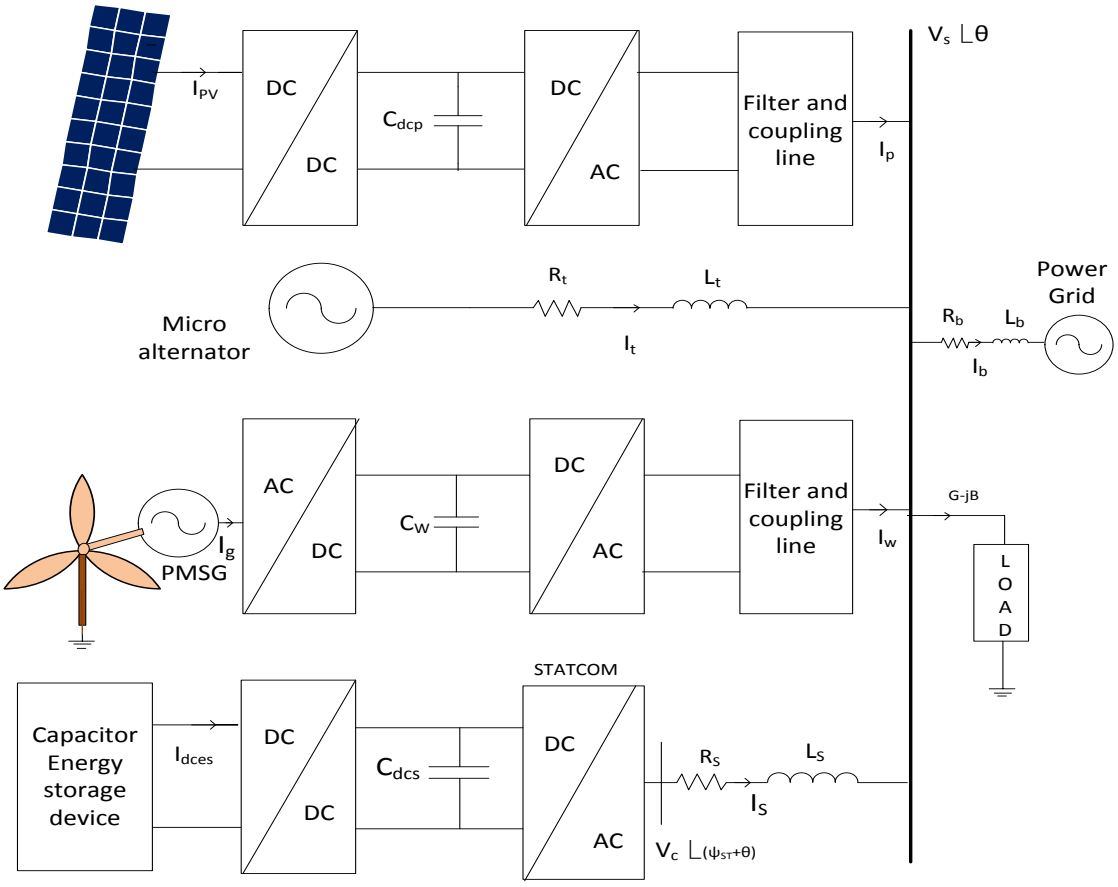

Figure 5.1 Complete microgrid

A composite state space model of the system shown in Figure 5.1 is obtained by equating the incoming and outgoing currents at the microgrid.

Microalternator current + PV current +Wind current +Statcom current=

Load current +Grid current

$$i_t + i_p + i_w + i_s = i_b + i_L \qquad (5.1)$$

Writing in d-q axes,

$$i_{td} + i_{pd} + i_{wd} + i_{sd} = i_{bd} + i_{Ld} \qquad (5.2)$$

$$i_{tq} + i_{pq} + i_{wq} + i_{sq} = i_{bq} + i_{Lq} \qquad (5.3)$$

Substituting (i_{td}, i_{bd}, and i_{Ld}) from (3.7),(4.5) and (4.3) respectively in (5.2),

$$\frac{-r_t V_{sd}+(e_q{}'-V_{sq})x_2}{z_1} + i_{pd} + i_{wd} + i_{sd} = \frac{(V_{sq}-V_b sin\delta)r_b+(V_{sq}-V_b cos\delta)x_b}{z_b} + gV_{sd} + bV_{sq} \quad (5.4)$$

Similarly, substituting (i_{tq}, i_{bq}, and i_{Lq}) from(3.8) ,(4.6) and (4.4) respectively in (5.3) we get,

$$i_{pq} + +i_{wq} + i_{sq} + \frac{V_{sd}z_1 - r_t{}^2 V_{sd} + r_t(e_q{}' - V_{sq})x_2}{x_2 z_1} = \frac{(V_{sq}-V_b cos\delta)r_b+(V_{sq}-V_b sin\delta)x_b}{z_b} \quad (5.5)$$

Solving (5.4) and (5.5) we get bus voltage components V_{sd} and V_{sq} as,

$$V_{sq} = \mathrm{D}\,(i_{pd} + i_{wd} + i_{sd}) + Ee_q{}' + \mathrm{F}\,(i_{pq} + i_{wq} + i_{sq}) + GV_b \quad (5.6)$$

$$V_{sd} = \frac{1}{A}[z_b z_1(i_{pd} + i_{wd} + i_{sd}) + z_b x_2 e_q{}' + V_b z_1(r_b \sin\delta + x_b \cos\delta) - \mathrm{B}V_{sq}] \quad (5.7)$$

The constants in the above are same as in (4.12).

Finally, substituting V_{sd} and V_{sq} in the individual component models, the nonlinear system equations are written as

$$\dot{x} = f(x,u) \quad (5.8)$$

Where the state vector x is given as $x = [x_{Gen}, x_{Controller}\, x_{PV}, x_{Wind},]$

where $x_{Gen} = [\,\delta, \omega, e'_q, E_{fd}]$

$x_{Controller} = [i_{sd}, i_{sq}, V_{dcs}\,]$

$x_{PV} = [i_{pfd}, i_{pfq}, i_{pd}, i_{pq}, V_{cpd}, V_{cpq}, i_{pv,}\ V_{dcp}]$

$x_{wind} = [\theta_s, \omega_t, i_{gd}, i_{gq}, \delta_w, \omega_w, i_{wfd}, i_{wfq}, i_{wd}, i_{wq}, V_{cwd}, V_{cwq}]$

The control u is given as $u = [u_{Controller}, u_{PV}, u_{Wind}]$

where, $u_{Controller} = [m_{st}, \psi_{st}]$, $u_{PV} = [m_p, \psi_p]$, $u_{Wind} = [m_{wr}, m_{wi}, \psi_{wi}]$

5.2 Linearized Model

The linearized model of the microgrid system shown in Figure 5.1 is obtained by expressing the linearized voltage components ΔV_{sd} and ΔV_{sq} in terms of system states and substituting in individual linearized component models.

From (5.6) and (5.7) the microgrid voltage components are rewritten as,

$$V_{sq} = \mathrm{D}\,(i_{pd} + i_{wd} + i_{sd}) + Ee_q' + \mathrm{F}\,(i_{pq} + i_{wq} + i_{sq}) + \left[\frac{1}{Den}[Z_1 C(r_b sin\delta + x_b cos\delta) + Ax_2 z_1(r_b cos\delta - x_b sin\delta)\right] V_b$$

$$V_{sd} = \frac{1}{A}[z_b z_1(i_{pd} + i_{wd} + i_{sd}) + z_b x_2 e_q' + V_b z_1(r_b \sin\delta + x_b \cos\delta) - \mathrm{B}V_{sq}]$$

On differentiating V_{sq} we get,

$$\Delta V_{sq} = \mathrm{D}(\Delta i_{pd} + \Delta i_{wd} + \Delta i_{sd}) + E\Delta e_q' + \mathrm{F}(\Delta i_{pq} + \Delta i_{wq} + \Delta i_{sq}) + V_b\left[\frac{1}{Den}[Z_1 C(r_b cos\delta_o - x_b sin\delta_o) - Ax_2 z_1(r_b sin\delta_o + x_b cos\delta_o)\right]\Delta\delta$$

$$\Delta V_{sq} = \mathrm{D}(\Delta i_{pd} + \Delta i_{wd} + \Delta i_{sd}) + E\Delta e_q' + \mathrm{F}(\Delta i_{pq} + \Delta i_{wq} + \Delta i_{sq}) + G_1\Delta\delta \qquad (5.9)$$

Similarly on differentiating V_{sd} and substituting the value of ΔV_{sq} we get,

$$\Delta V_{sd} = \frac{1}{A}[z_b z_1(\Delta i_{pd} + \Delta i_{wd} + \Delta i_{sd}) + z_b x_2 \Delta e_q' + V_b z_1(r_b \cos\delta_0 - x_b \sin\delta_0)\Delta\delta - \mathrm{B}\big(\mathrm{D}\{\Delta i_{pd} + \Delta i_{wd} + \Delta i_{sd}\} + E\Delta e_q' + \mathrm{F}(\Delta i_{pq} + \Delta i_{wq} + \Delta i_{sq}) + G_1\Delta\delta\big)]$$

$$\Delta V_{sd} = A_1\big(\Delta i_{pd} + \Delta i_{wd} + \Delta i_{sd}\big) + B_1(\Delta i_{pq} + \Delta i_{wq} + \Delta i_{sq}) + C_1\Delta e_q' + D_1\Delta\delta \qquad (5.10)$$

The constants are same as in section 4.1.

The values of ΔV_{sd} and ΔV_{sq} are substituted in the linearized differential equations of the component models to get the closed form equation

$$\left[\Delta \dot{X}_{overall}\right] = \left[A_{overall}\right]\left[\Delta X\right] + \left[B\right]\left[\Delta U\right]$$

where $\left[X\right] = [\delta \quad \omega \quad e_q^{'} \quad E_{fd} \quad i_{sd} \quad i_{sq} \quad V_{dcs} \quad i_{pv} \quad V_{dcp} \quad i_{pfd} \quad i_{pfq} \quad i_{pd} \quad i_{pq} \quad V_{opd}$

$V_{opq} \quad i_{gd} \quad i_{gq} \quad \theta_s \quad \omega_t \quad \delta_g \quad \omega_g \quad V_{dcw} \quad i_{wfd} \quad i_{wfq} \quad i_{wd} \quad i_{wq} \quad V_{cwd} \quad V_{cwq}]$ (5.11)

$$A_{overall} = \begin{bmatrix} (A_{GG})_{4x4} & (0)_{4x3} & (A_{GP})_{4x8} & (A_{GW})_{4x13} \\ (0)_{3x4} & (A_{SS})_{3x3} & (A_{SP})_{3x8} & (A_{SW})_{3x13} \\ (A_{PG})_{8x4} & (A_{PS})_{8x3} & (A_{PP})_{8x8} & (A_{PW})_{8x13} \\ (A_{WG})_{13x4} & (A_{WS})_{13x3} & (A_{WP})_{13x8} & (A_{WW})_{13x13} \end{bmatrix}_{28x28}$$

The sub matrices in $A_{overall}$ and control matrix B are given in Appendix B

5.3 Small signal analysis

The microgrid system shown in Figure 5.1 was simulated for small signal as well as nonlinear analysis. The initial loading of the DGs were PV=0.4pu, wind=0.4pu, microalternator=0.2pu with a load of 1pu operating at a steady state grid bus voltage of 0.965pu.The eigenvalues of the different DG units and the controllers are grouped and presented in Table 5.1.

Table 5.1 shows the eigenvalues of the complete microgrid model

DG unit	***Real part***	***Imaginary Part***
wind	-405.398	±3175.949i
	-235.555	±3030.692i
	-268.943	±2145.052i
	-4.648	±377.75i
	-0.349	±34.132i
	-0.063	±4.102i
	-1.166	
Microalternator	-0.043	±10.132i
	-0.582	±1.796i
	-235.551	±2276.736i
PV	-404.743	±873.714i
	-94.057	±378.210i
	-2.016	±0.483i
STATCOM	-62.987	±234.241i
	-99.166	

The eigenvalues identified as critical in terms of their location from jω axis are given in **Table 5.2.**

Table 5.2 Critical Modes

Eigenvalue values	**Component**	**Modes**
-0.063±4.102i	Wind turbine	Electromechanical modes
-0.349±34.132i	PMSG	Electromechanical modes
-0.043±10.132i	Micro alternator	Electromechanical modes

Figure 5.2 shows the variation of the real part of the dominant eigenvalue of the microalternator when the alternator power output is varied from 0.1pu to 0.5pu and wind power contribution is changed in steps of 0.1pu, 0.4pu, 0.7pu and 1.1p.u, respectively. PV power and load are kept constant at 0.2pu and (1+j0.15pu), respectively. It can be seen that as the wind power increases, the microgrid moves towards unstable regime. Also increased microalternator participation enhances the stability domain.

Figure 5.3 shows the real part of dominant eigenvalues of microalternator when the reactive power load is varied between 0.1pu and 0.7pu. The real power load was considered to be between 0.2pu and 0.8pu; the PV, wind and microalternator output each remaining constant at 0.2pu. It can be observed that for given PV, wind and microalternator output, the stability margin of the microgrid decreases as the reactive power demand increases. The microgrid becomes unstable if the real power demand goes below 0.2 pu.

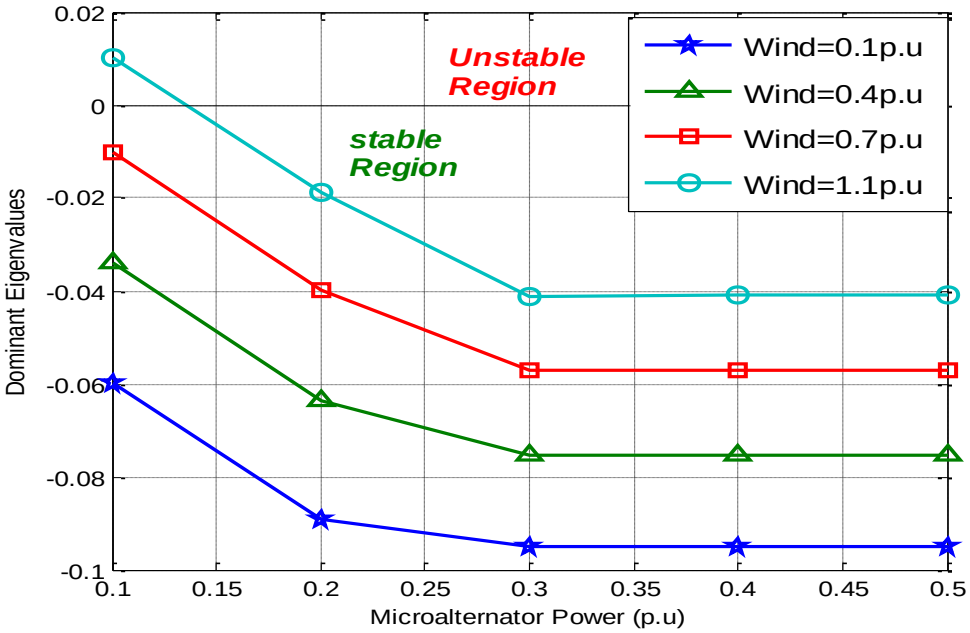

Figure 5.2 Dominant eigenvalues of microalternator for various wind generations, PV generation is 0.2p.u. , load is 1p.u

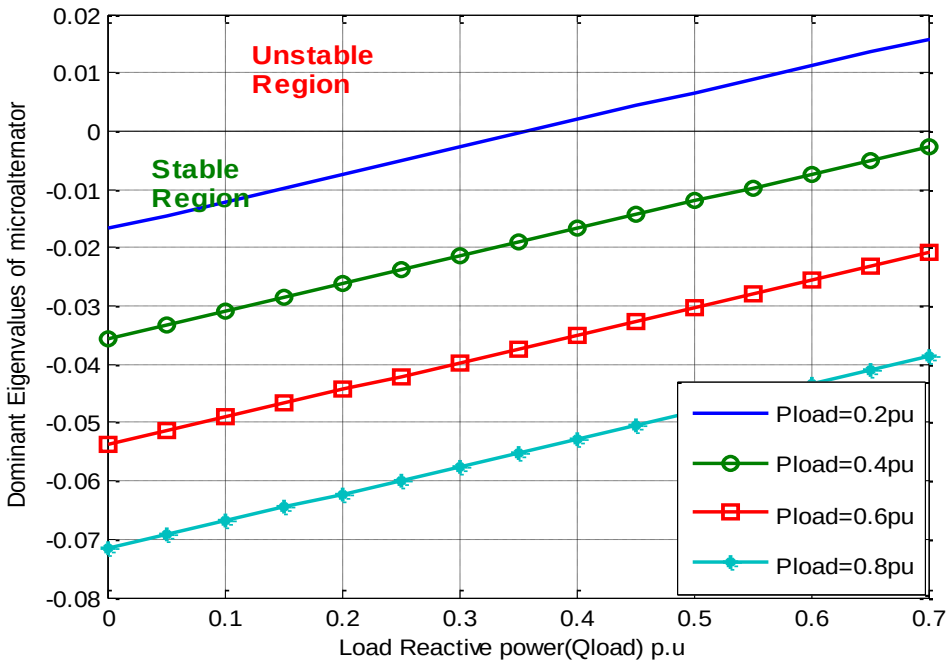

Figure 5.3 Dominant eigenvalues of microalternator, PV, wind and microalternator generation are each at 0.2p.u.

Figure 5.4 shows the real part of dominant eigenvalues of PV system as the PV power is changed against wind participation. In this case, microalternator power is kept constant at 0.2pu and the load power is 1pu(active load power). Again, it can be seen that greater wind and PV participations reduces the stability margin of the microgrid.

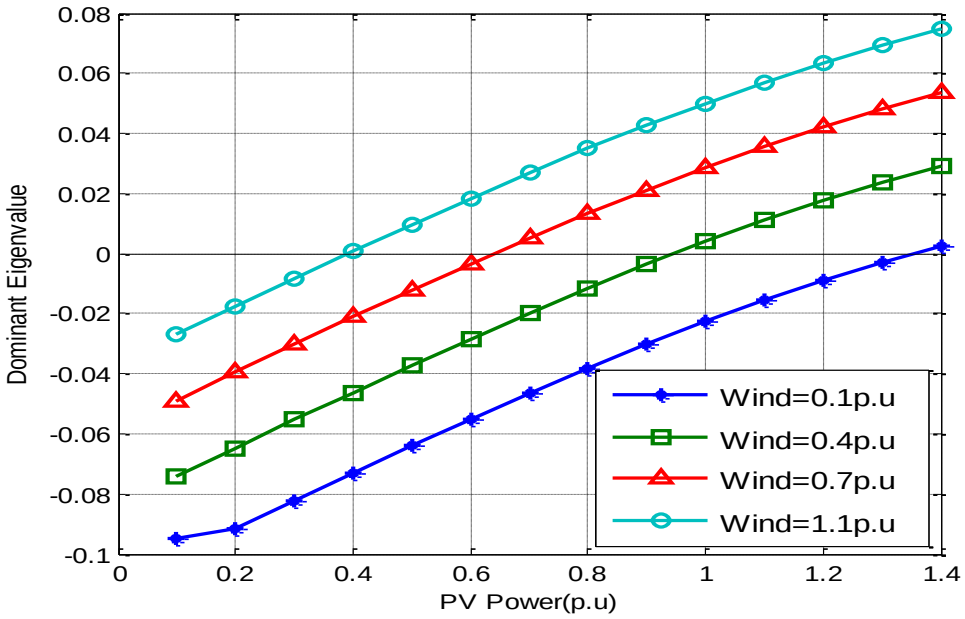

Figure 5.4 Dominant eigenvalues of PV for various wind generations, microalternator output is 0.2p.u. , load is 1p.u.

Figure 5.5-5.10 show the non-linear time domain response of the micro-alternator speed, microgrid voltage, PV DC-link voltage, Wind DC-link voltage, STATCOM DC-link voltage and STATCOM current following a 0.1pu input torque pulse of 0.3 sec when the microgrid system shown in Figure 5.1 is simulated. The study was carried out for two cases (a) wind 0.7pu and (b) wind 0.1pu. Microalternator power, PV power and load are kept constant at 0.2pu, 1pu and 1pu in both cases. For the first operating condition, microgrid is unstable. In case 2, wind power is decreased to 0.1pu hence the microgrid

shows the stable performance. It is observed that the nonlinear simulations verify the results through small signal analysis shown in Figure 5.4.

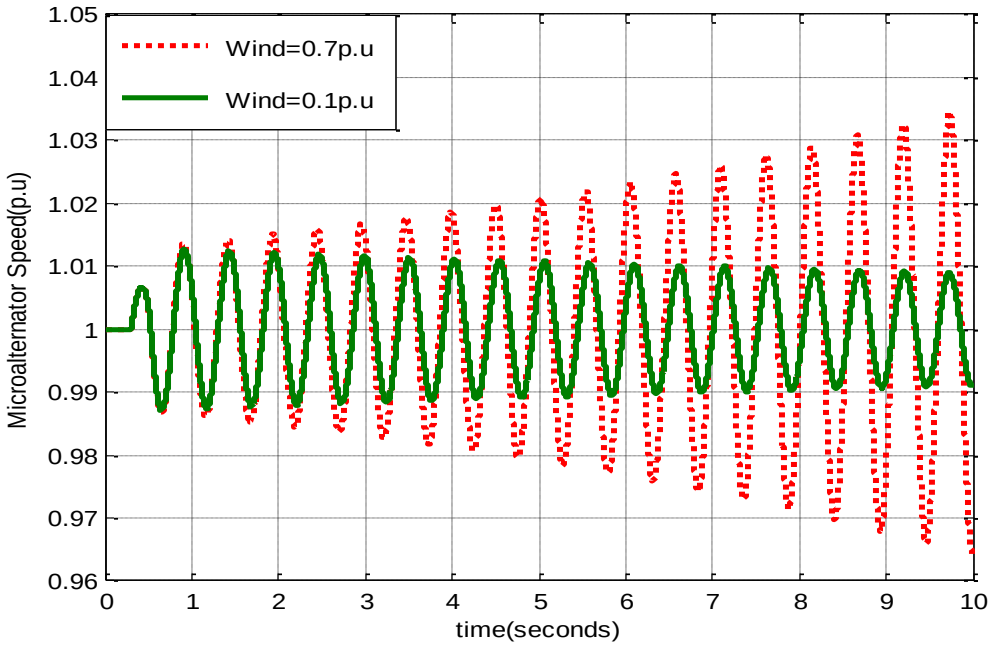

Figure 5.5 Speed variations of microalternator in complete microgrid following a 10% input torque pulse for 0.3sec.

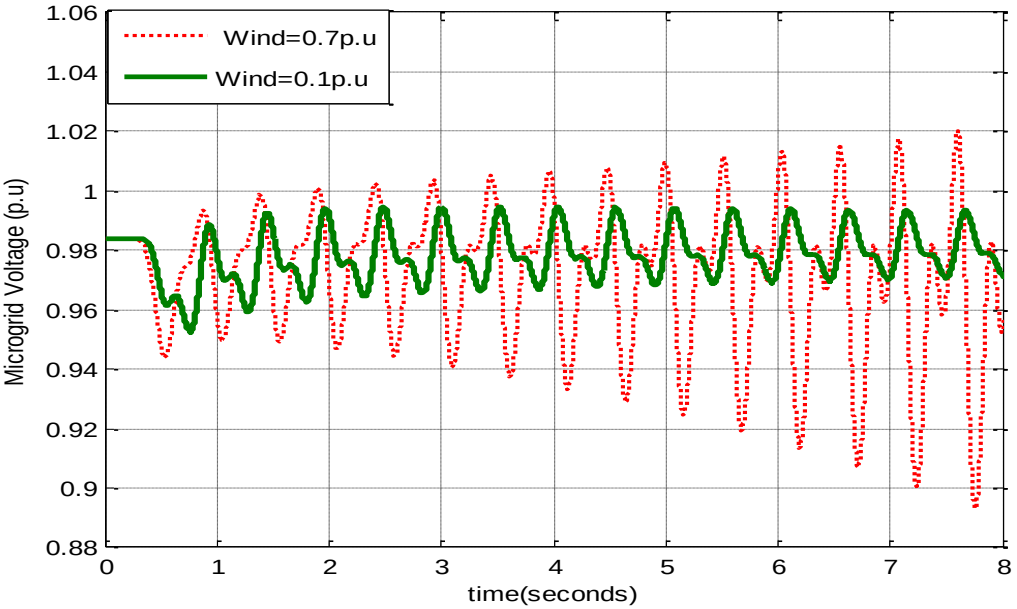

Figure 5.6 Variation in microgrid voltage following a 10% input torque pulse in microalternator for 0.3sec.

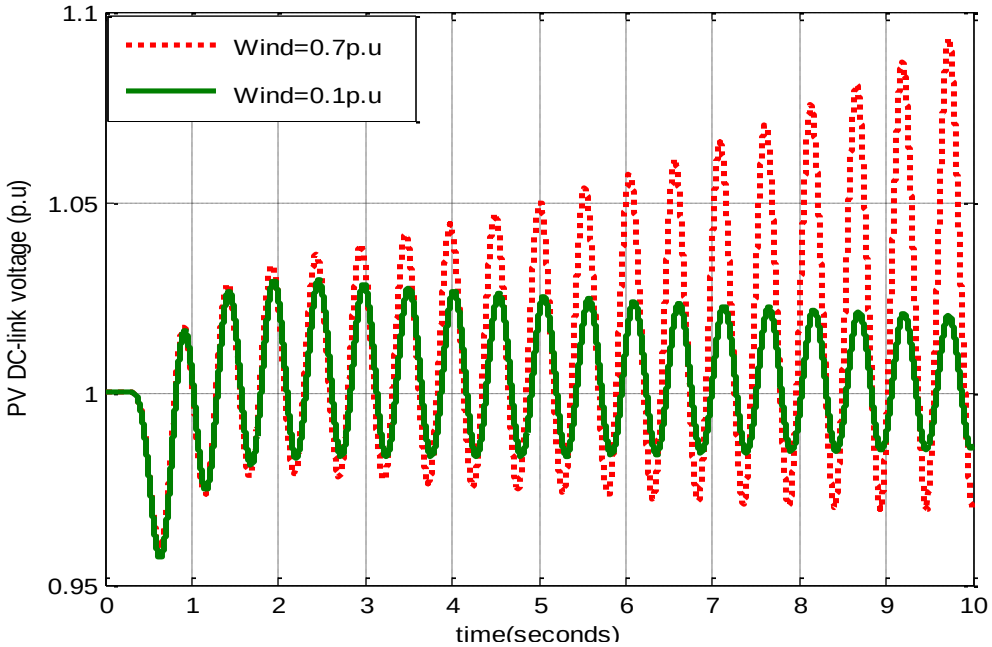

Figure 5.7 Variation in PV DC-link voltage in complete microgrid following a 10% input torque pulse in microalternator for 0.3sec.

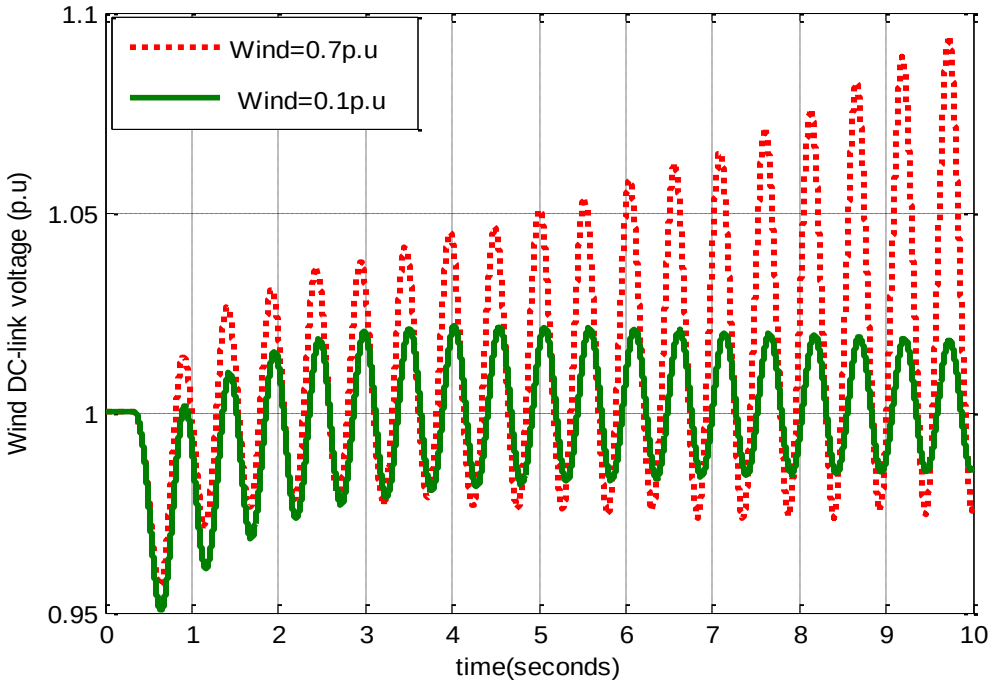

Figure 5.8 Variation in Wind DC-link voltage in complete microgrid following a 10% input torque pulse in microalternator for 0.3sec.

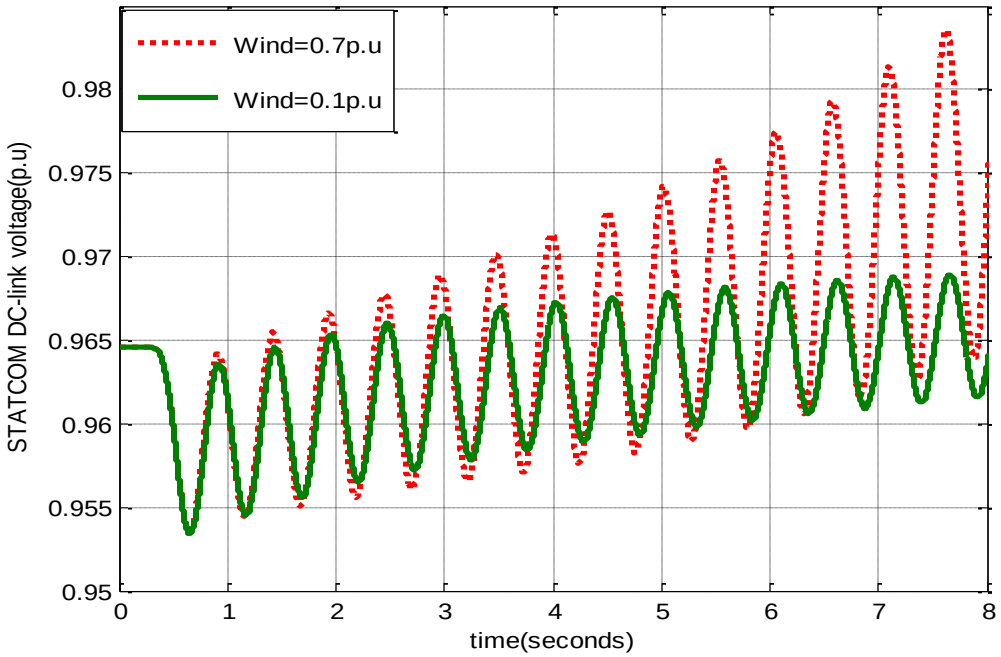

Figure 5.9 Variation in STATCOM DC-link voltage in complete microgrid following a 10% input torque pulse in microalternator for 0.3sec.

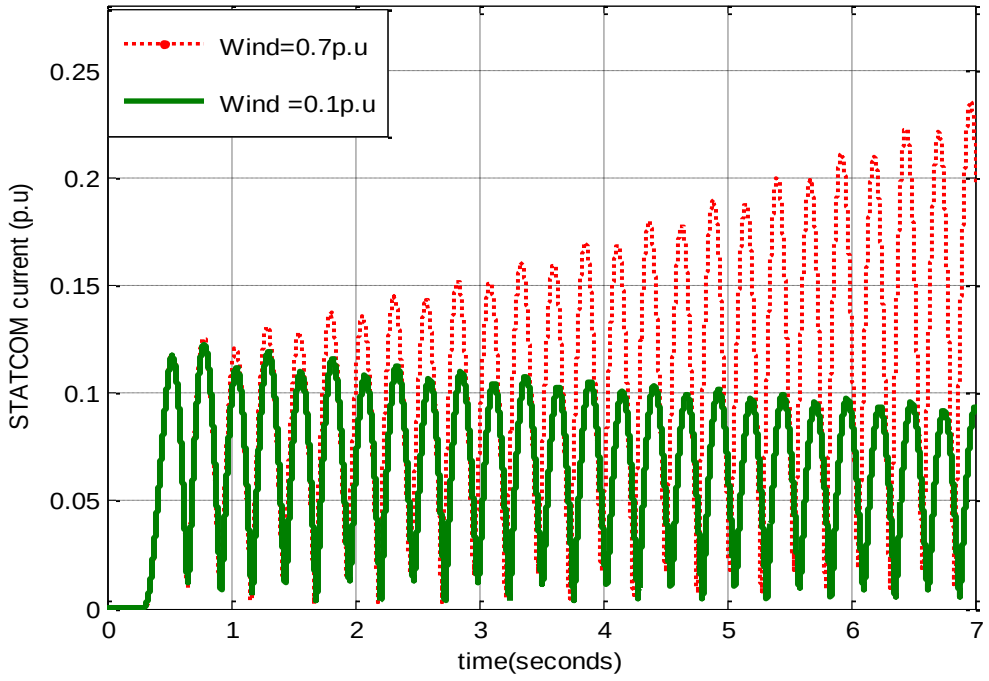

Figure 5.10 Variation in STATCOM current in complete microgrid following a 10% input torque pulse in microalternator for 0.3sec.

CHAPTER 6

CONTROL OF A MICROGRID

The microgrid model developed in chapter 5 consisting of PV, wind, microalternator along with a central energy controller has been identified with the hierarchy of 7 control inputs. This chapter evaluates all these controls and identifies damping characteristics associated with them, if any. The analysis also suggests the prospective signals which can be employed in the damping controller. Simulation studies are then carried out with some of the controls which provide the best damping performance.

6.1 Identification of stabilizing control

The state equations of the linearized model (5.11) are used to determine the eigenvalues of the system matrix $A_{overall}$ of the composite system. Out of these eigenvalues, there are some critical modes which are close to the imaginary axis. The eigenvalues corresponding to these modes are responsible for oscillations or instabilities in the microgrid under certain operating conditions. Critical modes dictate the initiation of the control action to improve the performance of the microgrid. The hierarchy of seven controls given as

$$\left[m_p, \psi_p, m_{wr}, m_{wi}, \psi_{wi}, m_{st}, \psi_{st}\right] \tag{6.1}$$

The control inputs are evaluated in terms of their potential for providing damping to the microgrid. The methods employed for the evaluation process are minimum singular value decomposition, Hankel singular value decomposition (HSVD) and the residue method.

6.1.1 Singular Value Decomposition

Mathematically, if S is a pxq complex matrix, then there exist unitary matrices L and U with dimensions of pxp and qxq, respectively[71], such that,

$$S=L\Sigma U \tag{6.2}$$

Where

$\Sigma=\begin{bmatrix}\Sigma_1 & 0\\ 0 & 0\end{bmatrix}$

$\Sigma_1=\text{diag}(\sigma_1, \dots\dots, \sigma_r)$

With $\sigma_1 \geq \cdots \geq \sigma_r \geq 0$ where r=min$\{m, n\}$ and

σ_1,….., σ_r are the singular values of S.

The p columns of L and q columns of U are called the left singular vectors and right singular vectors of S, respectively.

The minimum singular value σ_r represents the distance of the matrix S from all the matrices with a rank of r-1. The model controllability can be effectively quantified by utilizing this property. The control matrix B can be expressed as B= [b_1 $b_2 b_3$ b_4 b_5 b_6 b_7] where b_i is the column vector corresponding to the ith input. The minimum singular valueσ_{min}, of the matrix $[\lambda I - A|b_i]$ indicates the capability of the ith input to control the mode associated with the eigenvalueλ. It is known that higher the minimum singular value,σ_{min}, the higher is the controllability of this mode by the considered input. As such, the controllability of the dominant eigenvalue can be examined with all inputs in order to identify the most effective one to control the mode.

Singular value decomposition (SVD) is employed to measure the controllability of the dominant mode through the two control signals of PV system: (m_p, ψ_p), three control

signals of Wind system: (m_c, m_w, ψ_w) and two control signals of STATCOM: (m_{st}, ψ_{st}). The minimum singular value (σ_{min}), is estimated for varying power contributions from PV and wind separately. In scenario-1, the PV output power is kept constant and SVD analysis is carried out. In scenario-2, the power contribution from wind is kept constant. At each loading condition, the system model is linearized, the dominant mode is identified and the SVD based controllability measure is implemented.

The $\sigma_{\min}$ contribution from m_{st} and m_{wr} are negligible and hence are not shown.

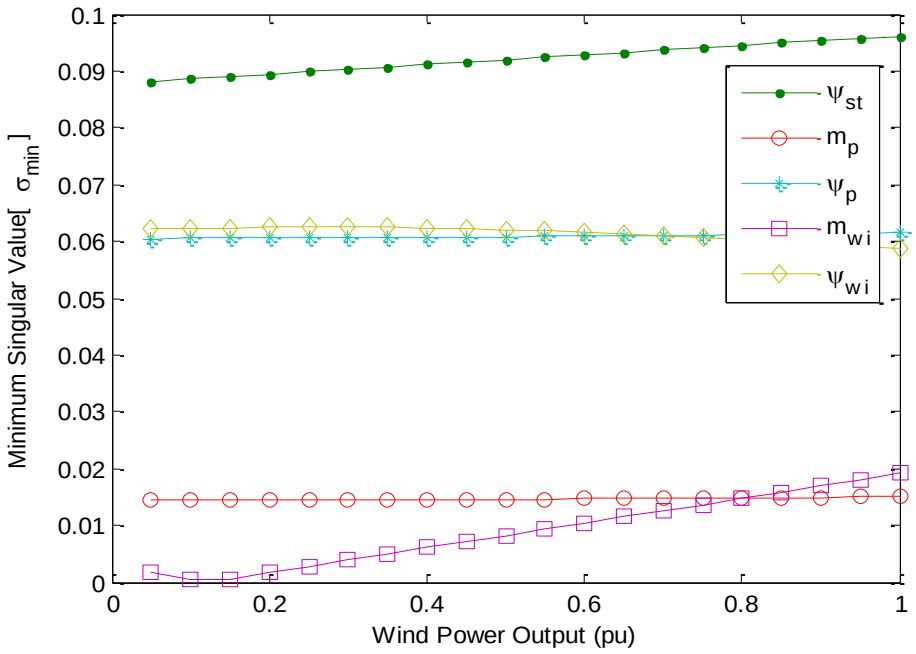

Figure 6.1 Minimum singular value of dominant control inputs for different wind power

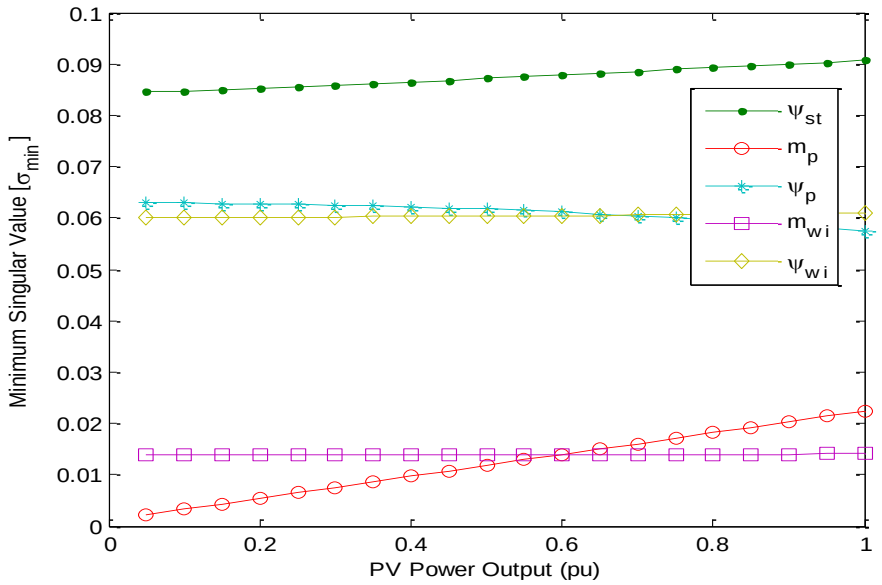

Figure 6.2 Minimum singular values of dominant control inputs for different PV power

The minimum singular values for all the inputs at different wind and PV powers were calculated. Figure 6.1 and Figure 6.2 show σ_{min} for some of the inputs. From the study of the minimum singular value, the following were observed.

- The STATCOM converter voltage phase angle (ψ_{st}) control has the largest damping content for both wind and PV system loadings.
- The order of the other signals in terms of damping contribution are $\psi_{st}, \psi_{p}, \psi_{wi}, m_{p}$, and m_{wi}.
- The m_{ST} and m_{wr} inputs have virtually no damping content.

6.1.2 Hankel singular value decomposition

In order to verify the results of singular value decomposition analysis, hankel singular value for identifying the controllability of the inputs is employed. Hankel singular values provide a measure of energy for a state in the system[72]. It is the basis for the balanced model reduction, in which high energy states are retained, while the low energy states are discarded.

Consider a linear system with n_x states, n_y outputs and n_u inputs, denoted by

G= {A, B, C}

where A, B and C are the state input and output matrices of the state space model.

The controllability and observability grammians, P and Q of the system are symmetric matrices and satisfy the lyapunov equations

$$AP + PA^T + BB^T = 0 \tag{6.3}$$

$$A^TQ + QA + C^TC = 0 \tag{6.4}$$

The hankel singular values $\sigma = \sigma_1 \leq \cdots \leq \sigma_{n_x}$ of the system are defined as the square root of eigenvalues of PQ i.e.

$$\sigma_m(G) = \sqrt{\lambda_m(PQ)}, \quad m = 1,2, \ldots\ldots, n_x \tag{6.5}$$

Hankel singular values measure the contribution of each state to evaluate the input/output behavior of the linear system. Actually, the larger the hankel singular value, the higher the energy contained by the state.

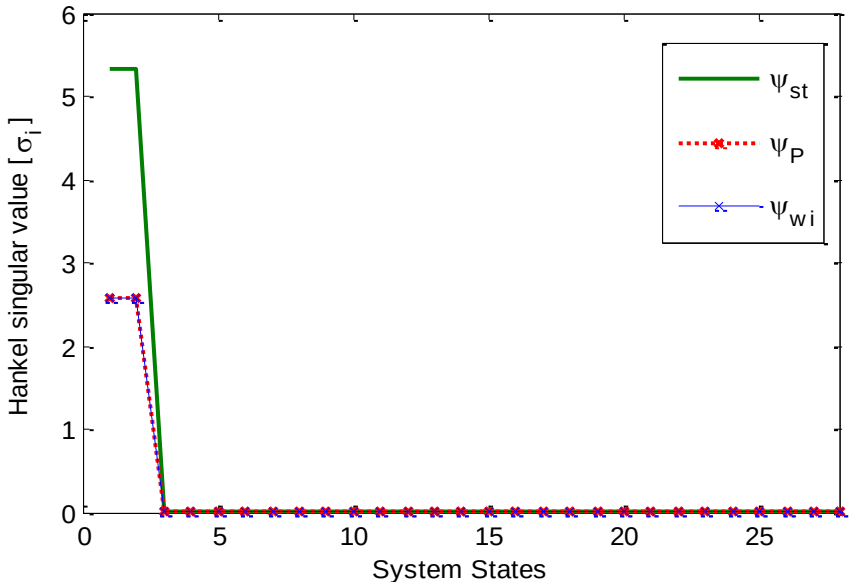

Figure 6.3 Hankel singular value decomposition with dominant control inputs.

Figure 6.3 shows the Hankel singular values against the system states (eigenvalues) for 5 dominant inputs $\psi_{st}, m_p, \psi_p, m_{wi}, \psi_{wi}$ .The singular values for the others are relatively small and hence are not shown. It can be observed that the order of the signals in comparison to those obtained through minimum singular value decomposition is the same, ψ_{st} having the highest controllability to affect the dominant mode followed by ψ_p.

6.1.3 Residue Method:

The residue of an eigenvalue of the linearized system gives the sensitivity of the mode between input and output for a SISO (single input single output).The transfer function of the SISO system

$$G(s) = \frac{\Delta y(s)}{\Delta u(s)} = C\Phi(sI - A)^{-1}B \qquad (6.6)$$

The plant function G(s) can be expanded in partial fractions of Laplace transform of y in terms of input(B)/ output(C) matrices and the controllability(ψ)/ observability(φ) measures.

$$G(s) = \sum_{i=1}^{N} \frac{C\emptyset(:,i)\psi(:,i)B}{(s-\lambda_i)} = \sum_{i=1}^{N} \frac{R_i}{(s-\lambda_i)} \qquad (6.7)$$

R_i is the residue corresponding to eigenvalueλ_i.

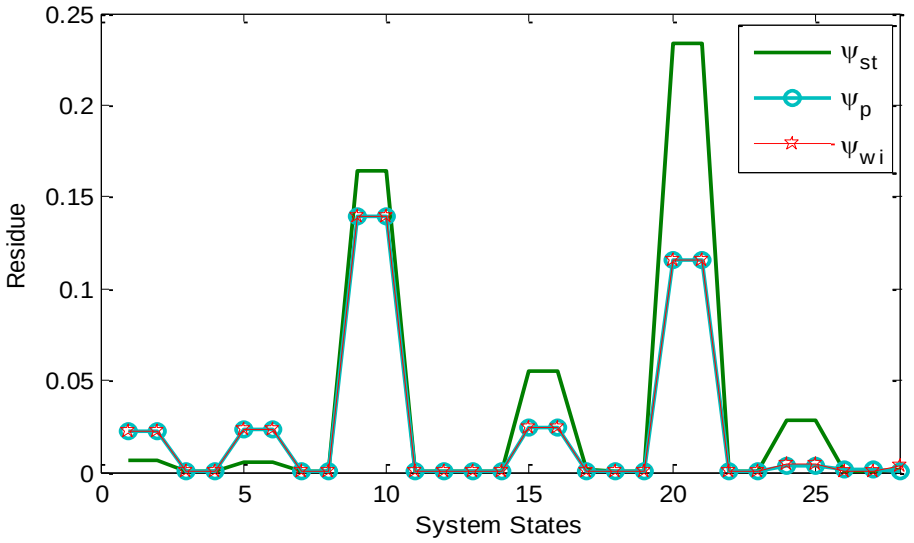

Figure 6.4 Residue analysis

The values of residues for 3 inputs for all the system states are shown in Figure 6.4. The rest are relatively small and are not shown. It can be observed that the residues corresponding to states 19 and 20 (microalternator rotor angle and speed) for control inputs $\psi_{st}$and ψ_p are the largest. So the signals angle and speed of the microalternator are the better candidates of stabilizing input in a damping control strategy.

6.2 Feedback Control System

The simulation results of small signal analysis in chapter 4 and 5 showed that the amount of participation by the different DGs can be critical in terms of system performance and stability. The central controller in the microgrid should generally monitor the real and reactive power generation and the system voltage. The controller should also be able to take emergency action to help the DG operating near the stability threshold. In this section a control strategy is designed based on the information obtained about possible inputs which can be modulated by the appropriate control signals.

From the decomposition analysis it was observed that the inputs ψ_{st} and ψ_P are more responsive to system damping needs. The residue analysis indicated that the microalternator electromechanical modes are the best candidates for any possible control action. Accordingly, the input signal to the controller configuration in Fig 13 is considered to be change in speed of the microalternator ($\Delta\omega$). The input to the plant is considered to be ψ_{st} and ψ_P.

For the input-output pair ($\psi_{st}, \Delta\omega$), the plant transfer function is given as

$$G_c(s) = C(sI-A)^{-1}B \qquad (6.8)$$

A PI controller is designed in this thesis to enhance performance of the microgrid system. The procedure is repeated for input-output of $(\psi_p, \Delta\omega)$.A PI controller is normally placed in the feedback. A washout is provided in cascade with the controller to deactivate it under steady state conditions.

The controller transfer function takes the form

$$G_c(s) = \frac{T_w s}{1+T_w s}\left(K_P + \frac{K_I}{s}\right) \qquad (6.9)$$

Where K_p and K_I are the parameters of the proportional controller. T_w is the time constant of the washout block. Starting with the linearized system equations, the gains of the controller is obtained through pole placement of the dominant poles to get the desired damping ratio.

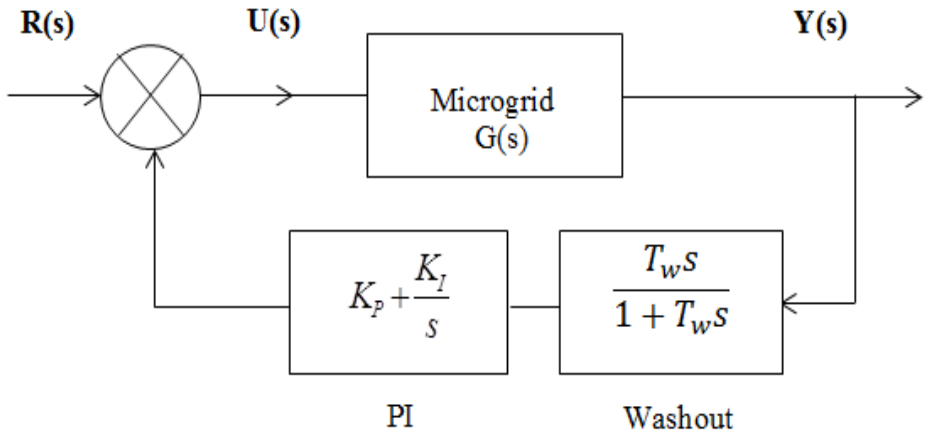

Figure 6.5 Feed forward control system

6.3 Pole Placement technique

Pole placement or full state feedback is a method employed in the feedback control system theory to place the poles of closed loop plant in the desired location in the s-plane. Placement of the poles for a specific damping ratio is desirable because it allows controlling the characteristics of the response by changing the eigenvalues of the system. This method is applicable only if the system is controllable.

From the equation (6.9), it can be shown that for any eigenvalue λ,

$$G_c(\lambda) = \frac{\lambda T_w}{1+\lambda T_w}\left(K_p + \frac{K_I}{\lambda}\right) \qquad (6.10)$$

For a dominant eigenvalue,$\lambda = \alpha + j\beta$, equation B

(6.8) can be written as

$$[C(\lambda I - A)^{-1}B]^{-1} = p + jq \qquad (6.11)$$

Also, equation (6.10) is written as

$$G_c(\lambda) = \frac{(\alpha + j\beta)T_w}{1 + (\alpha + j\beta)T_w}\left[K_p + \frac{K_I}{(\alpha + j\beta)}\right]$$

$$G_c(\lambda) = \frac{K_I T_w + K_p T_w(\alpha + j\beta)}{1 + \alpha T_w + j\beta T_w}$$

Substituting m=1+αT_w and n= βT_w

$$G_c(\lambda) = \frac{\{T_w K_I + T_w \alpha K_p + jT_w \beta K_p\}(m - jn)}{m^2 + n^2}$$

$$G_c(\lambda) = \frac{[(T_w K_I + T_w \alpha K_p)m + (T_w \beta K_p)n] + j[mT_w \beta K_p - n(T_w K_I + T_w \alpha K_p)]}{m^2 + n^2} \qquad (6.12)$$

Equating (6.11) and (6.12)

$$\frac{(T_w \alpha m + T_w \beta n)}{m^2 + n^2} K_p + \frac{T_w m}{m^2 + n^2} K_I = P \qquad (6.13)$$

$$\frac{(T_w \beta - T_w \alpha n)}{m^2 + n^2} K_p - \frac{T_w n}{m^2 + n^2} K_I = q \qquad (6.14)$$

The parameters of K_p and K_I can be obtained by solving (6.13) and (6.14)

$$K_P = \frac{[p(T_w n) + q(T_w m)](m^2 + n^2)^2}{(T_w \alpha m + T_w \beta n)T_w n + (T_w \beta - T_w \alpha n)T_w m} \qquad (6.15)$$

$$K_I = \frac{[p(T_w \beta - T_w \alpha n) - q(T_w \alpha m + T_w \beta n)](m^2 + n^2)^2}{(T_w \alpha m + T_w \beta n)T_w n + (T_w \beta - T_w \alpha n)T_w m} \qquad (6.16)$$

6.4 Simulation Results

In this section, non-linear time domain simulations have been carried out to assess the effectiveness of the controller. It has been observed in section 6.1 that the phase angles of STATCOM and PV inverter have the highest controllability. The effectiveness of only these control inputs to enhance the microgrid stability has been investigated.

In the absence of supervising control the dominant eigenvalues contributed by the microalternator yields a damping ratio of 0.004 for microalternator loading of 20%, PV 60% and Wind 70%. The damping ratio is small for the specific point of operation which is responsible for the oscillatory response when subjected to a 10% torque pulse for 0.3sec. The PI controller was designed to relocate the dominant eigenvalues so that the desired damping ratio of 0.2883 is achieved. The washout time constant was optimized at 1 sec. The objective of the simulation test is to test the inference drawn from the decomposition techniques.

Microalternator response

Figure 6.6 to Figure 6.9 show the variation in rotor angle, rotor speed, q-axis internal voltage and d-axis excitation of the microalternator following a 10% torque input for 0.3 sec. It can be seen that while the uncontrolled is on the verge of instability, the proposed energy storage controller is able to bring the system to stable manifold in less than 1 sec after the disturbance is applied. The energy storage backed supervisory controller is shown to stabilize the system very quickly. The supervisory controller thus allows enough time to redistribute the DG generation and load for safer operation of the system. It can be observed that the response with the PV system converter angle is also useful in controlling the power transients in the microgrid system. However, this is slightly inferior

compared to ψ_{st} control performance. This finding is consistent with the results obtained in Section 6.1.

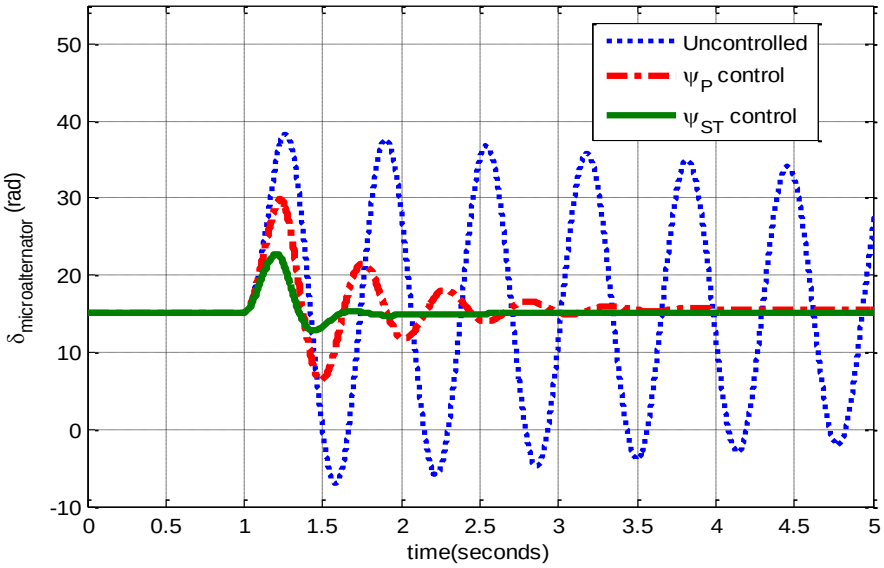

Figure 6.6 Rotor angle response of the microalternator

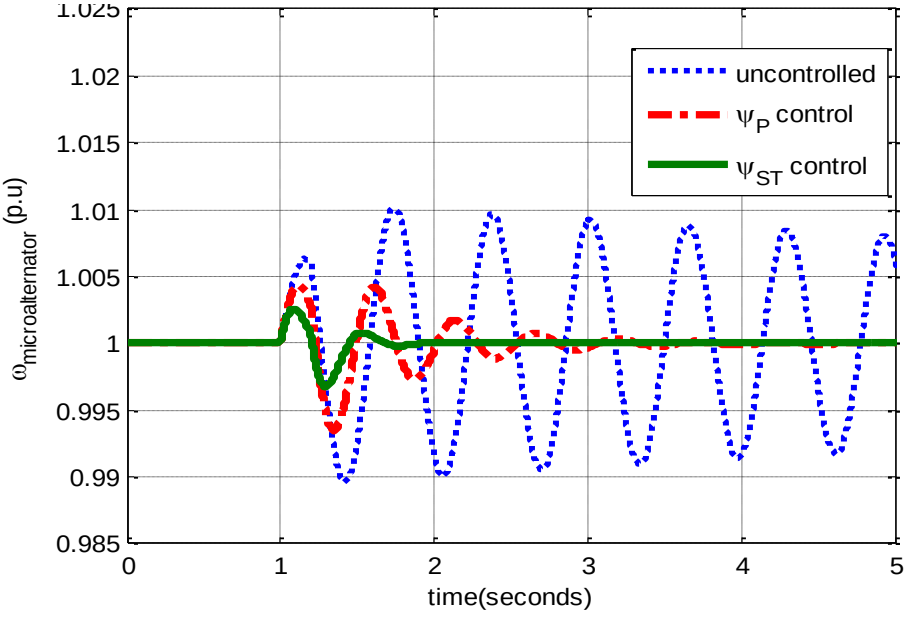

Figure 6.7 Speed response of the microalternator

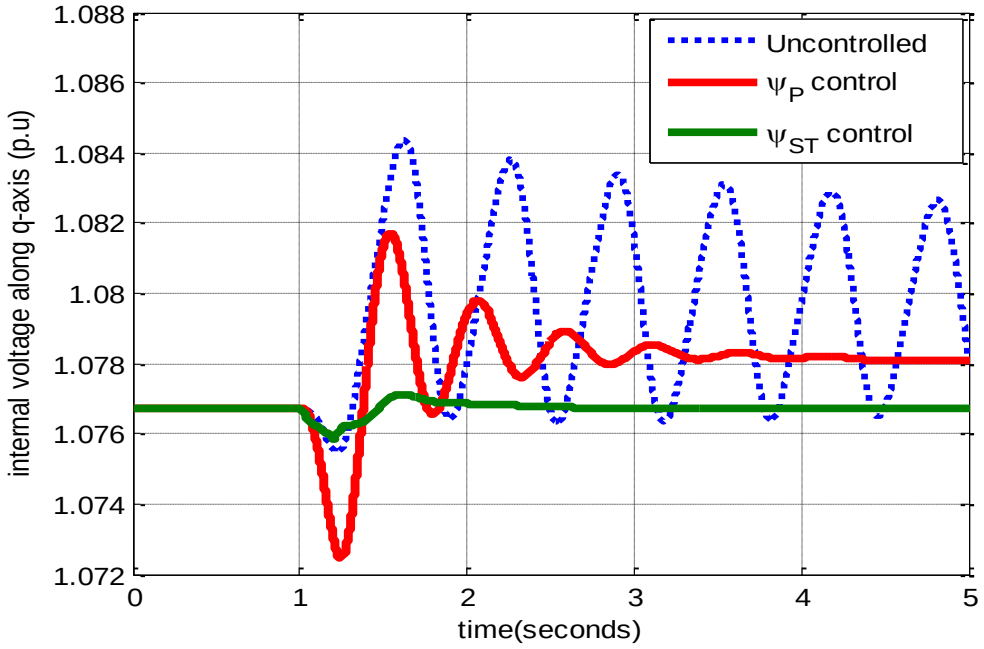

Figure 6.8 Internal voltage along q-axis response of the microalternator

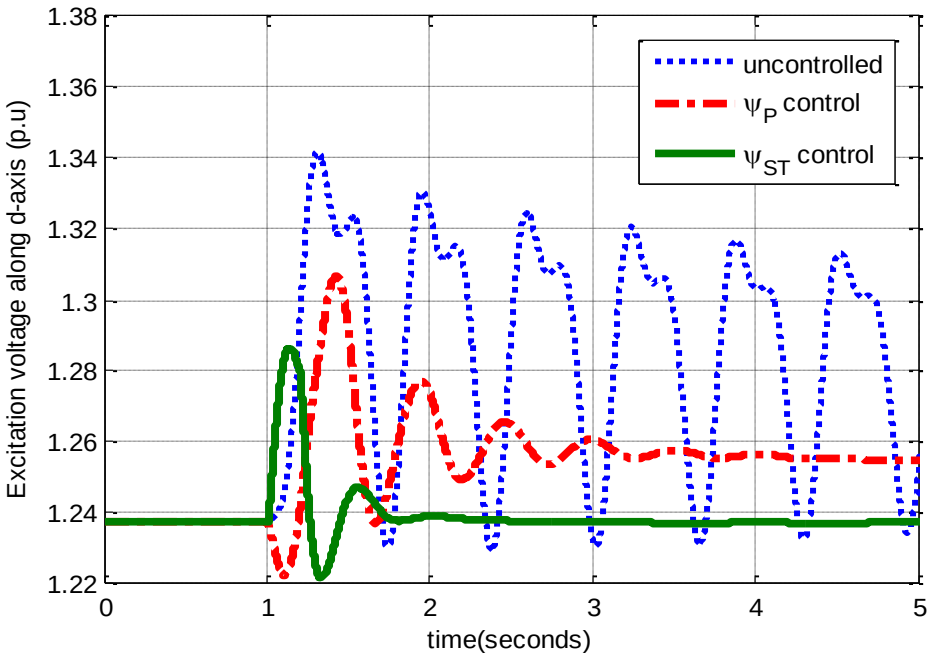

Figure 6.9 Excitation voltage along d-axis

Photovoltaic Response

In this section, nonlinear time domain responses of the photovoltaic quantities are shown when a 10% input torque pulse is applied for 0.3 sec in the microalternator. Figures 6.10 to Figure 6.14 show the responses of total PV array output current, PV inverter output filter current, PV coupling inductor current, voltage across the DC-link capacitor and voltage across the output filter capacitor respectively**.** The responses are shown for a normal loading of for microalternator loading of 20%, PV 60% and Wind 70%. It can be clearly seen that the STATCOM phase angle control not only damps the oscillations but also produce zero steady state error. The PV phase angle control except for the overshoot at the beginning also controls the instabilities in the microgrid.

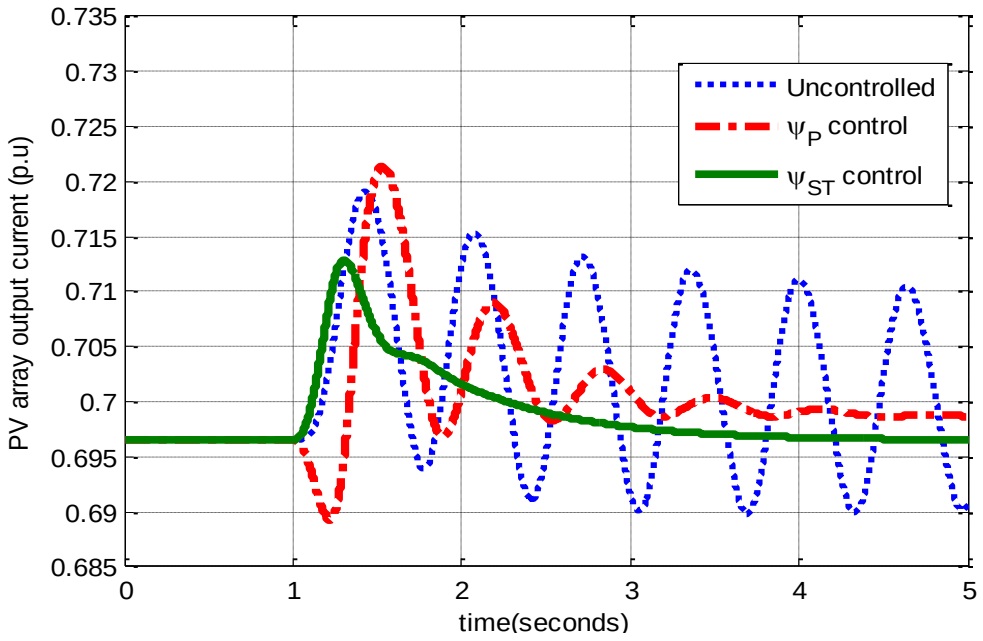

Figure 6.10 PV array output current

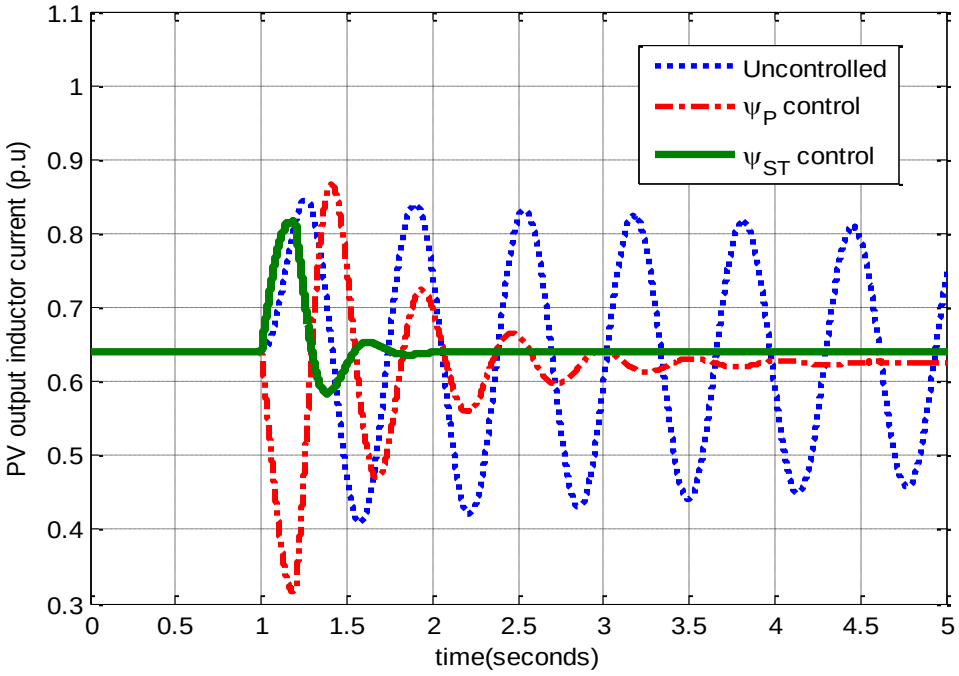

Figure 6.11 PV output filter current

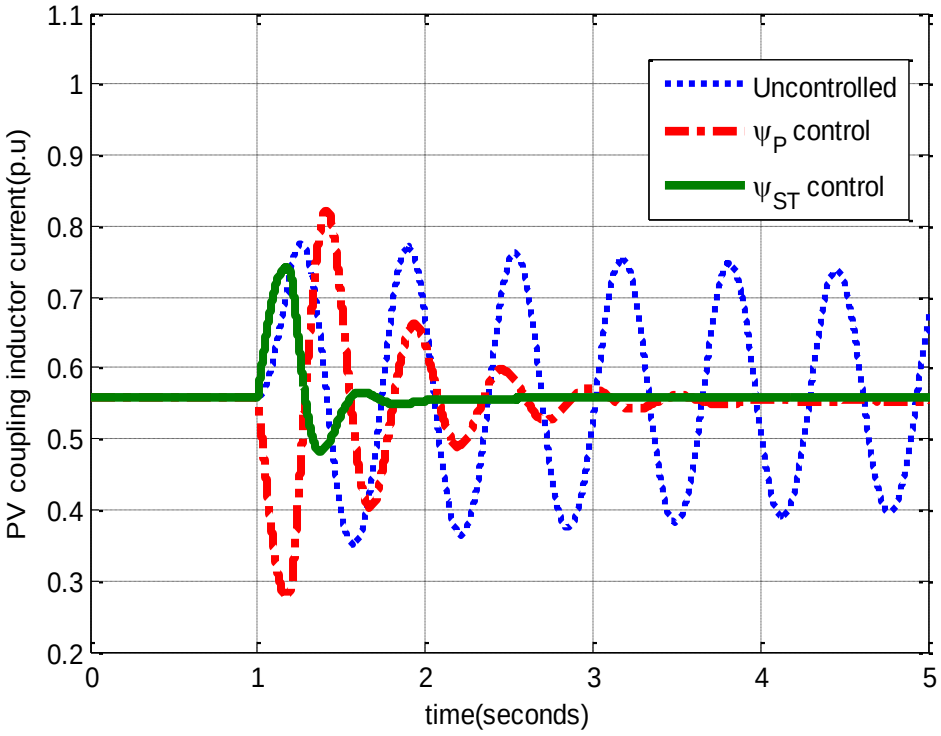

Figure 6.12 PV coupling inductor current

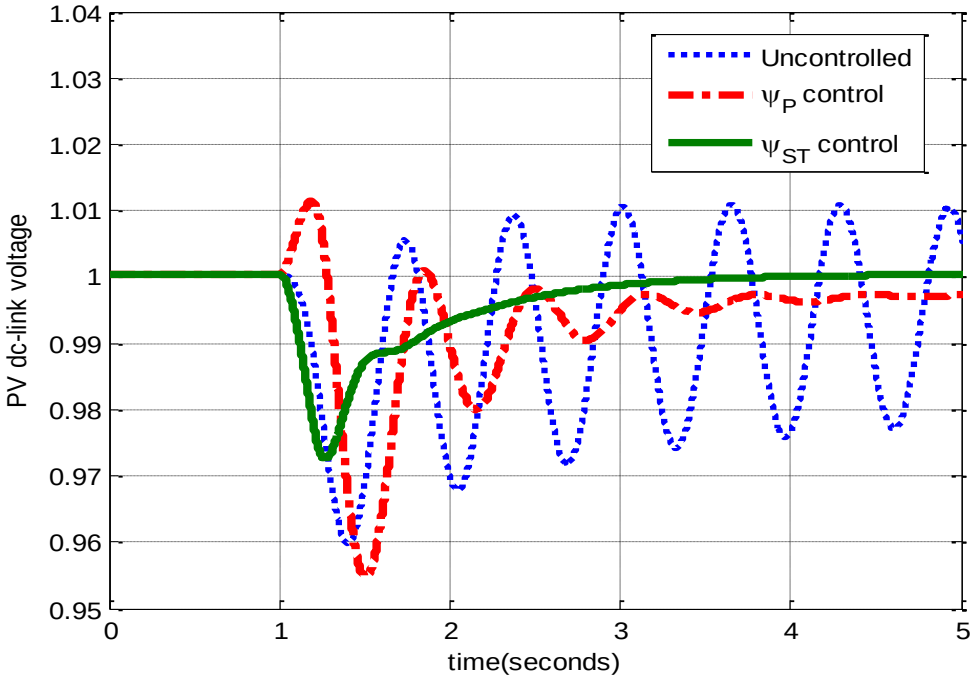

Figure 6.13 PV DC-link voltage

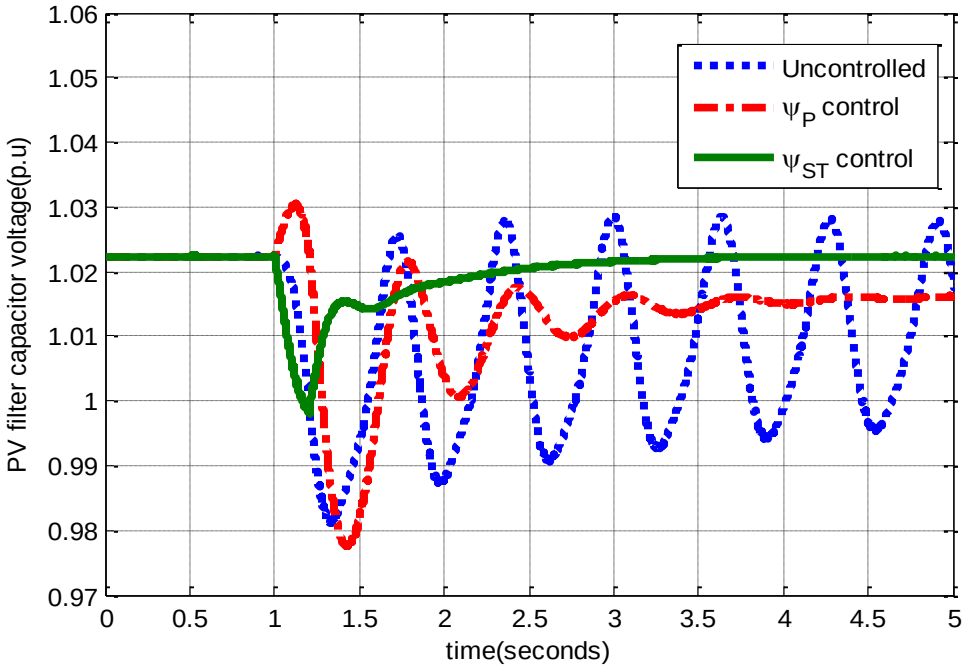

Figure 6.14 PV filter capacitor voltage

Wind system response

In this section, non-linear transient responses of some of the wind system variables have been shown. Figures 6.15 to 6.18 represent the responses of wind inverter output filter current, wind coupling inductor current, voltage across the DC-link capacitor and voltage across the output filter capacitor respectively**.** It can be observed that the inverter output currents before and after the filter returns to steady state in less than 1 sec after the disturbance is applied under ψ_{ST} control while the DC-link voltage and filter capacitor voltage recovers the steady state in 2 sec.

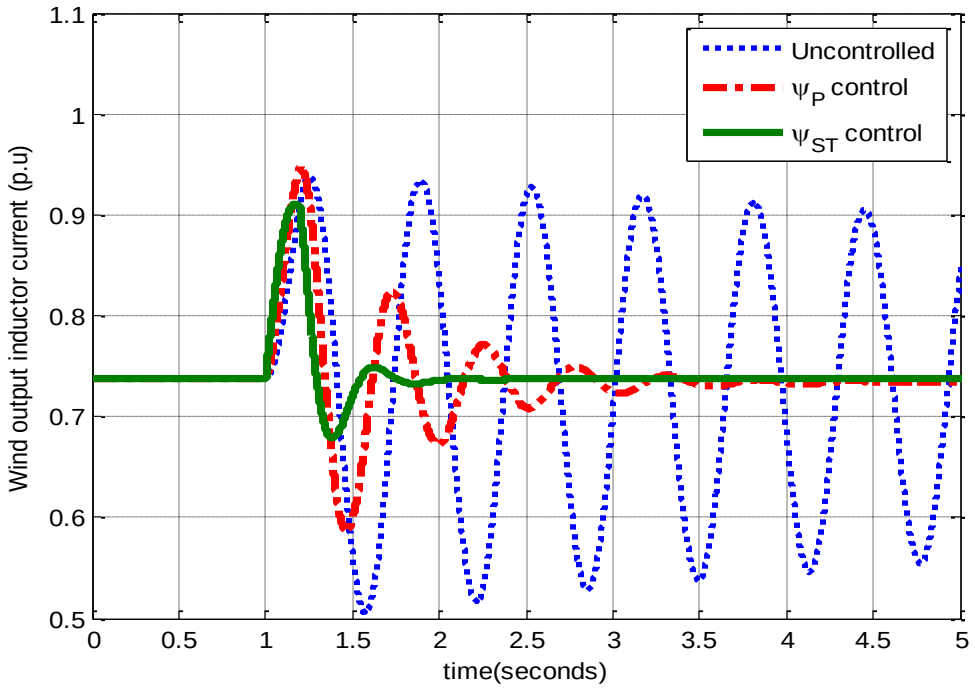

Figure 6.15 Wind output inductor current

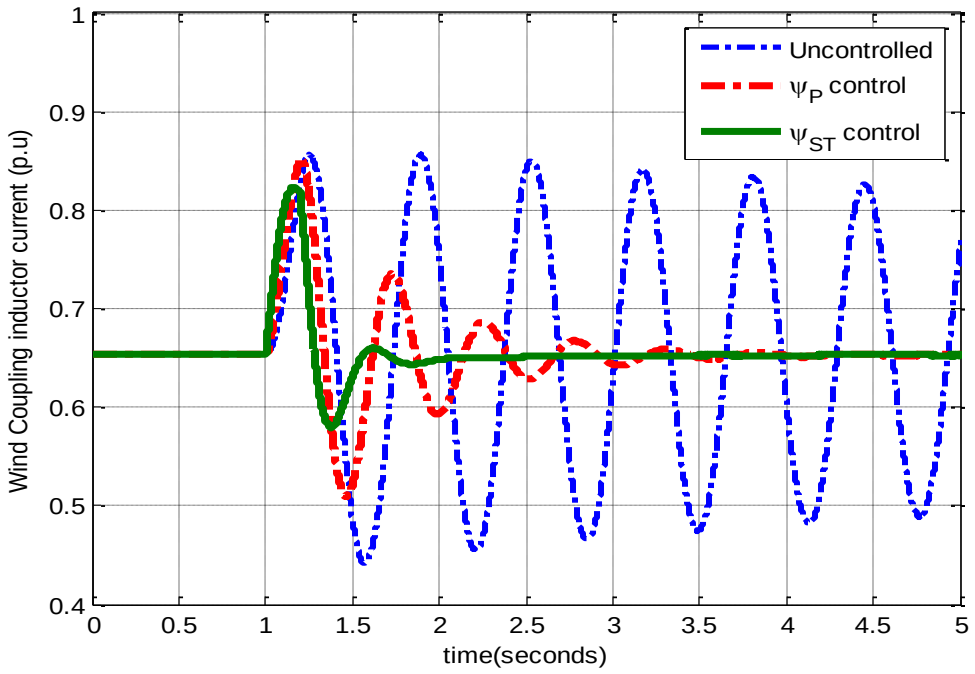

Figure 6.16 Wind coupling inductor current

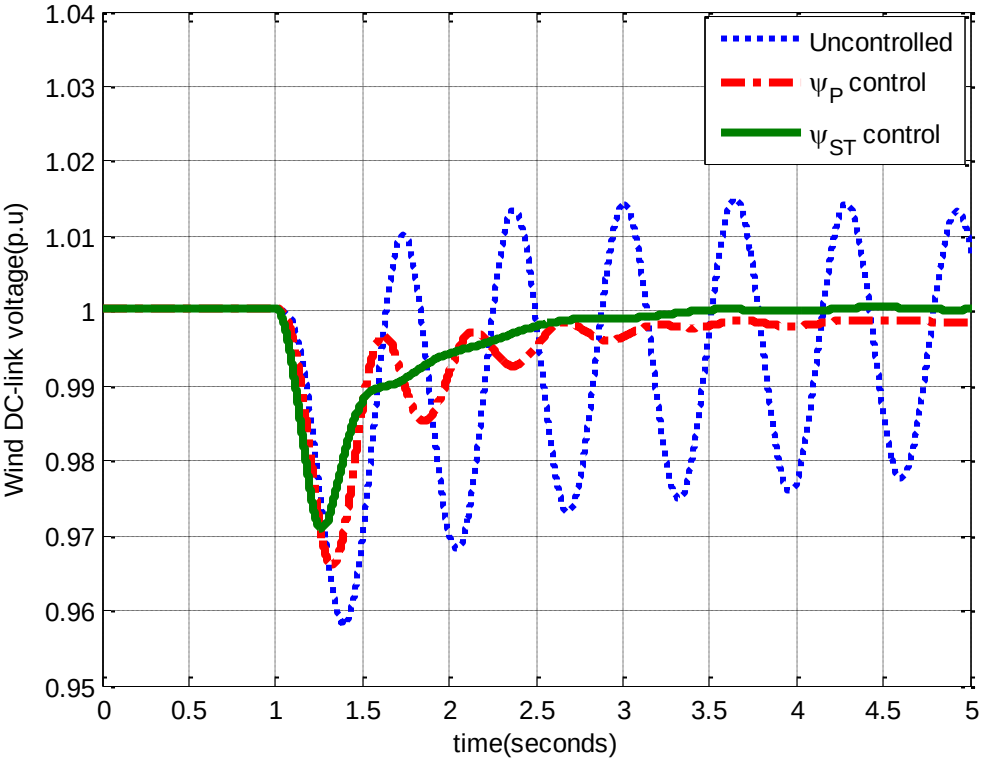

Figure 6.17 Wind DC-link voltage

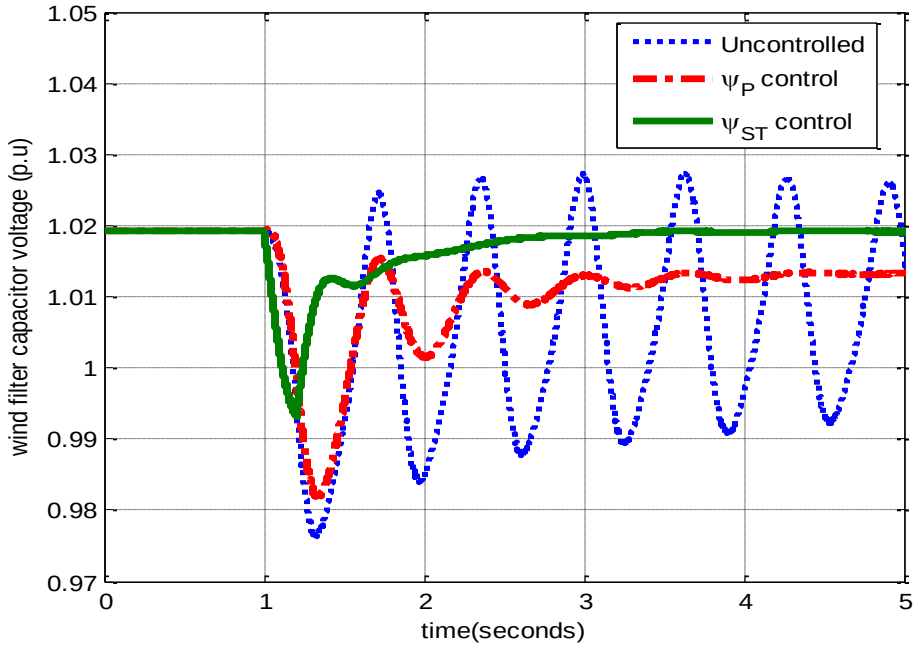

Figure 6.18 Wind filter capacitor voltage

Controller Response

In this section, nonlinear response of STATCOM output current and DC-link voltage is shown. The amount of disturbance and loadings of different DGs are kept same as before. Figure 6.19 and Figure 6.20 show the variations in STATCOM current and DC-link voltage respectively. It can be observed that ψ_{ST} control effectively damps the electromechanical oscillations and eliminates the steady state error. The PV phase angle (ψ_P) control does produce some steady state error and overshoot.

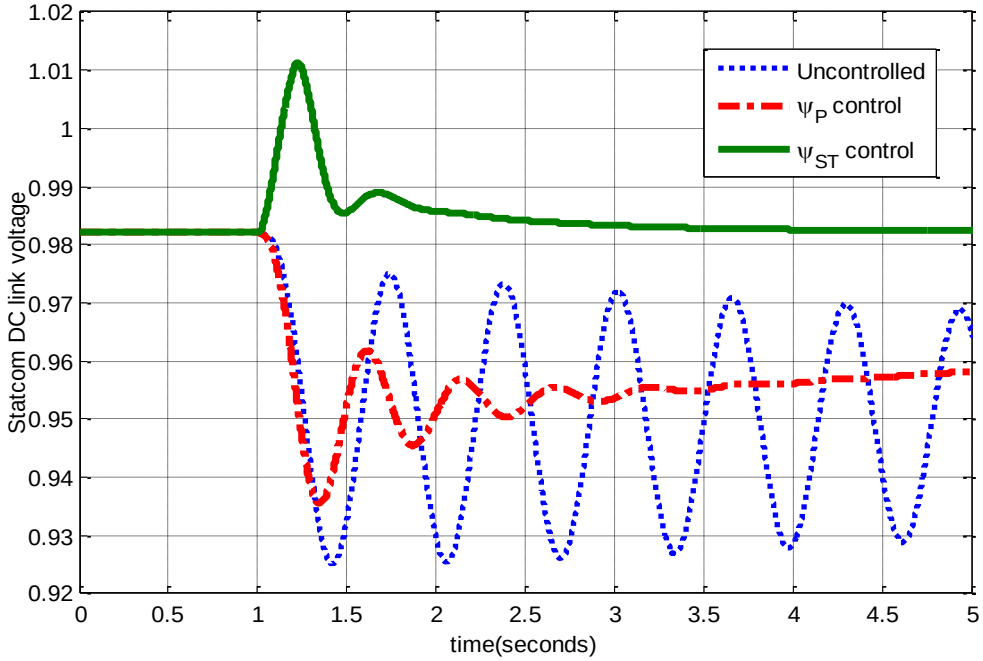

Figure 6.19 STATCOM DC-link voltage

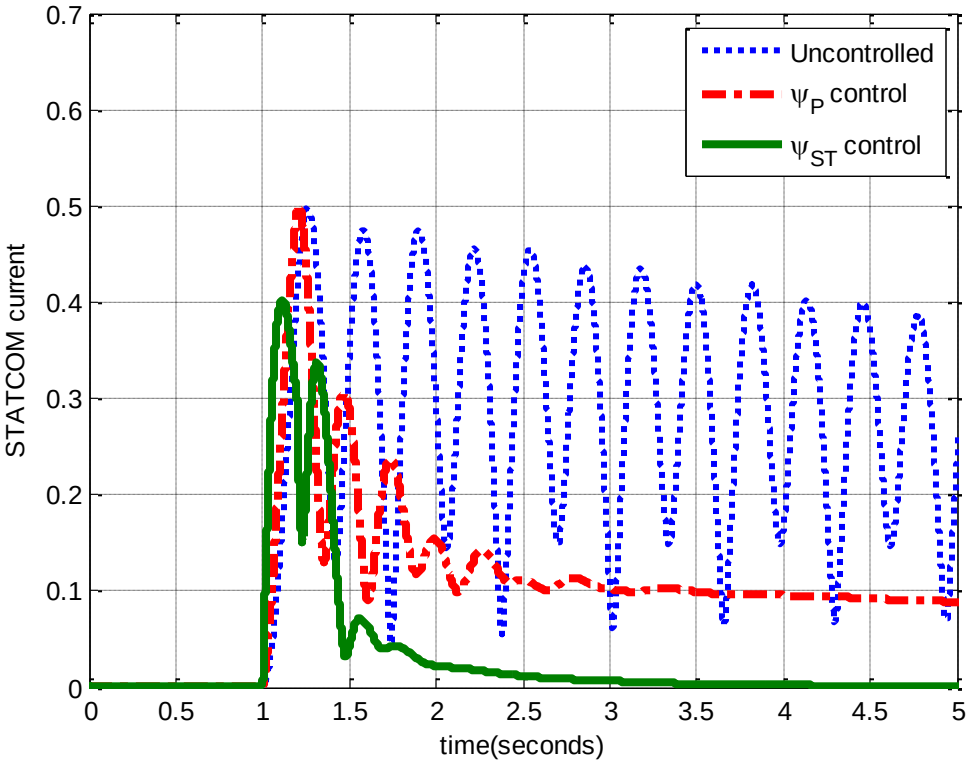

Figure 6.20 STATCOM current

Figure 6.21 and Figure 6.22 show the transient variations in microgrid bus voltage and the total real power deliver by the DG units respectively following a 10% input torque pulse in the microalternator for 0.3 sec

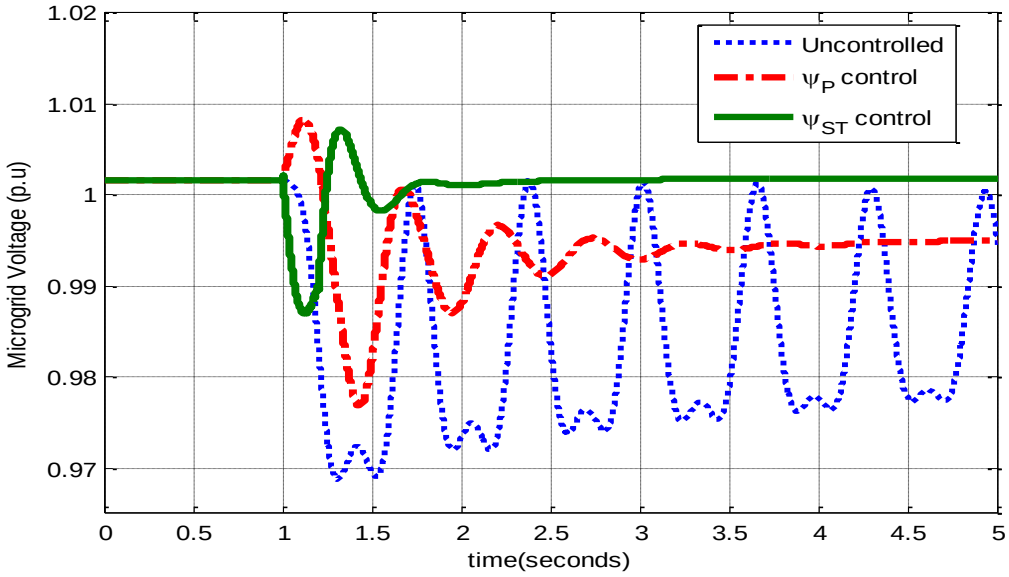

Figure 6.21 Variations in microgrid Voltage

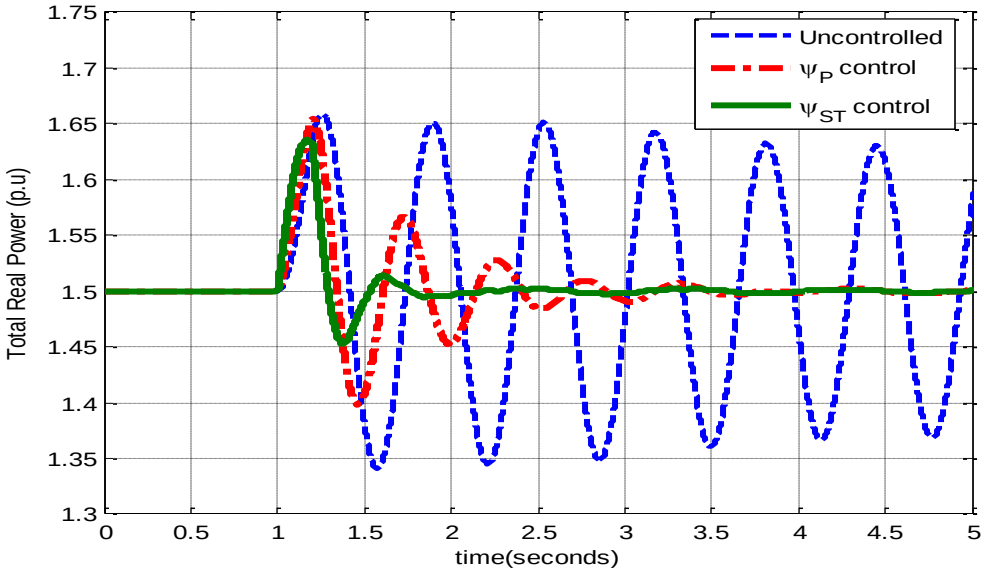

Figure 6.22 Variations in total real power.

6.5 Robustness of the controller

In this section, the robustness of the controller is evaluated by considering a different operating point of the microgrid system. This operating point corresponds to PV power 80%, wind 70% and microalternator 20%. From the small signal analysis of Figure 5.4, it can be observed that the operating point lies slightly in the unstable region. The system is tested again by applying a 10% input torque pulse in the microalternator for 0.3s. Figure 6.23 shows the responses with ψ_{st} and ψ_p controls indicating that the controller can keep the system stable transiently even in the unstable condition thus allowing enough time to redistribute the generation and load for safer operation of the system.

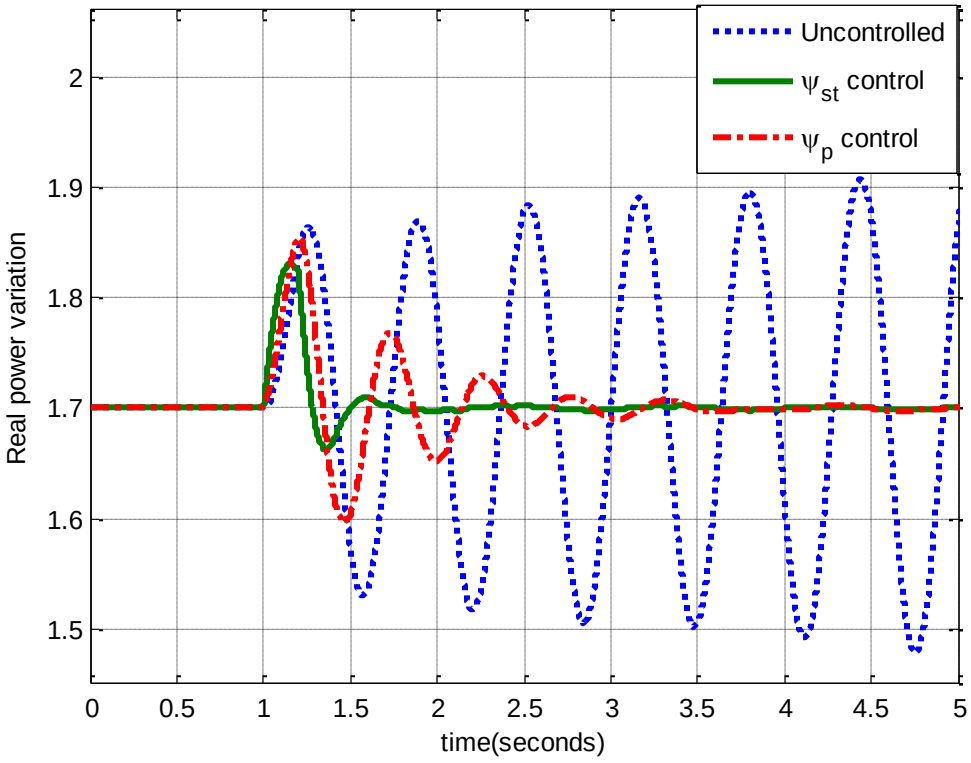

Figure 6.23 Variation of real power for a total initial power of 1.7pu.

The robustness of the controller can also be verified by observing the change in the damping ratio with the variation in some of the system parameters. The PI controller was designed for the damping ratio of 0.2883 with the system parameters presented in Appendix A. The operating point of the DG units was considered to be microalternator loading of 20%, PV 60% and Wind 70%. For fixed values of optimized control parameters K_p and K_I, the damping ratio is subjected to change with the variations in system parameters. Table 6.1 shows the damping ratio for the 20% increase or 20% decrease in the value of given parameter. It can be observed from the table that the damping ratio is not subjected to large changes with the variation in parameters thus showing the robustness of the controller.

Table 6.1: Damping ratios for the change in the system parameters from the their nominal values

Parameter	Damping ratio for 20% increase in the parameter	Damping ratio for 20% decrease in the parameter
$\boldsymbol{R_b}$	0.2955	0.28207
$\boldsymbol{x_b}$	0.3	0.27617
$\boldsymbol{R_t}$	0.28824	0.28808
$\boldsymbol{x_t}$	0.27955	0.29769
$\boldsymbol{R_p}$	0.2879	0.28882
$\boldsymbol{L_p}$	0.2906	0.28559
$\boldsymbol{R_w}$	0.28779	0.28898
$\boldsymbol{L_w}$	0.29076	0.28537

CHAPTER 7

CONCLUSION AND FUTURE WORK

7.1 Conclusion

The dynamic modeling of a microgrid including PV, wind in addition to microalternator has been developed in this work. Nonlinear and linear models of the individual components of the microgrid are obtained. The behavior of DG interactions has been analyzed through three different microgrid models. The first two microgrids consist of microalternator-PV and microalternator-wind, respectively. A composite configuration having PV, wind and microalternator DGs was then investigated along with a supervisory controller.

From small signal analysis of the smaller microgrids it was observed that for fixed amount of PV or wind participation, the stability of the microgrid worsens as the amount of micro-alternator power and system load decreases. For a particular microalternator output and load, there exists critical value of PV or wind power above which microgrid performance degrades. Non-linear simulations are carried out to verify the results obtained through small-signal analysis. Simulation studies of the composite system comply with the results of smaller microgrids. It is concluded from the analysis that for stable microgrid operation, microalternator output cannot be too low. Also, PV and wind contributions cannot exceed certain limit for stable operation of the microgrid.

The possibility of enhancing the stability boundaries for critical cases of generation mixes was investigated. A central supervisory controller with capacitor energy storage was found to provide extra damping to the system enhancing the transient stability domain. The phase angles of the STATCOM and PV have been identified to have better

ability to damp the oscillatory modes of the system. Residue analysis indicates that microalternator electromechanical modes are the best input for the controllers. A PI controller with STATCOM phase angle as the control input and microalternator speed as the feedback signal was shown to perform satisfactorily even for unstable loading conditions of the DG's. The controller gains were tuned through an optimal pole placement technique. It has been shown through nonlinear simulations that the supervisory control is capable of transferring the transiently unstable system to normal steady state operation then allowing time for the operators to redistribute the generation load mix transiting to safer range of operation.

7.2 Future Work

The following are the recommendations for further research in this work:

- Throughout the thesis, microgrid operates in connection with the grid. It will be interesting to study the operation of microgrid in autonomous mode. For this to happen, the microgrid should also include the finite energy storage device such as superconducting magnetic energy storage devices, supercapacitors, batteries etc. which can controls the real power flow in the microgrid.
- Controllers other than PI can be used. The effectiveness of the other controllers can be compared to that of PI.
- Various optimization techniques such as particle swarm optimization, genetic algorithm, etc. other than pole placement can be used to optimize controller parameters more efficiently.
- Power sharing techniques such as the droop controllers can be employed to share power efficiently among all DG units.
- Effect of different kinds of loads such as the transient load and also the impact of unbalance and single phase loads dynamic stability of microgrid can be studied.

APPENDIX A

System parameters and operating values

Microalternator:

Xd=1.3p.u., xq=0.47p.u., rt=0.1p.u., rb=0.15p.u., xb=0.2566p.u., xt=0.2p.u., M=1.2p.u.,

PV Plant:

Lp=0.2p.u., Lpf=0.2p.u., Cpf=0.2p.u., Rp=0.1p.u., Rpf=0.1p.u., Cdcp=1p.u.,

Wind Plant:

Lw=0.2p.u., Lwf=0.2p.u., Cwf=0.2p.u., Rw=0.1p.u., Rwf=0.1p.u., Cdcw=1p.u., Hg=0.6p.u, Ht=2p.u.

Linearization of the PV output LC filter and coupling inductance:

The PV inverter output filter current:

$$\Delta\dot{\imath}_{pfd} = \frac{-\omega_0 R_{pf}}{L_{pf}}\Delta i_{pfd} + \omega_0\left(\Delta i_{pfq} + i_{pfq0}\Delta\omega\right) + \frac{\omega_0}{L_{pf}}[m_p\cos(\psi_p+\theta)\Delta V_{dcp}$$

$$-m_p V_{dcpo}\sin\left(\psi_p+\theta\right)\Delta\psi_p + V_{dcpo}\cos\left(\psi_p+\theta\right)\Delta m_p] \quad - \frac{\omega_0\Delta V_{cpd}}{L_{pf}} - \frac{\omega_0 R_{pdr}}{L_{pf}}(\Delta i_{pfd} - \Delta i_{pq})$$

$$\Delta\dot{\imath}_{pfq} = \frac{-\omega_0 R_{pf}}{L_{pf}}\Delta i_{pfq} - \omega_0\left(\Delta i_{pfd} + i_{pfd0}\Delta\omega\right) + \frac{\omega_0}{L_{pf}}[m_p\sin\left(\psi_p+\theta\right)\Delta V_{dcp}$$

$$+m_p V_{dcpo}\cos\left(\psi_p+\theta\right)\Delta\psi_p + V_{dcpo}\sin\left(\psi_p+\theta\right)\Delta m_p] \quad - \frac{\omega_0\Delta V_{cpq}}{L_{pf}} - \frac{\omega_0 R_{pdr}}{L_{pf}}(\Delta i_{pfq} - \Delta i_{pq})$$

The PV output coupling inductance current:

$$\Delta\dot{i}_{pd} = \frac{-R_p}{L_p}\Delta i_{pd} + \omega_0\left(\Delta i_{pq} + i_{pq0}\Delta\omega\right) + \frac{1}{L_p}\left(\Delta V_{cpd} - \Delta V_{sd}\right) + \frac{\omega_0 R_{pdr}}{L_p}(\Delta i_{pfd} - \Delta i_{pd})$$

$$\Delta\dot{i}_{pq} = \frac{-R_p}{L_p}\Delta i_{pq} + \omega_0\left(\Delta i_{pd} + i_{pd0}\Delta\omega\right) + \frac{1}{L_p}\left(\Delta V_{cpq} - \Delta V_{sq}\right) + \frac{\omega_0 R_{pdr}}{L_p}(\Delta i_{pfq} - \Delta i_{pq})$$

The voltage across the filter capacitor:

$$\Delta\dot{V}_{cpd} = \omega_0\left(\Delta V_{cpq} + V_{cpq0}\Delta\omega\right) + \frac{1}{C_{pf}}\left(\Delta i_{pfd} - \Delta i_{pd}\right)$$

$$\Delta\dot{V}_{cpq} = -\omega_0\left(\Delta V_{cpd} + V_{cpd0}\Delta\omega\right) + \frac{1}{C_{pf}}\left(\Delta i_{pfq} - \Delta i_{pq}\right)$$

Linearization of the Wind output LC filter and coupling inductance:

The PV inverter output filter current:

$$\Delta\dot{\imath}_{wfd} = \frac{-\omega_0 R_{wf}}{L_{wf}}\Delta i_{wfd} + \omega_0\left(\Delta i_{wfq} + i_{wfq0}\Delta\omega\right) + \frac{\omega_0}{L_{wf}}\left[m_{wi}\cos(\psi_{wi}+\theta)\Delta V_{dcw}\right.$$

$$\left. - m_{wi}V_{dcwo}\sin(\psi_{wi}+\theta)\,\Delta\psi_{wi} + V_{dcwo}\cos(\psi_{wi}+\theta)\,\Delta m_{wi}\right] - \frac{\omega_0\Delta V_{cwd}}{L_{wf}}$$

$$- \frac{\omega_0 R_{wdr}}{L_{wf}}\left(\Delta i_{wfd} - \Delta i_{wq}\right)$$

$$\Delta\dot{\imath}_{wfq} = \frac{-\omega_0 R_{wf}}{L_{wf}}\Delta i_{wfq} - \omega_0\left(\Delta i_{wfd} + i_{wfd0}\Delta\omega\right) + \frac{\omega_0}{L_{wf}}\left[m_{wi}\sin(\psi_{wi}+\theta)\,\Delta V_{dcw}\right.$$

$$\left. + m_{wi}V_{dcwo}\cos(\psi_{wi}+\theta)\,\Delta\psi_{wi} + V_{dcwo}\sin(\psi_{wi}+\theta)\,\Delta m_{wi}\right] - \frac{\omega_0\Delta V_{cwq}}{L_{wf}}$$

$$- \frac{\omega_0 R_{wdr}}{L_{wf}}\left(\Delta i_{wfq} - \Delta i_{wq}\right)$$

The wind output coupling inductance current:

$$\Delta\dot{i}_{wd} = \frac{-R_w}{L_w}\Delta i_{wd} + \omega_0\left(\Delta i_{wq} + i_{wq0}\Delta\omega\right) + \frac{1}{L_w}\left(\Delta V_{cwd} - \Delta V_{sd}\right) + \frac{\omega_0 R_{wdr}}{L_w}\left(\Delta i_{wfd} - \Delta i_{wd}\right)$$

$$\Delta\dot{i}_{wq} = \frac{-R_w}{L_w}\Delta i_{wq} + \omega_0\left(\Delta i_{wd} + i_{wd0}\Delta\omega\right) + \frac{1}{L_w}\left(\Delta V_{cwq} - \Delta V_{sq}\right) + \frac{\omega_0 R_{wdr}}{L_w}\left(\Delta i_{wfq} - \Delta i_{wq}\right)$$

The voltage across the filter capacitor:

$$\Delta\dot{V}_{cwd} = \omega_0\left(\Delta V_{cwq} + V_{cwq0}\Delta\omega\right) + \frac{1}{C_{wf}}\left(\Delta i_{wfd} - \Delta i_{wd}\right)$$

$$\Delta\dot{V}_{cwq} = -\omega_0\left(\Delta V_{cwd} + V_{cwd0}\Delta\omega\right) + \frac{1}{C_{wf}}\left(\Delta i_{wfq} - \Delta i_{wq}\right)$$

APPENDIX B

In this chapter, linearized state space model of the microgrid system shown in Figure 5.1 is developed in detail.

Linearization of microalternator output parameters:

In this section, the microalternator output current, terminal voltage and output power are expressed in terms of chosen state variables to obtain the state space model of the microgrid.

Output current:

The microalternator output current along d-axis (3.7) from is given as,

$$i_{td} = \frac{-r_t V_{sd} + (e_q{}' - V_{sq})\{x_2\}}{Z_1}$$

$$\Delta i_{td} = \frac{-r_t}{Z_1}\Delta V_{sd} + \frac{x_2}{Z_1}(\Delta e_q{}' - \Delta V_{sq})$$

Substituting ΔV_{sd} and ΔV_{sq} from (5.10) and (5.9) in the above, we get

$$\Delta i_{td} = \frac{-r_t}{Z_1}\left[A_1\left(\Delta i_{sd} + \Delta i_{pd} + \Delta i_{wd}\right) + B_1\left(\Delta i_{sq} + \Delta i_{pq} + \Delta i_{wq}\right) + C_1\Delta E e_q{}' + D_1\Delta\delta\right]$$

$$+\frac{x_2}{Z_1}\left[\Delta e_q{}' - D\left[\Delta i_{sd} + \Delta i_{pd} + \Delta i_{wd}\right] + F\left[\Delta i_{sq} + \Delta i_{pq} + \Delta i_{wq}\right] + \Delta E e_q{}' + G\Delta\delta\right]$$

$$\Delta i_{td} = \left(\Delta i_{sd} + \Delta i_{pd} + \Delta i_{wd}\right)\left[\frac{-r_t}{Z_1}A_1 - \frac{x_2}{Z_1}D\right] + \left(\Delta i_{sq} + \Delta i_{pq} + \Delta i_{wq}\right)\left[\frac{-r_t}{Z_1}B_1 - \frac{x_2}{Z_1}F\right]$$
$$+ \Delta e_q{}'\left[\frac{-r_t}{Z_1}C_1 + \frac{x_2}{Z_1} - \frac{x_2 E}{Z_1}\right] + \Delta\delta\left[\frac{-r_t}{Z_1}D_1 - \frac{x_2}{Z_1}G\right]$$

$$\Delta i_{td} = i_{td1}\left(\Delta i_{sd} + \Delta i_{pd} + \Delta i_{wd}\right) + i_{td2}\left(\Delta i_{sq} + \Delta i_{pq} + \Delta i_{wq}\right) + i_{td3}\Delta e_q{}' + i_{td4}\Delta\delta \quad \text{(B. 1)}$$

where $i_{td1} = \frac{-r_t}{Z_1}A_1 - \frac{x_2}{Z_1}D$ $\quad i_{td2} = \frac{-r_t}{Z_1}B_1 - \frac{x_2}{Z_1}F$

$i_{td3} = \frac{-r_t}{Z_1}C_1 + \frac{x_2}{Z_1} - \frac{x_2 E}{Z_1}$ $\quad i_{td4} = \frac{-r_t}{Z_1}D_1 - \frac{x_2}{Z_1}G$

Similarly,

$$i_{tq} = \frac{V_{sd}z_1 - {r_t}^2 V_{sd} + r_t\left(e_q{}' - V_{sq}\right)x_2}{x_2 z_1}$$

Differentiating the above equation and substituting ΔV_{sd} and ΔV_{sq} from (5.10)

and (5.9) we get,

$$\Delta i_{tq} = \frac{1}{x_2 z_1}[(z_1 - r_t^2)\{A_1\left(\Delta i_{sd} + \Delta i_{pd} + \Delta i_{wd}\right) + B_1\left(\Delta i_{sq} + \Delta i_{pq} + \Delta i_{wq}\right) + C_1 \Delta E e_q{}']$$

$$+D_1\Delta\delta\} + r_t x_2\{\Delta e_q{}' - D\left(\Delta i_{sd} + \Delta i_{pd} + \Delta i_{wd}\right) + F\left(\Delta i_{sq} + \Delta i_{pq} + \Delta i_{wq}\right) + \Delta E e_q{}' + G\Delta\delta\}$$

$$\Delta i_{td} = \left[\frac{1}{x_2 z_1}(z_1 - r_t^2)A_1 - \frac{r_t D}{z_1}\right]\left(\Delta i_{sd} + \Delta i_{pd} + \Delta i_{wd}\right)$$
$$+ \left[\frac{1}{x_2 z_1}(z_1 - r_t^2)B_1 - \frac{r_t F}{z_1}\right]\left(\Delta i_{sq} + \Delta i_{pq} + \Delta i_{wq}\right)$$
$$+ \left[\frac{1}{x_2 z_1}(z_1 - r_t^2)C_1 - \frac{r_t E}{z_1}\right]\Delta e_q{}' + [\frac{1}{x_2 z_1}(z_1 - r_t^2)D_1 - \frac{r_t G}{z_1}]\Delta\delta$$

$$\Delta i_{tq} = i_{tq1}\left(\Delta i_{sd} + \Delta i_{pd} + \Delta i_{wd}\right) + i_{tq2}\left(\Delta i_{sq} + \Delta i_{pq} + \Delta i_{wq}\right) + i_{tq3}\Delta e_q{}' + i_{tq4}\Delta\delta$$

(B. 2)

where $i_{tq1} = \frac{1}{x_2 z_1}(z_1 - r_t^2)A_1 - \frac{r_t D}{z_1}$ $\quad i_{tq2} = \frac{1}{x_2 z_1}(z_1 - r_t^2)B_1 - \frac{r_t F}{z_1}$

$i_{tq3} = \frac{1}{x_2 z_1}(z_1 - r_t^2)C_1 - \frac{r_t E}{z_1}$ $\quad i_{tq4} = \frac{1}{x_2 z_1}(z_1 - r_t^2)D_1 - \frac{r_t G}{z_1}$

Linearizing microalternator terminal voltage:

The terminal voltage of microalternator is given as

$V_t = V_d + jV_q$

$V_t = x_q i_{tq} + j(e_q' - x_d' i_{td})$

$V_t^2 = V_d^2 + V_q^2$

Differentiating on both sides

$$\Delta V_t = \frac{V_{do}}{V_{to}}(\Delta V_d) + \frac{V_{qo}}{V_{to}}(\Delta V_q)$$

$$\Delta V_t = \frac{V_{do}}{V_{to}}\left(x_q \Delta i_{tq}\right) + \frac{V_{qo}}{V_{to}}(\Delta e'_q - x'_d \Delta i_{td})$$

Substituting the values of Δi_{td} and Δi_{tq}

$$\Delta V_t = \frac{V_{do}}{V_{to}} x_q \left[i_{tq1}\left(\Delta i_{sd} + \Delta i_{pd} + \Delta i_{wd}\right) + i_{tq2}\left(\Delta i_{sq} + \Delta i_{pq} + \Delta i_{wq}\right) + i_{tq3}\Delta e_q{}' \right.$$

$$\left. + i_{tq4}\Delta\delta \right] + \frac{V_{qo}}{V_{to}}\left[\Delta e'_q - x'_d\{i_{td1}\left(\Delta i_{sd} + \Delta i_{pd} + \Delta i_{wd}\right)\right.$$

$$\left. + i_{td2}\left(\Delta i_{sq} + \Delta i_{pq} + \Delta i_{wq}\right) + i_{td3}\Delta e_q{}' + i_{td4}\Delta\delta\}\right]$$

$$\Delta V_t = \left(\Delta i_{sd} + \Delta i_{pd} + \Delta i_{wd}\right)\left[\frac{V_{do} x_q i_{tq1}}{V_{to}} - \frac{V_{qo} x'_d i_{td1}}{V_{to}}\right] +$$

$$\left(\Delta i_{sq} + \Delta i_{pq} + \Delta i_{wq}\right)\left[\frac{V_{do} x_q i_{tq2}}{V_{to}} - \frac{V_{qo} x'_d i_{td2}}{V_{to}}\right] +$$

$$\Delta e'_q\left[\frac{V_{do} x_q i_{tq3}}{V_{to}} - \frac{V_{qo} x'_d i_{td3}}{V_{to}} + \frac{V_{qo}}{V_{to}}\right] + \Delta\delta\left[\frac{V_{do} x_q}{V_{to}} i_{tq4} - \frac{V_{qo} x'_d}{V_{to}} i_{td4}\right]$$

$$\Delta V_t = V_{t1}\left(\Delta i_{sd} + \Delta i_{pd} + \Delta i_{wd}\right) + V_{t2}\left(\Delta i_{sq} + \Delta i_{pq} + \Delta i_{wq}\right) + V_{t3}\Delta e_q{}' + V_{t4}\Delta\delta \qquad (B.3)$$

Where

$$V_{t1} = \frac{V_{do} x_q i_{tq1}}{V_{to}} - \frac{V_{qo} x'_d i_{td1}}{V_{to}} \qquad V_{t2} = \frac{V_{do} x_q i_{tq2}}{V_{to}} - \frac{V_{qo} x'_d i_{td2}}{V_{to}}$$

$$V_{t3} = \frac{V_{do} x_q i_{tq3}}{V_{to}} - \frac{V_{qo} x'_d i_{td3}}{V_{to}} + \frac{V_{qo}}{V_{to}} \qquad V_{t4} = \frac{V_{do} x_q}{V_{to}} i_{tq4} - \frac{V_{qo} x'_d}{V_{to}} i_{td4}$$

Linearizing the power output from microalternator

The real power output of the generator is described as

Pe= $V_d i_{td} + V_q i_{tq}$

$$\Delta P_e = V_{do}\Delta i_{td} + i_{tdo}\Delta V_d + V_{qo}\Delta i_{tq} + i_{tqo}\Delta V_q$$

$$\Delta P_e = V_{do}\Delta i_{td} + i_{tdo}(x_q \Delta i_{tq}) + V_{qo}\Delta i_{tq} + i_{tqo}(\Delta e'_q - x'_d \Delta i_{td})$$

$$\Delta P_e = \Delta i_{td}\left(V_{do} - i_{tqo}x'_d\right) + \Delta i_{tq}\left(i_{tdo}x_q + V_{qo}\right) + i_{tqo}\Delta e'_q$$

$$\Delta P_e = \left[i_{td1}\left(\Delta i_{sd} + \Delta i_{pd} + \Delta i_{wd}\right) + i_{td2}\left(\Delta i_{sq} + \Delta i_{pq} + \Delta i_{wq}\right) + i_{td3}\Delta {e_q}' + i_{td4}\Delta\delta\right]$$
$$\left(V_{do} - i_{tqo}x'_d\right) + \left[i_{tq1}\left(\Delta i_{sd} + \Delta i_{pd} + \Delta i_{wd}\right) + i_{tq2}\left(\Delta i_{sq} + \Delta i_{pq} + \Delta i_{wq}\right) + i_{tq3}\Delta {e_q}'\right.$$
$$\left. + i_{tq4}\Delta\delta\right]\left(i_{tdo}x_q + V_{qo}\right) + i_{tqo}\Delta e'_q$$

$$\Delta P_e = \left(\Delta i_{sd} + \Delta i_{pd} + \Delta i_{wd}\right)\left[\left(V_{do} - i_{tqo}x'_d\right)i_{td1} + \left(i_{tdo}x_q + V_{qo}\right)i_{tq1}\right]$$
$$+ \left(\Delta i_{sq} + \Delta i_{pq} + \Delta i_{wq}\right)\left[\left(V_{do} - i_{tqo}x'_d\right)i_{td2} + \left(i_{tdo}x_q + V_{qo}\right)i_{tq2}\right]$$
$$+ \Delta {e_q}'\left[\left(V_{do} - i_{tqo}x'_d\right)i_{td3} + \left(i_{tdo}x_q + V_{qo}\right)i_{tq3} + i_{tq0}\right]$$
$$+ \Delta\delta\left[\left(V_{do} - i_{tqo}x'_d\right)i_{td4} + \left(i_{tdo}x_q + V_{qo}\right)i_{tq4}\right]$$

$$\Delta P_e = \left(\Delta i_{sd} + \Delta i_{pd} + \Delta i_{wd}\right)P_{e1} + \left(\Delta i_{sq} + \Delta i_{pq} + \Delta i_{wq}\right)P_{e2} + \Delta {e_q}' P_{e3} + \Delta\delta P_{e4}$$

(B. 4)

The state space model of the microgrid system shown in Figure 5.1 is given as,

$$\left[\Delta \dot{X}_{overall}\right] = \left[A_{overall}\right]\left[\Delta X\right] + \left[B\right]\left[\Delta U\right]$$

where $\left[X\right] = [\delta \quad \omega \quad e_q^{'} \quad E_{fd} \quad i_{sd} \quad i_{sq} \quad V_{dcs} \quad i_{pv} \quad V_{dcp} \quad i_{pfd} \quad i_{pfq} \quad i_{pd} \quad i_{pq} \quad V_{opd}$

$V_{opq} \quad i_{gd} \quad i_{gq} \quad \theta_s \quad \omega_t \quad \delta_g \quad \omega_g \quad V_{dcw} \quad i_{wfd} \quad i_{wfq} \quad i_{wd} \quad i_{wq} \quad V_{cwd} \quad V_{cwq}]$ (0.1)

$$A_{overall} = \begin{bmatrix} (A_{GG})_{4x4} & (0)_{4x3} & (A_{GP})_{4x8} & (A_{GW})_{4x13} \\ (0)_{3x4} & (A_{SS})_{3x3} & (A_{SP})_{3x8} & (A_{SW})_{3x13} \\ (A_{PG})_{8x4} & (A_{PS})_{8x3} & (A_{PP})_{8x8} & (A_{PW})_{8x13} \\ (A_{WG})_{13x4} & (A_{WS})_{13x3} & (A_{WP})_{13x8} & (A_{WW})_{13x13} \end{bmatrix}_{28x28}$$

The submatrices are given as:

$$A_{SP} = \begin{bmatrix} (0)_{3x2} & (a_{SP})_{3x2} & (0)_{3x4} \end{bmatrix}_{3x8} \quad \text{where} \quad a_{SP} = \begin{bmatrix} -k_{ST}A_1 & -k_{ST}D \\ -k_{ST}B_1 & -k_{ST}F \\ 0 & 0 \end{bmatrix}_{3x2}$$

$$A_{PS} = \begin{bmatrix} (0)_{3x2} & (a_{PS})_{3x2} & (0)_{3x4} \end{bmatrix}^T_{3x8} \quad \text{where} \quad a_{SP} = \begin{bmatrix} -k_{p}A_1 & -k_{p}D \\ -k_{p}B_1 & -k_{p}F \\ 0 & 0 \end{bmatrix}_{3x2}$$

$$A_{SW} = \begin{bmatrix} (0)_{3x9} & (a_{SW})_{3x2} & (0)_{3x2} \end{bmatrix}_{3x13} \quad \text{where} \quad a_{SW} = \begin{bmatrix} -k_{ST}A_1 & -k_{ST}D \\ -k_{ST}B_1 & -k_{ST}F \\ 0 & 0 \end{bmatrix}_{3x2}$$

$$A_{WS} = \begin{bmatrix} (0)_{3x9} & (a_{wS})_{3x2} & (0)_{3x2} \end{bmatrix}^T_{3x13} \quad \text{where} \quad a_{SW} = \begin{bmatrix} -k_{W}A_1 & -k_{W}D \\ -k_{W}B_1 & -k_{W}F \\ 0 & 0 \end{bmatrix}_{3x2}$$

$$A_{PW} = \begin{bmatrix} (0)_{2x9} & (0)_{2x2} & (0)_{2x2} \\ (0)_{2x9} & (a_{PW})_{2x2} & (0)_{2x2} \\ (0)_{4x9} & (0)_{4x2} & (0)_{4x2} \end{bmatrix}_{8x13} \quad \text{where} \quad a_{PW} = \begin{bmatrix} -k_{p}A_1 & -k_{p}D_1 \\ -k_{p}B_1 & -k_{p}F \end{bmatrix}_{2x2}$$

$$A_{WP} = \begin{bmatrix} (0)_{9x2} & (0)_{9x2} & (0)_{9x2} \\ (0)_{2x2} & (a_{WP})_{2x2} & (0)_{2x2} \\ (0)_{2x2} & (0)_{2x2} & (0)_{2x2} \end{bmatrix}_{13x8} \quad \text{where} \quad a_{WP} = \begin{bmatrix} -k_{W}A_1 & -k_{W}D_1 \\ -k_{w}B_1 & -k_{W}F \end{bmatrix}_{2x2}$$

$$A_{SS} = \begin{bmatrix} -\frac{\omega_o}{L_s}(A_1 + r_s) & -\frac{\omega_o}{L_s}B_1 + \omega_o & -\frac{\omega_o}{L_s}m_{st}\cos\psi_{st} \\ -\frac{\omega_o}{L_s}D & -\frac{\omega_o}{L_s}(F + r_s) & -\frac{\omega_o}{L_s}m_{st}\sin\psi_{st} \\ -\frac{1}{C_{dcs}}m_{st}\cos\psi_{st} & -\frac{1}{C_{dcs}}m_{st}\cos\psi_{st} & 0 \end{bmatrix}_{3x3}$$

The matrices $A_{GG}, A_{PP}, A_{GP}, A_{PG}$ are defined in section 4.1 and the matrices A_{Gw}, A_{wG}, A_{ww} are defined in section 4.2.

The constants defined in the sub matrix A_{ww} are given as

$k_{gd} = \frac{\omega_0}{x_{dw}}$ $k_{gq} = \frac{\omega_0}{x_{qw}}$ $k_{gd1} = -k_{gd}m_{wr}V_{dcwo}\cos(\delta_w)$

$k_{wf} = \frac{\omega_o}{L_{wf}}$ $k_w = \frac{\omega_o}{L_w}$ $k_{gq1} = k_{gq}m_{wr}V_{dcwo}\sin(\delta_w)$

$k_{gd2} = k_{gd}x_{qw}i_{gq0}$ $k_{gq2} = -k_{gq}x_{dw}i_{gq0}$

$k_{gd3} = -k_{gd}m_{wr}\sin(\delta_w)$ $k_{gq3} = -k_{qd}m_{wr}\cos(\delta_w)$

$k_{dcw1} = \frac{1}{C_w}m_{wr}\sin(\delta_w)$ $k_{dcw2} = \frac{1}{C_w}m_{wr}\cos(\delta_w)$

$k_{dcw3} = \frac{1}{C_w}m_{wr}(i_{gd0}\cos(\delta_w) - i_{gq0}\sin(\delta_w))$

$k_{dcw4} = \frac{-1}{C_w}m_{wi}\sin(\delta_w)$ $k_{dcw5} = \frac{-1}{C_w}m_{wi}\cos(\delta_w)$

$k_{wf} = \frac{\omega_o}{L_{wf}}$ $k_w = \frac{\omega_o}{L_w}$ $k_{wf1} = k_{wf}m_{wr}\cos(\psi_{wi})$ $k_{wf1} = k_{wf}m_{wr}\sin(\psi_{wi})$

The control matrix B is given as

$$B=\begin{bmatrix}
(0)_{4x1} & (0)_{4x1} & (0)_{4x1} & (0)_{4x1} & (0)_{4x1} & (0)_{4x1} & (0)_{4x1} \\
B_{5a} & B_{5b} & 0 & 0 & 0 & 0 & 0 \\
B_{6a} & B_{6b} & 0 & 0 & 0 & 0 & 0 \\
0 & 0 & B_{7a} & B_{7b} & 0 & 0 & 0 \\
0 & 0 & B_{8a} & B_{8b} & 0 & 0 & 0 \\
0 & 0 & 0 & 0 & 0 & 0 & 0 \\
B_{14a} & B_{14b} & 0 & 0 & 0 & 0 & 0 \\
0 & 0 & B_{15a} & B_{15b} & 0 & 0 & 0 \\
0 & 0 & 0 & 0 & 0 & 0 & B_{16a} \\
0 & 0 & 0 & 0 & 0 & 0 & B_{17a} \\
0 & 0 & 0 & 0 & 0 & 0 & 0 \\
0 & 0 & 0 & 0 & 0 & 0 & B_{19a} \\
(0)_{2x1} & (0)_{2x1} & (0)_{2x1} & (0)_{2x1} & (0)_{2x1} & (0)_{2x1} & (0)_{2x1} \\
0 & 0 & 0 & 0 & B_{22a} & B_{22b} & B_{22c} \\
0 & 0 & 0 & 0 & B_{23a} & B_{23b} & 0 \\
0 & 0 & 0 & 0 & B_{24a} & B_{24b} & 0 \\
0 & 0 & 0 & 0 & 0 & 0 & 0
\end{bmatrix}_{28x7}$$

The constants defined in the control matrix are given below

$$\mathrm{K}_{st}=\frac{\omega_o}{L_s} \qquad B_{5a}=\mathrm{K}_{st}V_{dcso}\cos(\psi_{st}) \qquad B_{5b}=-\mathrm{K}_{st}m_{st}V_{dcso}\sin(\psi_{st})$$

$$B_{6a}=\mathrm{K}_{st}V_{dcso}\sin(\psi_{st}) \qquad B_{6b}=\mathrm{K}_{st}m_{st}V_{dcso}\cos(\psi_{st})$$

$$B_{7a}=\mathrm{K}_{pf}V_{dcpo}\cos(\psi_p) \qquad B_{7b}=-\mathrm{K}_{pf}m_pV_{dcpo}\sin(\psi_p)$$

$$B_{8a}=\mathrm{K}_{pf}V_{dcpo}\sin(\psi_p) \qquad B_{8b}=\mathrm{K}_{pf}m_pV_{dcpo}\cos(\psi_p)$$

$$B_{14a}=\frac{-1}{C_{dcs}}(i_{sdo}\cos(\psi_{st})+i_{sqo}\sin(\psi_{st})) \qquad B_{14b}=\frac{-m_{st}}{C_{dcs}}(-i_{sdo}\sin(\psi_{st})+i_{sqo}\cos(\psi_{st}))$$

$$B_{15a}=\frac{-1}{C_{dcp}}(i_{pfdo}\cos(\psi_p)+i_{pfqo}\sin(\psi_p)) \qquad B_{15b}=\frac{-m_p}{C_{dcs}}(-i_{pfdo}\sin(\psi_p)+i_{pfqo}\cos(\psi_p))$$

$$B_{16a}=-k_{gd}V_{dcwo}sin\delta_w \qquad B_{16b}=-k_{gq}V_{dcwo}cos\delta_w$$

$$B_{19a} = \frac{-1}{2H_g}(i_{gdo}V_{dcwo}sin\delta_w + i_{gqo}V_{dcwo}cos\delta_w)$$

$$B_{22a} = \frac{-1}{C_w}(i_{wfdo}\cos(\psi_{wi}) + i_{wfqo}\sin(\psi_{wi}) \quad B_{22b} = \frac{-m_{wi}}{C_w}(-i_{wfdo}\sin(\psi_{wi}) + i_{wfqo}\cos(\psi_{wi}))$$

$$B_{22c} = \frac{-1}{C_w}(i_{gdo}\sin(\delta_w) + i_{gqo}\cos(\delta_w)$$

$$B_{23a} = \mathrm{K}_{wf}V_{dcwo}\cos(\psi_{wi}) \qquad B_{23b} = -\mathrm{K}_{wf}m_{wi}V_{dcwo}\sin(\psi_{wi})$$

$$B_{24a} = \mathrm{K}_{wf}V_{dcwo}\sin(\psi_{wi}) \qquad B_{24b} = \mathrm{K}_{wf}m_{wi}V_{dcwo}\cos(\psi_{wi})$$

NOMENCLATURE

ω_0 : Synchronous speed

P_m, P_e : Mechanical input and electrical output of the microalternator

M, H : Machine inertia coefficient and inertia constant

E_{fd} : d-axis field voltage of microalternator

V_t : Terminal voltage of the microalternator

V_{tref} : Reference erminal voltage of the microalternator

x_d : d-axis synchronous reactance

$x_d^{'}$: d-axis transient reactance

$T_{do}^{'}$: Open circuit field constant

K_A, T_A : Gain and time constant of the exciter

E_g : Energy gap

P_{mw}, P_{ew} : Mechanical input and electrical output of the wind system

H_g : Inertia constant of the wind

x_{dw}, x_{qw} : d and q axes PMSG reactances

E_{fdw} : d-axis field voltage of PMSG

K_s : Stiffnes constant

R_{pf}, L_{pf}, C_{pf} : Resistance, inductance and capacitance of the PV output filter circuit

R_p, L_p : Resistance and inductance of the PV output coupling line.

R_{wf}, L_{wf}, C_{wf}: Resistance, inductance and capacitance of the wind output filter circuit

R_w, L_w : Resistance and inductance of the wind output coupling line.

R_s, L_s : Resistance and inductance of the STATCOM transmission line.

r_t, x_t : Resistance and reactance of the line between microalternator and microgrid

r_b, x_b : Resistance and reactance of the line between microgrid and main grid

g, b : Conductance and susceptance of the load

V_s, θ : Voltage magnitude and d-axis phase angle of microgrid

i_{gd}, i_{gq} : d-q axes PMSG currents

m_p, ψ_p : Modulation index and phase angle of the PV inverter respectively

m_{wi} : Modulation index of the wind generator side converter

m_{wi}, ψ_{wi} : Modulation index and phase angle of the wind inverter respectively

m_{st}, ψ_{st} : Modulation index and phase angle of the STATCOM respectively

REFERENCES

[1] P. P. Barker and R. W. De Mello, "Determining the impact of distributed generation on power systems. I. Radial distribution systems," 2000, pp. 1645-1656 vol. 3.

[2] F. Katiraei*, et al.*, "Micro-grid autonomous operation during and subsequent to islanding process," *Power Delivery, IEEE Transactions on,* vol. 20, pp. 248-257, 2005.

[3] R. H. Lasseter, "MicroGrids," 2002, pp. 305-308 vol. 1.

[4] J. A. P. Lopes*, et al.*, "Defining control strategies for microgrids islanded operation," *Power Systems, IEEE Transactions on,* vol. 21, pp. 916-924, 2006.

[5] R. Shah*, et al.*, "Impact of large-scale PV penetration on power system oscillatory stability," in *Power and Energy Society General Meeting, 2010 IEEE*, 2010, pp. 1-7.

[6] A. G. Tsikalakis and N. D. Hatziargyriou, "Centralized control for optimizing microgrids operation," 2011, pp. 1-8.

[7] P. F. Ribeiro*, et al.*, "Energy storage systems for advanced power applications," *Proceedings of the IEEE,* vol. 89, pp. 1744-1756, 2001.

[8] R. Lasseter*, et al.*, "Integration of distributed energy resources. The CERTS Microgrid Concept," 2002.

[9] F. Kanellos*, et al.*, "Micro-grid simulation during grid-connected and islanded modes of operation," 2005.

[10] F. Katiraei and M. Iravani, "Transients of a Micro-Grid system with multiple distributed energy resources."

[11] F. Katiraei and M. Iravani, "Power management strategies for a microgrid with multiple distributed generation units," *Power Systems, IEEE Transactions on,* vol. 21, pp. 1821-1831, 2006.

[12] W. Deng*, et al.*, "Research on dynamic stability of hybrid wind/PV system based on Micro-Grid," 2008, pp. 2627-2632.

[13] R. Yan and T. K. Saha, "Development of simplified models for a single phase grid connected photovoltaic system," 2011, pp. 1-6.

[14] R. J. Wai and W. H. Wang, "Grid-connected photovoltaic generation system," *Circuits and Systems I: Regular Papers, IEEE Transactions on,* vol. 55, pp. 953-964, 2008.

[15] M. A. Eltawil and Z. Zhao, "Grid-connected photovoltaic power systems: Technical and potential problems--A review," *Renewable and Sustainable Energy Reviews,* vol. 14, pp. 112-129, 2010.

[16] M. E. Ropp and S. Gonzalez, "Development of a MATLAB/simulink model of a single-phase grid-connected photovoltaic system," *Energy Conversion, IEEE Transactions on,* vol. 24, pp. 195-202, 2009.

[17] A. Canova*, et al.*, "Electrical impact of photovoltaic plant in distributed network," *Industry Applications, IEEE Transactions on,* vol. 45, pp. 341-347, 2009.

[18] E. Liu*, et al.*, *Distribution system voltage performance analysis for high-penetration photovoltaics*: National Renewable Energy Laboratory, 2008.

[19] Y. T. Tan*, et al.*, "A model of PV generation suitable for stability analysis," *Energy Conversion, IEEE Transactions on,* vol. 19, pp. 748-755, 2004.

[20] S. Achilles*, et al.*, *Transmission system performance analysis for high-penetration photovoltaics*: National Renewable Energy Laboratory, 2008.

[21] G. Li*, et al.*, "Design of a Photo-Voltaic System to Enhance Network Dynamic Stability," 2010.

[22] R. Shah*, et al.*, "Impact of large-scale PV penetration on power system oscillatory stability," pp. 1-7.

[23] T. Ackerman, "Wind Power in Power Systems. Royal Institute of Technology Stockholm, Sweden," ed: John wiley & Sons, Ltd, 2005.

[24] F. González-Longatt*, et al.*, "Dynamic Behavior of Constant Speed WT based on Induction Generator Directly connect to Grid," 2007.

[25] P. Ledesma*, et al.*, "Transient stability of a fixed speed wind farm," *Renewable Energy,* vol. 28, pp. 1341-1355, 2003.

[26] L. M. Fernández*, et al.*, "Dynamic models of wind farms with fixed speed wind turbines," *Renewable Energy,* vol. 31, pp. 1203-1230, 2006.

[27] W. Qiao*, et al.*, "Dynamic modeling of wind farms with fixed-speed wind turbine generators," pp. 1-8.

[28] J. Ribrant and L. M. Bertling, "Survey of failures in wind power systems with focus on Swedish wind power plants during 1997–2005," *Energy Conversion, IEEE Transactions on,* vol. 22, pp. 167-173, 2007.

[29] P. Vas, *Electrical machines and drives: a space-vector theory approach* vol. 25: Oxford University Press, USA, 1992.

[30] M. Mansour*, et al.*, "Comparative study of fixed speed and variable speed wind generator with pitch angle control," 2011, pp. 1-7.

[31] K. Tan and S. Islam, "Optimum control strategies in energy conversion of PMSG wind turbine system without mechanical sensors," *Energy Conversion, IEEE Transactions on,* vol. 19, pp. 392-399, 2004.

[32] F. Mei and B. C. Pal, "Modelling of doubly-fed induction generator for power system stability study," 2008, pp. 1-8.

[33] W. Zhiqun*, et al.*, "IMPACTS OF DISTRIBUTED GENERATION ON DISTRIBUTION SYSTEM VOLTAGE PROFILE [J]," *Automation of Electric Power Systems,* vol. 16, 2004.

[34] Z. Yang*, et al.*, "Preliminary study on the technical requirements of the grid-connected microgrid," in *Electric Utility Deregulation and Restructuring and Power Technologies (DRPT), 2011 4th International Conference on*, 2011, pp. 1656-1662.

[35] D. Menniti*, et al.*, "A method to improve microgrid reliability by optimal sizing PV/Wind plants and storage systems," in *Electricity Distribution - Part 1, 2009. CIRED 2009. 20th International Conference and Exhibition on*, 2009, pp. 1-4.

[36] S. Park*, et al.*, "A study on the stand-alone operating or photovoltaic/wind power hybrid generation system," 2004, pp. 2095-2099 Vol. 3.

[37] T. Tadokoro*, et al.*, "A photovoltaic-diesel hybrid generation system for small islands," 1994, pp. 708-715 vol. 1.

[38] F. Valenciaga*, et al.*, "Power control of a solar/wind generation system without wind measurement: a passivity/sliding mode approach," *Energy Conversion, IEEE Transactions on,* vol. 18, pp. 501-507, 2003.

[39] H. J. Choi*, et al.*, "An analysis of PEMFC & photovoltaic 500W hybrid system," pp. 522-524.

[40] F. Katiraei*, et al.*, "Small-signal dynamic model of a micro-grid including conventional and electronically interfaced distributed resources," *Generation, Transmission & Distribution, IET,* vol. 1, pp. 369-378, 2007.

[41] J. M. Guerrero*, et al.*, "Hierarchical control of droop-controlled AC and DC microgrids—A general approach toward standardization," *Industrial Electronics, IEEE Transactions on,* vol. 58, pp. 158-172, 2011.

[42] Y. Mohamed and E. F. El-Saadany, "Adaptive decentralized droop controller to preserve power sharing stability of paralleled inverters in distributed generation microgrids," *Power Electronics, IEEE Transactions on,* vol. 23, pp. 2806-2816, 2008.

[43] M. Prodanovic and T. C. Green, "Control and filter design of three-phase inverters for high power quality grid connection," *Power Electronics, IEEE Transactions on,* vol. 18, pp. 373-380, 2003.

[44] J. H. R. Enslin and P. J. M. Heskes, "Harmonic interaction between a large number of distributed power inverters and the distribution network," *Power Electronics, IEEE Transactions on,* vol. 19, pp. 1586-1593, 2004.

[45] D. P. Ariyasinghe and D. M. Vilathgamuwa, "Stability analysis of microgrids with constant power loads," 2008, pp. 279-284.

[46] A. Al-Hinai and A. Feliachi, "Dynamic model of a microturbine used as a distributed generator," 2002, pp. 209-213.

[47] X. Xialing, *et al.*, "Probabilistic analysis of small signal stability of microgrid using point estimate method," in *Sustainable Power Generation and Supply, 2009. SUPERGEN '09. International Conference on*, 2009, pp. 1-6.

[48] W. Huang, *et al.*, "Discussion on application of super capacitor energy storage system in microgrid," in *Sustainable Power Generation and Supply, 2009. SUPERGEN '09. International Conference on*, 2009, pp. 1-4.

[49] G. Zhang, *et al.*, "Research on Battery Supercapacitor Hybrid Storage and its application in MicroGrid," in *Power and Energy Engineering Conference (APPEEC), 2010 Asia-Pacific*, 2010, pp. 1-4.

[50] E. Bilbao, *et al.*, "Design and development of a supercapacitor-based microgrid dynamic support system," in *Power Electronics and Applications, 2009. EPE '09. 13th European Conference on*, 2009, pp. 1-10.

[51] A. Hamdan, "An investigation of the significance of singular value decomposition in power system dynamics," *International Journal of Electrical Power & Energy Systems,* vol. 21, pp. 417-424, 1999.

[52] I. Y. Chung, *et al.*, "Control parameter optimization for a microgrid system using particle swarm optimization," pp. 837-842.

[53] M. Liserre, *et al.*, "Design and control of an LCL-filter-based three-phase active rectifier," *Industry Applications, IEEE Transactions on,* vol. 41, pp. 1281-1291, 2005.

[54] I. Y. Chung, *et al.*, "Control parameter optimization for multiple distributed generators in a microgrid using particle swarm optimization," *European Transactions on Electrical Power,* vol. 21, pp. 1200-1216, 2011.

[55] M. El-Sherbiny*, et al.*, "Optimal pole shifting for power system stabilization," *Electric Power Systems Research,* vol. 66, pp. 253-258, 2003.

[56] K. De Brabandere*, et al.*, "Control of microgrids," 2007, pp. 1-7.

[57] S. Barsali*, et al.*, "Control techniques of dispersed generators to improve the continuity of electricity supply," 2002, pp. 789-794 vol. 2.

[58] A. Mehrizi-Sani and R. Iravani, "Potential-function based control of a microgrid in islanded and grid-connected modes," *Power Systems, IEEE Transactions on,* vol. 25, pp. 1883-1891, 2010.

[59] I. J. Balaguer*, et al.*, "Intelligent control for intentional islanding operation of microgrids," pp. 898-903.

[60] C. Cho*, et al.*, "Active Synchronizing Control of a Microgrid," *Power Electronics, IEEE Transactions on,* vol. PP, pp. 1-1, 2011.

[61] M. A. Hassan and M. A. Abido, "Optimal Design of Microgrids in Autonomous and Grid-Connected Modes Using Particle Swarm Optimization," *Power Electronics, IEEE Transactions on,* vol. 26, pp. 755-769, 2011.

[62] Y. N. Yu, "Electric power system dynamics," *ACADEMIC PRESS, INC., 111 FIFTH AVE., NEW YORK, NY 10003, USA, 1983, 256,* 1983.

[63] H. L. Tsai*, et al.*, "Development of generalized photovoltaic model using MATLAB/SIMULINK," 2008.

[64] J. J. Wysocki and P. Rappaport, "Effect of temperature on photovoltaic solar energy conversion," *Journal of Applied Physics,* vol. 31, pp. 571-578, 1960.

[65] V. Quaschning and R. Hanitsch, "Numerical simulation of current-voltage characteristics of photovoltaic systems with shaded solar cells," *Solar Energy,* vol. 56, pp. 513-520, 1996.

[66] K. Hussein*, et al.*, "Maximum photovoltaic power tracking: an algorithm for rapidly changing atmospheric conditions," 1995, pp. 59-64.

[67] Q. Zhao and F. C. Lee, "High-efficiency, high step-up DC-DC converters," *Power Electronics, IEEE Transactions on,* vol. 18, pp. 65-73, 2003.

[68] G. Bon-gwan and N. Kwanghee, "A DC link capacitor minimization method through direct capacitor current control," in *Industry Applications Conference, 2002. 37th IAS Annual Meeting. Conference Record of the*, 2002, pp. 811-817 vol.2.

[69] N. Mahamad*, et al.*, "Application of LC filter in harmonics reduction," 2004, pp. 268-271.

[70] Y. Ming*, et al.*, "Modeling of the Wind Turbine with a Permanent Magnet Synchronous Generator for Integration," in *Power Engineering Society General Meeting, 2007. IEEE*, 2007, pp. 1-6.

[71] M. Abido, "Analysis and assessment of STATCOM-based damping stabilizers for power system stability enhancement," *Electric Power Systems Research,* vol. 73, pp. 177-185, 2005.

[72] M. Farsangi*, et al.*, "Choice of FACTS device control inputs for damping interarea oscillations," *Power Systems, IEEE Transactions on,* vol. 19, pp. 1135-1143, 2004.

Vitae

- Mohammed Touseef hussain.
  - ✓ Permanent Address: Hyderabad, INDIA
  - ✓ Present Address: Dhahran, Saudi Arabia.
  - ✓ Contact no: +966502040226
  - ✓ Email: touseefhussainhere@yahoo.co.in
  - ✓ Date of birth: March 16, 1987.
- Received Bachelor of Engineering (B.E) degree in Electrical and Electronics Engineering from Deccan College of Engineering and Technology (DCET), Osmania University, Hyderabad, INDIA in May 2009.
- Joined the Department of Electrical Engineering at King Fahd University of Petroleum and Minerals (KFUPM), Dhahran, Saudi Arabia as Research Assistant in February 2010.
- Received Master of Science (M.S) degree in Electrical Engineering from KFUPM, Saudi Arabia in April 2012.